Unusual Particle Motions

in the Liquid Crystal Phases

A thesis submitted to the University of Manchester

for the degree for PhD in the Faculty of

Engineering and Physical Sciences

2014

JIYOUNG OH

School of Physics and Astronomy/Condensed

Matter, Atomic and Biological Physics

Abstract

The motions of particles dispersed in liquid crystals can be influenced by the application of an electric field, the effect depending on the field frequency and field amplitude. Sandwich cells under the application of electric field are widely used as the tool in order to investigate the fundamental research relating to electro-optic display technology. Therefore, the aim of this experimental work is to find and investigate novel motion of the particles dispersed in the liquid crystal phases, held within a sandwich cell.

For the liquid crystal–particle systems in the sandwich cells in this thesis, the particle shapes, temperature and cell geometry are all shown to have an influence on the regime of the particle's motions, with different phenomena observed using three different phases of liquid crystals. The experiments are designed to find and investigate the novel motion of the micron sized silica particles in the liquid crystal phases.

In the chiral nematic phase, spherical particles are shown to exhibit linear motion, which is related to the electrophoretic mobility. Such spherical particles are also observed to show circular motion which is found to have a field dependency that can be related to Quincke rotation. A maximum frequency for motion occurs which is found to possibly be related to the effect of the ion diffusion in the liquid crystal-particle composite system. The direction of the circular motion is found to be independent of the handedness of the chiral nematic material.

In the isotropic phase of a chiral nematic liquid crystal, the spherical particles do not exhibit any linear motion, which shows the system does not follow the traditional electrophoresis observed in normal isotropic liquids. The circular motion of the spherical particle that is observed in the isotropic phase is analysed in terms of the Quincke rotation and again shows the Maxwell relaxation time.

The electric-field induced motion of elongated particles in four different nematic systems is examined. In this case of planar aligned systems, linear motion is observed, in which the velocity shows a minimum for particles of the same length as the cell gap. A novel field-induced defect texture appears in the homeotropic device containing a nematic liquid crystal of negative dielectric anisotropy. Interestingly, the motion of the particle is found to be strongly coupled with the defects formed.

Acknowledgements

Most of all I thank to Professor Helen Gleeson who holds my hands with the great inspiration, wide range of knowledge, precious equipment and her respected leadership. Without the help and support I would not be keeping doing the PhD course. The way to go up the hill looked not good to me but now I am ready to climb another hills and mountains.

I would like to thank Doctor Ingo Dierking for his guidance, providing material and support as well. I want to thank Professor Cliff Jones who is always willing to communicate with such a nice mind. I appreciate to respected academic Professor Jian Lu and Professor David Dunmur who cared me to finish my thesis. Also, I thank all the members of the liquid crystal group in University of Manchester for their encouragement, friendship and interesting discussions.

I wish to thank Professor Myung-Ja Kim, CTO Ji-Min Cha, Professor Kyung-Ok Kwon, and Professor Woo-Kul Lee who have been transferring to me the nice vision in Research & Development. Also, I wish to say thank my friends; Sojin, Eunju, Heekyung, Eunjin, Sunjung, Yuna, Shinhee, Mrs. Stewart, Mrs. Wood, Father Burnard, the Watertons, the Gunstones, and Edie & Cath.

In addition, I would like to appreciate the University of Manchester for the Windfall scholarship allocated during my time as a PhD. Student in Physics. I wish to acknowledge British liquid crystal society, and Institute of Physics for their sponsoring for my academic travels and presentations. WIEST, WES, and MICRA are also thankfully delivering bright idea to me because their philosophies and their tools of working are going to be useful to the interdisciplinary area of science as future work.

Finally, I want to thank my family. The endless support and the power of love have been providing from Min, Se-Eun, Hak-Sun, my parents and brother Jun. It is such a blessing that I have you. I am happy to say, "Love you."

Declaration

No portion of the work preferred to in this thesis has been submitted in support of an application for another degree or qualification of this or any other university or other institute of learning.

Copyright

The Author

The author graduated from Dae-Gok Elementary School, Sook-Myung Girl’s Middle & High School. She graduated with a Bachelor and Master of Chemistry from Sook-Myung Women’s University. She started her PhD at University of Manchester, School of Physics and Astronomy in 2008 titled "Unusual Particle Motions in Liquid Crystal Phases" She is under the supervision of Prof. Helen Gleeson and Dr. Dierking.

List of Publication

Micron-sized spherical particle's unusual motion in chiral nematic phase

Ingo Dierking, Jiyoung Oh, Helen Gleeson.

PRE (Processing manuscript)

Micron-sized elongated particle's motions in nematic phases under the application of electric field.

Jiyoung Oh, Helen Gleeson, Ingo Dierking.

PRE (Processing manuscript)

A novel texture of nematic defect with an elongated particle

Helen Gleeson, Ingo Dierking, Jiyoung Oh.

Science (Preparing manuscript)

Conference Contributions

BLCS 2009, 6th ~ 8th of April, 2009, HP Center, Bristol, UK

Poster Presentation at the British Liquid Crystal Society conference

MCND 2010, 18th of June, 2010, Alan Turing Building, Oxford road, Manchester, UK

Oral presentation at the seminar of Manchester Centre for Nonlinear Dynamics

ILCC 2010, 11th ~ 16th of July, 2010, Krakow, Poland.

Poster Presentation at the International Liquid Crystal Conference

CMMP11, 13th ~ 15th of December, 2011, Lancashire County Cricket Club, Manchester.

Poster presentation at the IOP (Institute of Physics) conference of Condensed Matter and Materials Physics organised by the IOP Condensed Matter and Materials Division

To My family

Especially to Angela Jung

Contents

List of Figures

Chapter 1

light and illuminates the sample uniformly (h) focus is a dial-button to regulate the height of the stage for focusing light onto sample (i) polarizer (j) lens (k) lower body of the microscope (l) light source (m) mirror reflects the light source.

Figure 1.10 A diagram of a polarizing filter and light wave propagating perpendicular to the polarizing filter domain. (a) An electric field of unpolarized light which is oscillating randomly in all directions. (b) Polarizer; the black coloured arrow line depicts the direction of polymer grid and the red coloured arrow line describes the polarizer's axis (c) Transmitted component of the electric wave which is perpendicular to the polymer molecules (d) Propagation direction of the light wave.

Figure 1.11 A geometric diagram of a birefringent liquid crystal material and light ray showing the polarization of light striking the polarizer and analyser. (a) a polarizer; the red arrow is a symbol of transmittance axis (b) the propagation of light; the direction of a light wave moves (c) a liquid crystal material's optical axis as depicted with a green arrow; θ is the angle between optic axis and propagation direction of the light wave (d) An analyser containing a transmittance axis symbolised by the red arrow, and the purple arrow shows a projection of the optic axis on the analyser plate; φ is the angle between the liquid crystal's optic axis projected on the analyser domain and transmittance axis of the analyser.

Figure 1.12 The optical active material. (a) incident plane polarized light (b) a chiral liquid crystal phase (c) exiting light of changed plane of polarization (d) propagation direction of light.

Figure 1.13 Two nematic textures. Image (a) shows a well aligned E44 (Merk co.,) texture, with a homogenous colour with dark regions corresponding to particles used to separate the glass substrates (spacers). Image (b) shows surface disclination lines appearing like threads in a planar boundary condition. The disclination lines (180° turn of director in plane of substrates) in the texture are similar in appearance to threadlike textures. Threads are line singularities with π disclinations and end at the substrates, connected with brushes or make closed loops. For more information, see. [32] [Photo courtesy of Dr. H. Milton and Dr. I. Dierking]

Figure 1.14 A nematic schlieren texture. Two- and four-fold brushes can be observed, leading into singularities. The curved dark brushes gather to point singularities; topological defect with values s = ± (number of brushes/4). [Photo courtesy of Dr. S. Lagerwall & B. Stebler]

Figure 1.15 A cholesteric oily-streaks Grandjean texture. The helical axis of the chiral nematic phase is oriented perpendicular to the substrate plane except the area of defects named oily-streaks defects. [Photo courtesy of Dr. I. Dierking]

Figure 1.16 A fingerprint texture of a chiral nematic phase. The helical axis located in the plane of the substrate. The line pattern is due to the helical structure of the liquid crystal phase. [Photo courtesy of Dr. I. Dierking]

Chapter 2

Figure. 2.1 [P. Poulin, H. Stark, T. C. Lubensky, and D. A. Weitz, "Novel Colloidal Interactions in Anisotropic Fluids". *Science*, 21 March, 1997, Volume 275, No.5307, pp.1770-1773.] (A) Microscope image of a nematic multiple emulsion taken under crossed polarizers. (B) A chain of water droplets under high magnification. (C) A nematic drop containing a single water droplet.

Figure 2.2 [J-C. Loudet, P. Barois & P. Poulin, "Colloidal ordering from phase separation in a liquid- crystalline continuous phase". *Nature*, 5 October, 2000, Volume 407, pp.611-613.] (A) Highly ordered arrays made of monodisperse droplets form. (a) System composition: liquid crystal, 98.0 wt%; silicone oil, 2.0 wt%. Black arrow denotes direction of polymer rubbing on the device substrate. Scale bar, 50 μm. (b) System composition: liquid crystal, 98.4 wt%; silicone oil, 1.6 wt%. Black arrow denotes direction of polymer rubbing. Scale bar, 35 μm. (c) Chains aligned in different directions (picture of system between crossed polarizers). They are obtained by rubbing different regions of the substrate in different directions. System composition: liquid crystal, 98.4 wt%; silicone oil, 1.6 wt%. White arrows denotes direction of polymer rubbing. Scale bar, 60 μm.
(B) As time passes, the droplet size becomes larger. The black lines represent the axis of preferential orientation of the liquid-crystal molecules. For small particles, the liquid crystal is slightly distorted, and its alignment at the surface of the particle may adopt different orientations. (C) For large particles, the alignment is normal to the particle surface. This induces the formation of a companion defect located near the particle. The global structure has dipolar symmetry. (D) The distortions for an assembly of dipolar droplets that form parallel chains. The defect between neighboring droplets inhibits the coalescence.

Figure. 2.3 [I. Muševič, M. Škarabot, U. Tkalec, M. Ravnik, and S. Žumer, "Two-Dimensional Nematic Colloidal Crystals Self-Assembled by Topological Defects",

Science, 18 August, 2006, Volume 313, No.5789, pp.954-958.] (A) Micrograph of a d = 2.32 μm silica sphere in an h = 5 μm layer of 5CB with a hyperbolic hedgehog defect (black spot on top). (B) The nematic order around the colloid has the symmetry of an electric dipole. (C) Dipoles spontaneously form dipolar (ferroelectric) chains along the rubbing direction. (D) The same type of colloid in a thin (h = 2.5 μm) 5CB layer. The two black spots on the right and left side of the colloid represent the Saturn ring. (E) The nematic order has in this case the symmetry of an electric quadrupole. (F) Quadrupoles spontaneously form kinked chains perpendicular to the direction of rubbing.

Figure 2.4-1 [N. Hijnen, T. A. Wood, D. Wilson, and P. S. Clegg, "Self-Organization of Particles with Planar Surface Anchoring in a Cholesteric Liquid Crystal". *Langmuir*, 21 JULY, 2010, Volume 26, Issue 16, pp.13502–13510.] High-magnification birefringence images of melamine particles (d = 3 μm) in a cholesteric liquid crystal. (a) Images (p = 1.5 μm) taken at a sample thickness of ∼5 μm in the top row and images taken at a sample thickness of ∼10 μm in the bottom row. The bottom-row images are of the same three particles but with a different choice of focal plane. The particles can be seen to be touching. (b) Images (p = 0.4 μm) taken at a sample thickness of ∼5 μm and at higher magnification in the top row and images taken at a sample thickness of ∼15 μm in the bottom row. (c) Confocal images at high magnification of melamine particles (10 vol. %) in the nematic (top row) and the cholesteric (bottom row) with p = 0.4 μm.

Figure 2.4-2 [N. Hijnen, T. A. Wood, D. Wilson, and P. S. Clegg, "Self-Organization of Particles with Planar Surface Anchoring in a Cholesteric Liquid Crystal". *Langmuir*, 21 JULY, 2010, Volume 26, Issue 16, pp.13502–13510.] (A) Radial distribution functions of the melamine (d = 3 μm) particles in a nematic liquid crystal and cholesteric liquid crystals of different pitch lengths obtained from the analysis of confocal images of particles in planes. (B) Cartoons showing the proposed organisation of the cholesteric liquid crystal around the particles. (a) Top view of the onionlike arrangement. (b) Helical order between two particles viewed from the side; $\lambda^{-1/2}$ lines may form in the gap. (c) Plane of particles in contact as viewed from the side.

Figure 2.5 [D. Pires, J. B. Fleury, and Y. Galerne, "Colloid Particles in the Interaction Field of a Disclination Line in a Nematic Phase". *PHYSICAL REVIEW LETTERS*, 15, June, 2007, Volume 98, pp.247801.] (A), (B), (C) Photographs (width 50 μm) taken before the bead is captured by the disclination line at times t = -240 s, -56 s, -2 s, respectively. The particle is indicated with round black spot, and the line shows

disclination line. Note that the line is slightly distorted by the attraction exerted by the particle.

Figure 2.6 [S. Juodkazis, M. Shikata, T. Takahashi, S. Matsuo and H. Misawa, "Fast optical switching by a laser-manipulated microdroplet of liquid crystal". *APPLIED PHYSICS LETTERS*, 14 JUNE, 1999, VOLUME 74, NUMBER 24, pp.3627-3629.] (A) Angularly controlled orientation of a LC (liquid crystal) droplet by plane-polarized irradiation. The images made by light passed through a polarizer–droplet–analyser bear the signature of polar alignment of LC molecules (schematically shown on the right), which scatter the passing light. The regions, which are marked by black ellipses in a schematic drawing of the LC droplet, to those where the passing light is not scattered (less transmitive regions on the video frames). By polarization control of the incident beam, the LC droplet was accordingly aligned to the polarization plane of the incident beam, as shown in the five video frames (a)~(e). The polarization was controlled by a λ/2 plate (scale bar: 10 μm). (B) Spinning of an LC droplet by circularly left polarized light (marked by arrow). The spinning of a nematic LC droplet can be recognized by viscous orbiting of smaller particle (enclosed in circle) on consecutive snap shots (a)~(f) made with 30 ms separation. The rotation speed of the droplet itself was higher than the 30 Hz resolution of the video recorder (scale bar: 10μm). (C) An optical switching as transmission changes of the rotating LC droplet (the diameter of the droplet was 1.8 μm; the irradiation power was 700 mW). The switching time of 280 μs was determined between the highest and the lowest transmission, and corresponded to the droplet's rotation by a π/4 angle. (b) The power dependencies of rotation frequency for the droplets of 1 μm (squares) and 2.3 μm (triangles) in diameter. The theoretical limit of rotation frequency for the 1 μm diameter droplet (solid line) was calculated by Equation of $\Gamma = -8\pi\eta(a/2)^3\omega$ as the transfer of all light spin $\Gamma_{max} = (P/\hbar\omega)\cdot\hbar$ into the rotation, where P is the irradiation power.

Figure 2.7 [H. F. Gleeson, T. A. Wood, and M. R. Dickinson, "Laser manipulation in liquid crystals: an approach to microfluidics and micromachines". *Philosophical Transactions of the Royal Society A*, 2006, Volume 364, Number 1847, pp.2789-2805.] Photograph of a 6μm diameter polystyrene particle dispersed in MLC-6648 (Merk) and viewed between crossed polarizers, showing the symmetric transmission pattern (approx. 1000×).

Figure 2.8 [J. L. Sanders, Y. Yang, M. R. Dickinson, and H. F. Gleeson, "Pushing, pulling and twisting liquid crystal systems: exploring new directions with laser manipulation". *Philosophical Transactions of the Royal Society A*, 2013, Volume 371, Number 1988, pp.20120265.] Time evolution showing the continuous rotation of

nematic and chiral nematic LC droplets in circularly and elliptically polarized optical tweezers. (*a*) A nematic bipolar droplet rotates about its centre, where a nearby small droplet can be seen orbiting owing to their hydrodynamic interaction. (*b*) The centre of the radial nematic droplet orbits as a circle. (*c*) A Frank–Pryce droplet rotates about its centre. (*d*) The centre of a variational Frank–Pryce droplet orbits as a circle in company with its spin rotation.

Figure 2.9-1 [A. Nych, U. Ognysta, M. Škarabot, M. Ravnik, S. Žumer, and I. Muševič, Assembly and control of 3D nematic dipolar colloidal crystals. *Nature Communications*, 2012, Volume 4, Article number: 1489.] Laser-tweezers assembly of a 3D dipolar colloidal crystal observed under crossed polarizers. (a,b) Microscopic images of 2.32 μm dipolar silica microspheres in the homeotropic cell filled with 5CB nematic liquid crystal. In (a), the topological point defect is above the microsphere, in (b), the defect is below it. Left panels are taken without polarizers, right panels are taken between crossed polarizers. Scale bar, 2 μm. (c) Quasi-2D checkerboard structure formed by 4.32 μm silica particles in ~10 μm-thick homeotropic cell filled with ZLI-2806. The lattice was observed with completely open condenser aperture diaphragm enhancing the 'checkerboard'-like look of the crystal. No polarizers were used. Scale bar, 10 μm. (d) A vertical cross-section of a quasi-2D checkerboard colloidal crystal of 4 μm colloidal particles, obtained from confocal microscope imaging of a structure like in (c). The alternating arrangement of the microspheres with topological defects above and below them is clearly seen. The defects are not resolved in this image, they are located at the points where the two bright lobes that encircle each particle come together.

Figure 2.9-2 [Laser-tweezers assembly of a 3D dipolar colloidal crystal observed under crossed polarizers by I. Muševič *et al*. *Nature Communications*, 2012, Volume 4, Article number: 1489.] (a) Three isolated colloidal particles of 4 μm diameter in the ZLI-2806-filled homeotropic cell of ~25 μm thickness appear as bright objects with a dark cross in the centre. Using laser tweezers, one particle is brought close to the other and they spontaneously form a chain of two particles in a direction perpendicular to the plane of the image. The pair appears like a single but larger and brighter particle (3rd image from the left). The third particle is brought to the couple and it spontaneously forms a dipolar colloidal chain of three particles on top of each other. (b) Three chains, each made of three dipolar particles, are brought close to each other and they start to assemble into a frustrated colloidal trio. Note the tilting of the chains. (c) Two colloidal blocks of 2 × 2 × 3 particles self-assemble into 2 × 4 × 3 blocks. (d) Colloidal blocks of 2 × 6 × 3 and 4 × 6 × 3 particles assemble into the final 6 × 6 × 3 dipolar colloidal crystal. The assembly at the initial stage was guided by the laser tweezers

until blocks started to attract themselves. Scale bar, 10 μm. In all images, the small red cross is the optical trap, used to direct t representation of the fluorescent confocal polarizing microscopy image of a 6 × 6 × 3 3D dipolar colloidal crystal. Here, the fluorescence intensity was inverted to show the in-plane arrangement of the particles in the XY, YZ and XZ planes. Scale bar, 5 μm. (c) Numerical simulation of a 3D dipolar nematic colloidal crystal. Point topological defect opened into small loops, somewhat larger as observed in experiments, and are visualized as iso-surfaces of fixed nematic degree of order *S*. Scale bar, 1 μm. (d) Free energy of one colloidal crystal unit cell as a function of the lattice constants A and B in units of particle radius R. (e) Schematic drawing of the crystal structure showing the tetragonal Bravais lattice with basis.

Figure 2.9-3 [Structure of a 3D dipolar nematic colloidal crystal by I. Muševič *et al. Nature Communications*, 2012, Volume 4, Article number: 1489.] (a) Fluorescent confocal polarizing microscopy images of two horizontal cross-sections of a 3D, 6 × 6 × 3 dipolar colloidal crystal, assembled from 4 μm diameter colloidal particles in the homeotropic aligned nematic liquid crystal ZLI-2806. The images were acquired by refocusing along the *z*-axis direction by 2.6 μm . Scale bar, 5 μm. (b) The 3D representation of the fluorescent confocal polarizing microscopy image of a 6 × 6 × 3 3D dipolar colloidal crystal. Here, the fluorescence intensity was inverted to show the in-plane arrangement of the particles in the XY, YZ and XZ planes. Scale bar, 5 μm. (c) Numerical simulation of a 3D dipolar nematic colloidal crystal. Point topological defect opened into small loops, somewhat larger as observed in experiments, and are visualized as iso-surfaces of fixed nematic degree of order *S*. Scale bar, 1 μm. (d) Free energy of one colloidal crystal unit cell as a function of the lattice constants A and B in units of particle radius R. (e) Schematic drawing of the crystal structure showing the tetragonal Bravais lattice with basis.

Figure 2.10-1 [I. Dierking, G. Biddulph, and K. Matthews, “Electromigration of microspheres in nematic liquid crystals”. *PHYSICAL REVIEW E*, 2006, Volume 73, pp.011702.] (a) Side view of the employed Hele-Shaw cell with cell gap d =10 μm. At zero electric field the nematic director **n** is approximately parallel to the bounding substrates. Particle motion is observed in the plane perpendicular to the direction of the applied electric field. (b) Top view of the cell as observed in the polarized microscopic experiments. At zero applied field the director **n** is uniformly oriented along a preferred direction. Particle motion is observed parallel to this direction and perpendicular to the applied ac electric field direction.
he colloidal assembly.

Figure 2.10-2 [Schematic illustration of the experimental conditions by I. Dierking *et al.* 2006. *PHYSICAL REVIEW E*, 2006, Volume 73, pp.011702.] (A) Exemplary time series of the collection of microspheres towards a cluster of particles by a collapsing defect loop in the nematic phase at zero applied electric field. (a) $t - t_0 = 6$ s, (b) $t - t_0 = 3$ s, (c) $t - t_0 = 0$ s. The value of $t - t_0$ describes the time to defect annihilation. The displayed image size is 120 ×120 μm^2. (B) Exemplary time series showing the repulsion of particles from a cluster during electric application at amplitude E = 8 $V\mu m^{-1}$ and frequency f = 13 Hz. (a) t = 0 s, (b) t = 2 s, and (c) t = 4 s. The displayed image size is 120 ×120 μm^2.

Figure 2.10-3 [Displacement and Velocity dependence by I. Dierking *et al.*2006. *PHYSICAL REVIEW E*, 2006, Volume 73, pp.011702.] (A-a) Velocity dependence of a single microsphere as a function of applied sinusoidal field amplitude *E*. The particle velocity v increases linearly above a threshold field of $E_{th} = 5\ V\mu m^{-1}$, as depicted for several independent measurement series. (A-b) The frequency dependence of the particle velocity exhibits a maximum and microsphere motion ceases for increasing frequency of the applied electric field. Note that an equivalent behaviour is also observed for other applied wave forms, with the velocity maximum shifted towards higher frequencies for the square wave field. (B-a) Particle displacement L as a function of time for different ionic dopant concentrations. At short times $t < 5$ s, microsphere motion appears to be nonlinear for the doped samples. (B-b) For the linear regime, $t > 5$ s, the particle velocity increases with increasing ionic dopant concentration and approaches saturation at approximately $C_{ion} = 0.4\%$ by weight.

Figure 2.11-1 [I. Dierking, P. Cass, K. Syres, R. Cresswell, and S. Morton, Electromigration of microspheres in ferroelectric smectic liquid crystals. *PHYSICAL REVIEW E, 2007, Volume 76, pp.021707*.] Schematic illustration of the experimental geometry. (a) Side view of the cell where smectic layers are oriented in the "bookshelf-geometry" between two substrates with planar boundary conditions, separated by a distance of 10 μm. Particles of diameter D = 3−4 μm are dispersed within the ferroelectric liquid crystal matrix. Electric fields are applied perpendicular to the substrate plane. (b) Top view of the cell, indicating the two director orientations of the FLC in response to the applied electric ac field. The observed microsphere translation occurs along the smectic layer plane.

Figure 2.11-2 [Exemplary time series of texture photographs during particle translations by I. Dierking *et al. PHYSICAL REVIEW E, 2007, Volume 76, pp.021707*.] The black arrows indicate the position of an isolated *D* = 3μm microsphere. Particle

motion is linear in time and proceeds within the smectic layer plane, which is indicated by the white line in the left part of the figure. Displayed image size is 130 μm×100 μm.

Figure 2.11-3 [The microsphere velocity by I. Dierking *et al. PHYSICAL REVIEW E, 2007, Volume 76, pp.021707.*] (A) Frequency dependence of the microsphere velocity for the D = 4 μm particles. Despite relatively large scattering, the data clearly indicates a (linear) increase of the particle velocity with frequency of the applied electric field. (B) Temperature dependence of the D = 4 μm microsphere velocity at a fixed electric field amplitude of E = 2.8 Vμm^{-1} and frequency f = 205 Hz. The observed increase in microsphere velocity can be attributed to the decrease in liquid crystal viscosity by increasing the temperature.

Figure 2.12 [I. Lazo and O. D. Lavrentovich, "Liquid-crystal-enabled electrophoresis of spheres in a nematic medium with negative dielectric anisotropy". *Philosophical Transactions of the Royal Society A*, 2013, Volume 371, No.1988, pp.20120255.] (A) Scheme of electrophoretic experiment for spheres showing opposite polarities of p_y in an LC with $\Delta\varepsilon < 0$ aligned along $\mathbf{n}_0 = (0, 1, 0)$. (a) Out-of-plane configuration with the electric field $\mathbf{E} = (0, 0, E_z)$. (b) In-plane configuration with the electric field $\mathbf{E} = (E_x, 0, 0)$. The inset shows a polarizing microscope texture of a spherical particle with a hyperbolic hedgehog near its bottom. (B) Electrically controlled levitation of $2a$ = 9.6 μm spherical particles in MLC7026-000. (a) z-Position of microspheres in the bulk as a function of the electric field. Fluorescent confocal polarizing microscopy textures of a vertical cross section of the nematic cell with a colloidal sphere (b) for negative E_z and (c) for positive E_z. The white scale bar corresponds to 5 μm.

Chapter 3

Figure 3.1 The schematic illustration of composition of a sample cell.

Figure 3.2 Schematic of the experimental set up for observation of particles in liquid crystals.

Figure 3.3 Exemplary linear displacement of the particle as a function of time.

Figure 3.4 Exemplary trace of the circular motion of a spherical particle in an applied electric field.

Chapter 4

Crystals. 2. Liquid Crystals Containing a Nonracemic 2,3-Epoxy Alcohol Unit. Journal of American Chemical Society. 1986, Volume 108, 7424-7425]

Figure 4.10 The textures of (S,S,)-EPHDBPE at certain temperatures with particle inclusions. (a) crystalline state of the material. (b) chiral nematic texture with pitch jumps (c) chiral nematic phase with oily streaks. (d) Grandjean planar texture without defects which is the best texture for the experimental work in this chapter.

Figure 4.11 The pitch length of the chiral nematic phase as a function of temperature. The black circles are the experimental value of length. The graph shows a helix inversion temperature around 82.5℃. [Taken from Dierking *et al*., Liquid Crystals, *Investigations of the structure of a cholesteric phase with a temperature induced helix inversion and of the succeeding S_c* phase in thin liquid crystal cells.* 1993, Volume 13, No. 1, pp.45-55.]

Figure 4.12 Schematic diagram of a sample cell with a side view when particle motion is observed at 90.3℃. There are the homogeneous boundary conditions for liquid crystal alignment on the substrates, and a planar boundary condition around the silica particle.

Figure 4.13 The data plot of the square of the critical field versus the square of angular velocity. The straight line shows the fit to equation 4.2 which gives the values of E_{cr} and τ_{MW} indicated in the text. y = ω^2, M0 = E^2, m2 = E_{cr}^2 , m1 = τ_{MW}^2 .

Figure 4.14 The twisting power of the liquid crystal material as a function of temperature. The black circles are experimental values by the Cano-Grandjean method and the white circles are values calculated from the colour change observation. [18] The experimental results are both fit well showing helix inversion as temperature changes. (The negative values indicate a left handed and the positive values indicate a right handed helicoidal structure.) The zero point is where the pitch length is infinite (∞) at the inversion temperature (~ 82.5 ℃) . [Taken from Dierking *et al*., *Investigations of the structure of a cholesteric phase with a temperature induced helix inversion and of the succeeding S_c* phase in thin liquid crystal cells.* Liquid Crystals, 1993, Volume 13, No. 1, pp.45-55.]

Figure 4.15 The schematic diagram of the ample cell with a side view which shows pitch at longer pitch regime (an example at 87℃) and shorter pitch regime at 90.5℃. In a case of 87℃, the helical pitch can be 2π turns far away from the spherical particle, but around the particle the liquid crystal's helical structure cannot be periodic(without

2π truns), while in higher temperature there could be spatial periodicity with 2π turns up and down of the particle inclusion. **L** is cell gap, the substrate is ITO coated glass plate.

Figure 4.16 The data plot of amplitude of electric field versus linear velocity. The straight line shows the fit to an equation $\nu = a(E-E_{cr})$, gives the values of E_{cr} indicated on the figure (~1.4 V/μm). y = ν, M0 = *E*, m2 = E_{cr} .

Figure 4.17 The data plot of amplitude of electric field versus linear velocity. The straight line shows the fit to an equation $\nu = a(E-E_{cr}) + b(E-E_{cr})^3$, gives the values of E_c indicated on the figure (~0.4 V/μm). y = ν, M0 = *E*, m2 = E_{cr} .

Chapter 5

Figure 5.1 The stability regime of the motions of the silica spheres in the isotropic phase at 110℃. Three types of motions, random motion – circular motion – no motion are observed. The black squares are showing the boundary of 'Random motion' (chaotic flying) regime and 'No motion' (no movement) regime as the amplitude and frequency of the applied electric field were varied. The red circles represent the regions of electric field induced 'Circular motion' (circle shaped motions) of the particles.

Figure 5.2 An exemplary circular trajectory of the micron-sized silica sphere at 110.0 ℃. The applied electric field has a value of $E = 4.6\ V\mu m^{-1}$ and f = 160 Hz.

Figure 5.3 The angular velocity of the micron-sized silica sphere as a function of frequency of the applied electric field. The applied electric field is $E = 5\ V\mu m^{-1}$.

Figure 5.4 The angular velocity of the micron-sized silica sphere as a function of the applied electric field. The frequency f = 160 Hz.

Figure 5.5 The diameter of a circular motion of the micron-sized silica sphere as a function of frequency of the electric field applied. The applied electric field is $E = 5\ V\mu m^{-1}$.

Figure 5.6 The diameter of a circular motion of the micron-sized silica sphere as a function of electric field applied to the system. The frequency f = 160 Hz.

Figure 5.7 The data plot of square of critical field versus square of angular frequency. The straight line shows the fit to equation 5.2 which gives the values of E_{cr} and τ_{MW} indicated on the figure.

Figure 5.8 Schematic diagram of the confinement of a spherical particle in an isotropic liquid crystal phase. When electric field applied across the cell depth, a stable Quincke rotation is available as the condition $\varepsilon_s/\sigma_s > \varepsilon_l/\sigma_l$ is given by this system.

Chapter 6

Figure 6.1 A schematic diagram of homogeneous boundary conditions in a calamitic liquid crystal material in an arbitrary cell gap (a side view). The elongated particle's geometry can be observed as lying particles (**LP**) or standing particles (**SP**), each with positional distributions between the two substrates (it is not possible to detect the angles of 3 dimensional positions).

Figure 6.2 The stability regime of the motions of the elongated particles in a nematic phase with homogeneous boundary conditions, and a negative dielectric anisotropy liquid crystal material.

Figure 6.3 (a) A lying particle in the liquid crystal material in the cell showing a difference of angle between the director and the particle's long axis; the white double arrow line is the director and the yellow line is the particle's long axis. (b) The linear velocity of the elongated silica particle as a function of angular difference between the long axis of the particle and director alignment along the rubbing direction of the cell. The observation is at f = 50 Hz and E = 10 Vμm^{-1}. The diameter of the particle is 1.5 μm and length is 8.33 μm.

Figure 6.4 The linear velocity of the elongated silica particle as a function of particle's length scale. The applied electric field is f = 10 Hz and E = 10 Vμm^{-1}. The length is 5 μm ~ 10 μm.

Figure 6.5 A stability regime of the motions of the elongated particles in a nematic phase. With homogeneous boundary conditions and a positive dielectric anisotropy liquid crystal material. The Fréedericksz threshold is at 2.6 Vμm^{-1}.

Figure 6.6 An exemplary photograph showing the length distribution of the moving

particles (in a state of LP) in the sample cell. The linear velocity of the elongated silica particle as a function of particle's length scale could be measured in this texture with the motion of different particles. The moving directions have no dependency with respect to the director.

Figure 6.7 The linear velocity of the elongated silica particle as a function of particle's length scale 3 μm ~ 12 μm at f = 8 Hz and E = 1.5 Vμm^{-1} in homogeneous boundary condition with positive dielectric anisotropic nematic liquid crystal.

Figure 6.8 The schematic diagram of homeotropic boundary condition of calamitic liquid crystal material in an arbitrary cell gap (a side view). Elongated particle's geometry is observed lying particles (**LP**) and standing particles (**SP**) with the position distributions (not possible to detect the angles of 3-dimensional positions) between the two substrates.

Figure 6.9 A stability regime of the motions of the elongated particles in a negative dielectric anisotropy nematic phase with homeotropic boundary conditions. The threshold for defect formation in this geometry is 0.6 Vμm^{-1}.

Figure 6.10-1 A negative dielectric liquid crystal phase with homeotropic boundary conditions including an elongated particle. (a) initial state (HT) at 1*t*. The liquid crystal director and the particle are all perpendicular to the substrates. (b) after applying an electric field, (the threshold field is 0.6 V μm^{-1}) the texture changes and topological defects appears. At 87*t*, the particle is at the interface between the defect domains. (c) Just before the transition to the point defects in the texture at 96*t*.

Figure 6.10-2 A negative dielectric liquid crystal phase with homeotropic boundary conditions including an elongated particle. (a) the particle is kept in the interface during stabilizing the topological defect at 108*t*. (b) around the particle, there are still a fluctuations of the defects exists at 141*t*. (c) the particle is standing in the middle of the point defect and starts to exhibit circular motion holding the centre of the defect at 469*t*.

Figure 6.10-3 A negative dielectric liquid crystal phase with homeotropic boundary conditions including an elongated particle. The particle combined with a defect and shows a 360º circular motion with the clockwise movement from the view. The pictures from (a) at 1580*t* to (d) at 1641*t*.

Figure 6.10-4 A negative dielectric liquid crystal phase with homeotropic boundary conditions including an elongated particle. From (a) at 7641*t* ~ (e) at 7741*t*, the defects become smaller and disappear, the particle shows a displacement along the edge of the defect and is propelled away when the defects disappear by annihilation.

Figure 6.11-1 The angular velocity of the elongated silica particle as a function of the applied electric field. The frequency f = 800 Hz. (HT, $\Delta\varepsilon < 0$, Standing particles).

Figure 6.11-2 The diameter of a circular motion of the elongated particle as a function of amplitude of the applied electric field. The frequency of the field is f = 800 Hz. (HT, $\Delta\varepsilon < 0$, Standing particles).

Figure 6.12 A stability regime of the motions of the elongated particles in a positive dielectric anisotropy nematic phase with homeotropic boundary conditions.

Figure 6.13 The angular velocity of the elongated particles in the nematic liquid crystal phase, the velocity is shown as a function of amplitude of the electric field. The standing particle's circular motion becomes faster as the amplitude of the field is higher. (HT, $\Delta\varepsilon > 0$, f = 400Hz).

Figure 6.14 A linear fit to the graph that describes the diameter of the circular motion with respect to the applied electric field (from Figure 6.11-2).

Figure 6.15 A square law dependence fitted to the data of figure 6.11-2.

Figure 6.16 The relationship between the square of the angular velocity and the square of the applied electric field for the circular motion of elongated particles coupled with defects. The fit describes a Quincke-type rotation.

Figure 6.17-(a) and (b) Linear and cubic fits applied to the dependence of the angular velocity to the applied electric field for the circular motion of the elongated particles coupled with defect motion.

List of Tables

List of Symbols

Chapter 1

$\mathbb{T}, \mathbb{T}'$	terminal groups of liquid crystal structure
$\mathbb{R}, \mathbb{R}'$	ring groups of liquid crystal structure
$\mathbb{I}$	linking group of liquid crystal structure
$\mathbb{L}, \mathbb{L}'$	lateral group of liquid crystal structure
Δc	variation of the concentration
ΔT	variation of the temperature
$\mathbf{n}$	director
S	order parameter
Θ	individual angle between the long molecular axis and the director
P	pitch length of chiral nematic liquid crystal phase
N	nematic liquid crystal phase
N*	chiral nematic liquid crystal phase
ε	dielectric permittivity
ε_e	extraordinary dielectric permittivity
ε_o	ordinary dielectric permittivity
$\Delta\varepsilon$	dielectric anisotropy

$\varepsilon_{\parallel}$	parallel dielectric permittivity
$\varepsilon_{\perp}$	perpendicular dielectric permittivity
n	refractive index
n_e	extraordinary refractive index
n_o	ordinary refractive index
Δn	birefringence
$n_{\parallel}$	parallel refractive index
$n_{\perp}$	perpendicular refractive index
δ	phase difference of propagation of light
κ	wave number
λ	wavelength
d	distance of wave travels
m	integer
I	transmitted intensity of light
I_0	incident light intensity is after polarizer
φ	azimuthal angle
θ	the angle between optic axis and propagation direction of the light wave
s	topological defect

Chapter 2

k	Boltzmann's constant
T	absolute temperature
ΔG	total free energy of the colloidal system
E_D	energy of the droplet-defect dipole
R	separation (distance between the defect and the droplet centre)
K	elastic constant
A	a number of order unity
a	the diameter of the dispersed particle
R_0	equilibrium separation (distance between the defect and the droplet centre)
Q	topological charge
$U_{\alpha\beta}$	dipole-dipole potential of defect α and defect β
p_α^z	dipole moment of defect α along the z axis
p_β^z	dipole moment of defect β along the z axis
n	director
λ	wavelength
Γ	torque
η	viscosity of the liquid
a	diameter of the spherical droplet
ω	angular velocity of the rotating droplet

$\hbar$ reduced Planck constant (or Dirac constant)

P irradiation power

E amplitude of applied electric field

f frequency of the applied electric field

v velocity of a silica particle

L displacement of silica particle

t time dimension

C_{ion} ionic dopant concentration

LC liquid crystal

D silica particle's diameter

FLC ferroelectric liquid crystals

p polarity

$\Delta\varepsilon$ dielectric anisotropy

Chapter 3 ~ Chapter 7

P helical pitch length

n director

(S,S,)-EPHDBPE 4-[(S,S)-2,3-epoxyhexyloxy]-phenyl-4-(decy1oxy)-benzoate

C crystalline solid state

S_1	smectic phase
S_c*	chiral smectic phase
N*	chiral nematic phase
I	isotropic liquid state
PhI	phase inversion
Un	unstable planar texture
ω	angular velocity
τ_{MW}	Maxwell-Wagner interfacial polarization relaxation time
E	applied electric field
E_{cr}	critical field
f_{max}	maximum frequency
τ_{DEL}	delay time
r	radius of the particle
D	ion diffusion coefficient
D_{iso}	ion diffusion coefficient in isotropic phase
T	absolute temperature
L	cell gap
ν	linear velocity
$T_{\mathrm{Iso\text{-}N^*}}$	transition temperature of the material from chiral nematic liquid crystal to isotropic phase
η	viscosity of fluid

σ_{lc} conductivity of liquid crystal

σ_s conductivity of spherical particle

ε_0 dielectric permittivity of vacuum

ε_{lc} dielectric permittivity of liquid crystal

ε_s dielectric permittivity of spherical particle

Chapter 1
Introduction to Liquid Crystal Physics

Liquid crystals are a series of phases of matter which possess properties between solids and liquids. The properties of these phases include the exhibition of optical anisotropy (except a blue phase) associated with some crystals and fluidity of a liquid. Since these material have properties in between those of a solid and a liquid, a liquid crystal phase is also called a mesophase and liquid crystal materials are termed mesogens. A mesogen which has temperature dependence in the formation of phases is named a 'thermotropic liquid crystal'. If the formation of a liquid crystal phase is controlled by dissolution of amphiphilic molecules in solvent, the mesophase is called a 'lyotropic liquid crystal'. One of the historic examples of lyotropic liquid crystal is myelin in water which exhibited birefringence, reported in a microscopic study in 1854. [1] The observation of the mesophases formed by cholesteryl benzoate and cholesteryl acetate was performed in 1888 and invoked the interest of scientists in research on thermotropic liquid crystals. These two categories are the main classes of liquid crystals. [2]

In 1956, Flory's work calculated that ratio between the principal axes of the mesophase's molecule is bigger than 4, and the mesophase was only appeared for non-spherical molecules, and the typical dimensions of liquid crystal molecules are 20 ~ 40 Å (for the long axis) and 4 ~ 5 Å (for the short axis). [3]

The introduction section of this thesis starts with the fundamental structure scheme, alignments and anisotropic physical properties of thermotropic liquid crystals,

together with a description of a useful tool for the observation of the liquid crystal phases, polarizing microscopy.

1.1 Liquid Crystal Molecular Structure

Liquid crystal molecules usually have two parts to their structure, the rigid core and the flexible functional groups. Typically, the core structure is composed of phenyl or biphenyl groups and the flexible end groups incorporate alkyl or alkoxy chains. The overall structure of each group for different molecules is related to the types of structure assigned as either calamitic (rod-like) or discotic mesogens (disc-like). [4]

The thermotropic liquid crystal phases this thesis deals with can be differentiated by molecular shape into three categories. Figure 1.1 shows a calamitic liquid crystal with a rod-like shape, a discotic liquid crystal which has disk-like molecular shape and a sanidic liquid crystal with the shape of molecule like bricks. [5]

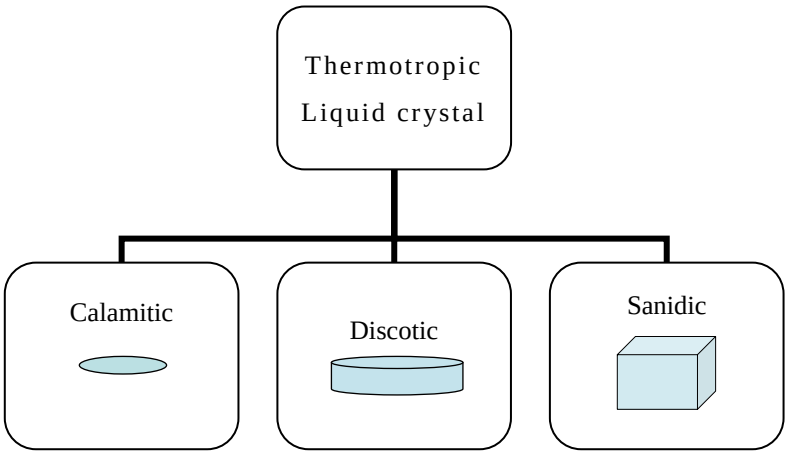

Figure 1.1 A schematic diagram of three types of thermotropic liquid crystals defined by their molecular shapes.

This thesis is concerned with calamitic liquid crystals. Table 1.1 is a brief introduction to some of the structural systems included in calamitic liquid crystals. [6]

Typical molecular structure	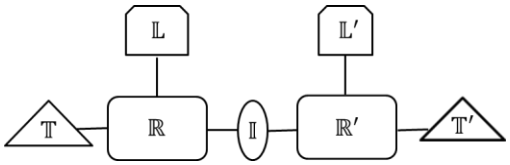			
The components	$\mathbb{T}$, $\mathbb{T}'$ *Terminal group*	$\mathbb{R}$, $\mathbb{R}'$ *Ring group*	$\mathbb{I}$ *Linking group*	$\mathbb{L}$, $\mathbb{L}'$ *Lateral substituents*
Function names	n- Alkyl chains branched Alkyl chain Alkenyl chain Alkoxy group	biphenyl terphenyl diphenylethane stilbene tolane Schiffs base Azobenzene Azoxybenzene Phenyl benzoate Phenyl thiobenzoate	-CH=CH- $-CH_2O-$ -N=N- $-OCH_2CH_2O-$ -COO- -N=N-O $-CH_2CH_2-$ -CH=N- -CH=N-N=CH- $-(CH_2CH_2)_2-$	H F Cl Br CN NO_2

Table 1.1 Chemical groups which compose liquid crystal structure. [6]

1.2 Liquid Crystal Phases

A brief introduction to the phases formed by liquid crystals is shown in Figure 1.2, with the image representing one or more liquid crystal mesophases formed by liquid crystal molecules.

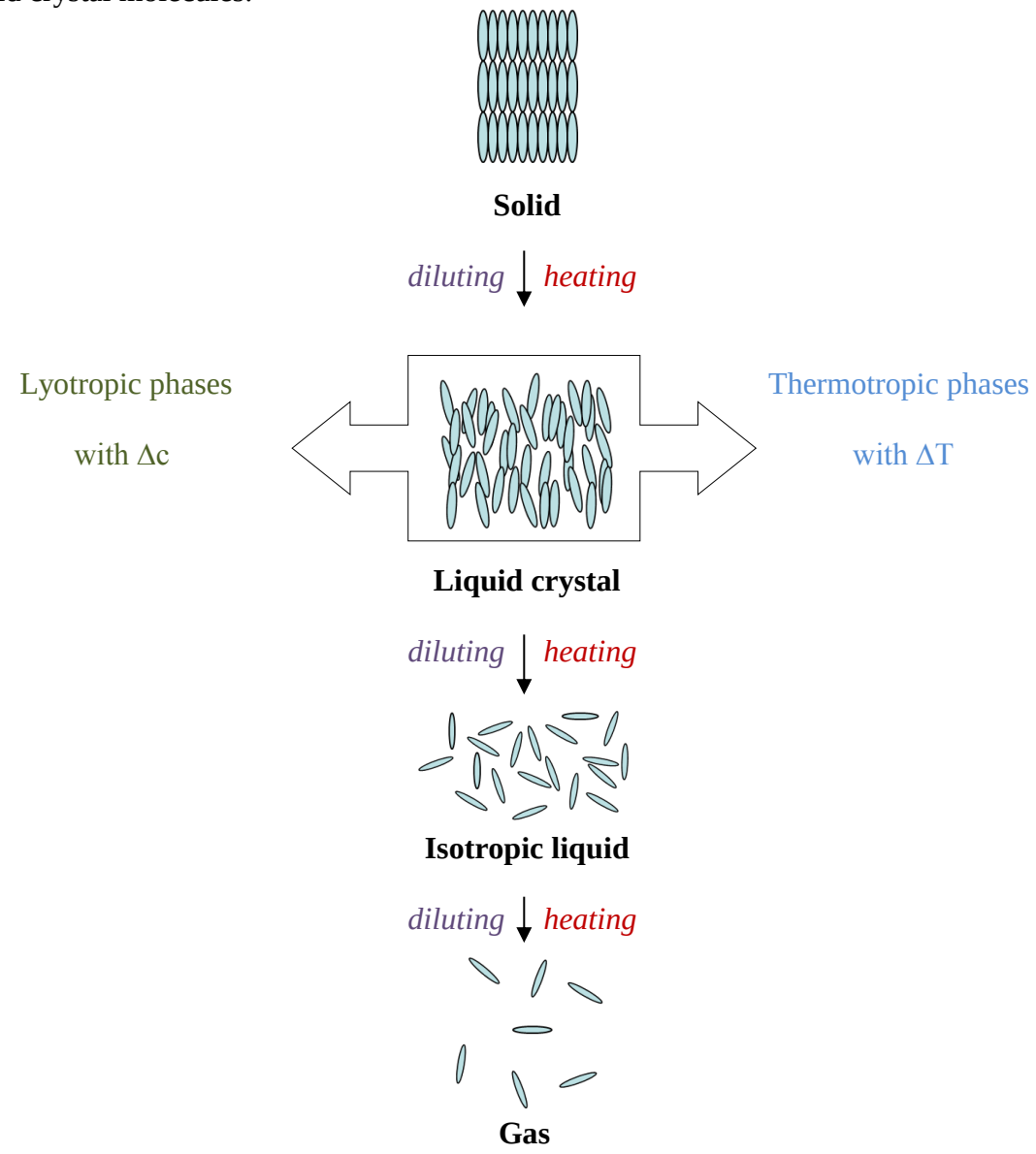

Figure 1.2 The scheme of states of matter. T is the temperature of the system and c is the concentration.

The gas and isotropic liquid phase do not have any order, but as the temperature reduces, the material may experience a phase transition to the nematic phase or smectic phases, which both possess orientational order characterised by a director **n** defining the average direction of an ensemble of molecules. The smectic phases also have some degree of positional order and hexatic smectics with higher ordered phases have bond orientational order. Ordering of anisotropic material which has not a spherical shape can be explained using the three types of orders, which are orientational order, positional order, and bond orientational order. [7]

The anisotropy of the state can be expressed by the director (**n**) and an order parameter (*S*). The unit vector describing the average direction of liquid crystal molecules is the director, **n**. The order parameter can be measured by calculating the difference of each molecular axis from the average direction of the molecules. [8] Liquid crystal has different order in different phases, which means the order of different liquid crystals phases are not the same. Liquid crystals have electrical anisotropy, diamagnetic anisotropy and birefringence is observed due to optical anisotropy. In addition, elastic deformation can occur due to the anisotropic elastic properties of the system, viscosity from flow anisotropy; different parameter values depend on the direction of the measurement because the properties are different parallel and perpendicular to the director. The simplest phases, the nematic and chiral nematic phases are introduced in section 1.2.1 and 1.2.2 as these phases form the basis of the experimental work presented in this thesis. The methods used for making the director orientation uniform in-between two glass substrates and the realignment of the bulk structure will also be illustrated in the following sections.

1.2.1 Nematic Phase

The nematic phase has the simplest structure of the liquid crystal phases, with the molecules oriented along an average direction called the director. The name of 'nematic' came from the Greek word meaning '*thread*' after the observing textures of lines from a nematic liquid crystal sample using a polarizing microscope. The director is abbreviated as **n**, and the schematic illustration in Figure 1.3 (a) shows **n** is using an arrow. The individual angles made by each molecule are shown in Figure 1.3 (b); the distribution of angles defines the orientational order of the phase. The states of **n** and -**n** of the director are indistinguishable as the nematic phase has symmetry operation and do not have polarity. The nematic phase is consists of molecules with long-range orientational order and no positional order of the centre of masses. [8]

For the simplest liquid crystal phase, a calamitic nematic liquid crystal structure, we can model the system as cylindrical molecules, we often use a Hermitian orientational order parameter as a scalar order parameter. It can be used to describe the phase transition from an isotropic liquid to the nematic liquid crystal phase. [9]

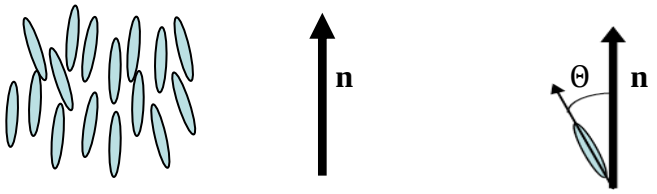

(a) (b)

Figure 1.3 (a) A schematic illustration of the structure of the nematic phase. The liquid crystal is a calamitic type and the director **n** is the average direction of the molecules. (b) The individual angle, Θ, between the long molecular axis and the director is shown.

The order parameter will be introduced in this chapter for the use as a description of the physical property of the nematic crystals in section 1.4.1.

1.2.2 Chiral Nematic Phase

The chiral nematic phase exhibits chirality, the name 'chiral' has originated from the Greek word '*hand*' as hand has been a representative example of chiral objects which do not have mirror symmetry. The chiral nematic phase was the first liquid crystal phase to be studied and is historically also called the cholesteric phase, named after the cholesteryl derivatives investigated by Reinitzer. [2] Chirality in nature was firstly noticed by Pasteur in 1848 when he was observing salts of tartaric acid; their solutions showed optical activity which rotated the plane of the linearly polarized light clockwise for one 'handedness' and for the other the rotation of the plane was counter clockwise. [10] Lord Kelvin coined the word 'chirality' and a concept of the asymmetrical tetrahedral carbon atom was introduced by Le bel and van't Hoff in 1874. [11-13]

Chiral molecules give rise to a helical structure of the liquid crystal phase; a chiral nematic phase forms a helical structure with a pitch length **P**, which is a 2π radian rotation of the director **n** (a full rotation), and **P/2** becomes the periodicity due to the equivalence of **n** and –**n.** The pitch is temperature dependent, as the director varies more with higher thermal energy and this dependence introduces a shorter pitch in the higher temperature as a result. The bulk chiral nematic liquid crystal phase shows a brilliant colour effect even when we watch with our naked eyes, this colour

effect comes from Bragg reflection, the selective reflection of circularly polarized light appears when the pitch of the helical structure is of the same order as the wave length of visible light. [14] The liquid crystal molecules are located (on average) along the director fields and a rotation of the directors can be seen along the helix in Figure 1.4.

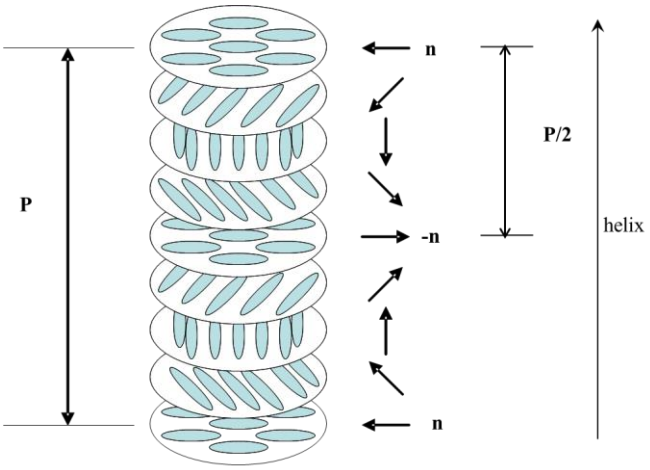

Figure 1.4 Schematic representation of the chiral nematic liquid crystal phase structure with pitch length **P** (2π rotation) and periodicity **P/2**. (**n** = -**n**) The asymmetric molecules cause gradual rotation of the director, describing the helix.

1.3 Alignment of Liquid Crystals

For the investigation and observation of a liquid crystal material, the first research step is choosing the liquid crystal phase to use and the next step is aligning the liquid crystal phase in-between the supporting substrates (normally glass). The glass substrates can have a weak or strong interaction with the liquid crystal directors and a certain angle of tilting can occur at the surface (known as pretilt). Thus, the

phase of liquid crystal and the surface treatment of the glass substrates cause a specific alignment of the liquid crystals between two glass plates.

In 1911, alignment of liquid crystals was first performed through orientation on a solid phase by Mauguin. [15] Surface alignment methods were investigated in detail from the 1970's, because of the importance of their applications in display area. Surface treatment methods of the substrates have been developed using chemical materials, handling process of the chemicals, applying physical force, and using a radiation source (UV) to accomplish certain anchoring conditions. [16] Such methods are important for both the industrial application and for scientific observations using optical equipment (microscopy).

The following section is going to introduce a few of examples of the surface treatment methods and two major geometries of the calamitic liquid crystals at the interface of the sample cell.

1.3.1 Homeotropic Alignment

One of the common vertical alignment methods is using surfactant as a chemical agent for the surface treatment. The treatment of the glass substrates with amphiphilic molecules dissolved in an organic solvent followed by the evaporation of the organic solvent from the substrates causes deposition of the surfactant molecule on the substrates. The surfactant thin film can be a monolayer or multilayer film depending upon the technique used. [17-18] Homeotropic alignment is the structure as shown in Figure 1.5. When the view is from the side of the liquid crystal cell, the

cell contains the nematic liquid crystal director which is oriented perpendicular to the glass substrates.

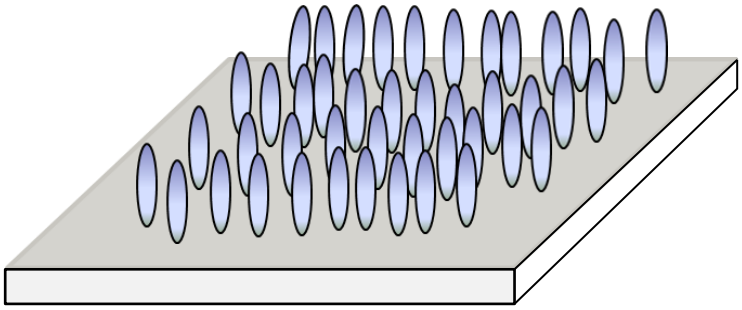

Figure 1.5 An illustration of the homeotropic alignment structure. This liquid crystal sample cell shows schematically the calamitic nematic liquid crystal phase in-between glass plates. (A lower glass substrate is shown here.) The director of the liquid crystal is perpendicular to the two glass substrates.

1.3.2 Homogeneous Alignment

Liquid crystals can also be aligned planar to the glass substrates, which means the director of the liquid crystal is parallel to the surface of the substrates. Surface treatment methods have been developed using different kind of chemicals such as polyimide or nylon, and evaporation processes, rubbing techniques and temperature control. The microscopic grooves on the surface of the substrates caused by rubbing can play an important role in the interaction of the thin film of the surface and the liquid crystal which is to be aligned on it. [19-20] Indeed, the microscopic alignment mechanism of a layer with polymer chains that has been rubbed by fibers can include

the formation of characteristic periodicities (grooves) and the alignment which can tend to align the polymer chains can rely on the combination of unidirectional grooves and rubbing. The rubbing process induces an interaction between the liquid crystal director and oriented polymer chains on the surface. The strength of the alignment is controlled by regulating the rotation frequency of the rubbing mechanism, with the number of rubbing cycles, pressure, unidirectional motion used optimised to owe the best surface to form the preferred uniform liquid crystal unidirectional alignment. Figure 1.6 is a schematic view from the side of a device, illustrating the homogeneous alignment of nematic liquid crystals. As we can vary the distance between the substrates, the extent of the planar alignment can be varied, typically to distances of ~50 μm.

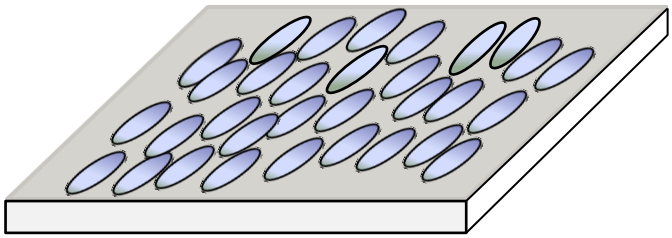

Figure 1.6 Schematic illustration of the structure of homogeneous liquid crystal alignment in between two glass substrates. (A lower substrate is shown here.)

1.4 Physical Properties of Liquid Crystal Materials

Liquid crystals are partially ordered fluids, as has been mentioned previously. This state of matter is different from solids and isotropic liquids, as the liquid crystal

phases can be differentiated by the relevant order parameter. Liquid crystal molecules have an anisotropic electron density within the structure which can result in a dipole moment and cause anisotropic polarizability. Characteristic interactions with light and electric fields occur and the anisotropic properties make possible various applications of the liquid crystals. Some of the physical properties of liquid crystals are described below.

1.4.1 Order in Liquid Crystals

The way we can describe the state of a liquid crystal is in terms of three different parameters. They are positional order, orientational order and bond orientational order (which is associated with smectic phase). The positional order is critical to characterise the types of liquid crystal state, and it can be deduced by looking at the liquid crystal's texture (when observed using a polarizing microscope) and measured from X-ray diffraction patterns which can determine the smectic layer thickness and larger correlations. The bond orientational order is the measurement of the extent which the core structure and functional groups within the liquid crystal molecule are ordered, measured by using nuclear magnetic resonance techniques to investigate relative orientation of the molecular constituents caused by short-range intermolecular and intermolecular forces. [7] However, for the practical applications of liquid crystals, the most important parameter is orientational order parameter *S*. [8]

The director is the average direction of the orientation of the molecules of the liquid crystal sample. Orientational order in nematic phase is described by the order parameter S

$$S = \frac{1}{2}\langle 3\cos^2\Theta - 1\rangle \quad , \tag{1.1}$$

where the brackets denote the statistical average of all the molecules in the sample, and Θ is the angle between the director and the long molecular axis of an individual molecule as shown in Figure 1.3. In Equation 1.1, S is a temperature dependent function as the thermal average is taken over an ensemble of molecules. If no orientational order exists in the material, such as in the isotropic phase, the order parameter will be zero. On the other hand, with a perfect crystal the order parameter would be equal to 1. The experimentally found values of S are ~ 0.3 at nematic-isotropic transition, and upon cooling the order parameter becomes around $S \approx 0.6$. [4-5]

1.4.2 Anisotropic Physical Properties

The anisotropic physical properties of liquid crystals give rise to anisotropy in the following physical properties: refractive index (birefringence), dielectric constant, magnetic susceptibility, electric conductivity, modulus of elasticity, coefficient of viscosity. These anisotropic properties give rise to many factors which have been critically useful for industrial application.

In this section, we provide an introduction to two major anisotropy related properties, which is the electric permittivity and polarizability of the liquid crystal molecules.

1.4.2.1 Dielectric Anisotropy

The structural shape of a liquid crystal molecule causes the electrical anisotropy property in the material. Due to the anisotropy of the liquid crystal molecule, a permanent dipole results from asymmetrical charge distribution within the liquid crystal molecule under an applied electric field, or without an applied field. The permanent dipoles arise from covalent bonds from atoms of different electronegativity which have an unbalanced distribution of charge, and the liquid crystal molecule containing a permanent dipole might or might not be polar depending on the symmetry of the dipoles within the main core structure or functional group. Induced dipoles are caused by the distortion of the electron cloud when an electric field is applied, as electrons are shared by atoms with similar electronegativity and become redistributed by the field.

The permittivity of a positive dielectric liquid crystal, parallel to the director, is usually observed when an electric field is applied approximately along the long axes of the liquid crystal molecules, and permittivity perpendicular to the direction results from the application of an electric field applied perpendicular to the director. The anisotropic shape of liquid crystal molecules and their anisotropic distribution in the nematic phase gives rise to the difference between the parallel dielectric permittivity $\varepsilon_{\parallel}$

and perpendicular dielectric permittivity $\varepsilon_{\perp}$ and is defined as the dielectric anisotropy $\Delta\varepsilon$

$$\Delta\varepsilon = \varepsilon_{\parallel} - \varepsilon_{\perp} \quad , \tag{1.2}$$

the dielectric anisotropy is dimensionless, and can have two kinds of values. A positive dielectric anisotropy acts to reorient the director along the direction of the applied electric field. On the other hand, a negative dielectric anisotropy material would align perpendicular to an applied electric field. [21]

The relative contributions of the permanent and induced dipoles to the dielectric properties of a liquid crystal are frequency dependent. For example, Phenylbenzoates (a long two ringed molecule with high barriers to rotation of the molecule around the short axes) forms a nematic phase and the sign of $\Delta\varepsilon$ changes at a certain frequency, named a dielectric sign inversion frequency, with the relaxation of $\varepsilon_{\parallel}$ observed with a negative slope as a function of frequency. [22]

1.4.2.2 Optical Anisotropy

When we look at the simplest liquid crystal phase which is the nematic liquid crystal in a glass beaker or flask, it appears like a milky translucent fluid. The structure of a nematic liquid crystal material leads to optical anisotropy in the material itself, and the random orientation of domains in the bulk material causes discontinuities in refractive indices, leading to the observation of the scattering when unaligned in a beaker or flask.

In the simplest liquid crystal system, which is a case of a uniform alignment of the director for a uniaxial liquid crystal material, the refractive index anisotropy can be observed as two different indices. As a light wave passes polarized parallel to the director of the liquid crystal, it experiences a different refractive index compared to light wave polarized perpendicular to the director of the liquid crystal. Due to the differences in refractive indices parallel and perpendicular to nematic liquid crystal direction in the uniform alignment, these materials are termed as birefringent.

The two refractive indices can be further explained by considering the refractive index indicatrix. For the explanation, an optical indicatrix is shown in Figure 1.7. [23]

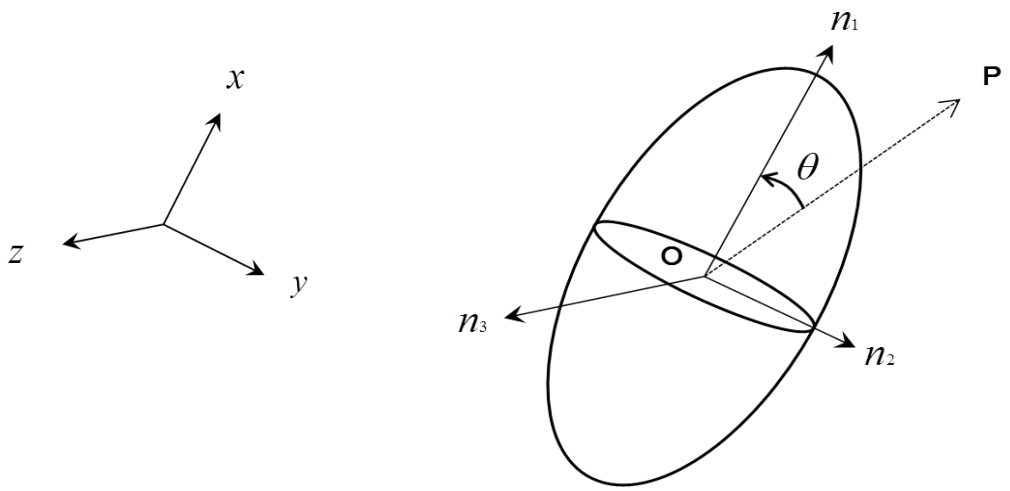

Figure 1.7 A uniaxial ellipsoid illustrating the anisotropic nature of liquid crystal refractive indices, where OP is a light ray and n_1, n_2, n_3 are the principal refractive indices. The directions *x, y, z* are the principal axes of the electric permittivity tensor.

This ellipsoid is defined by the equation (With the terms defined in Figure 1.7.)

$$\frac{x^2}{n_1^2}+\frac{y^2}{n_2^2}+\frac{z^2}{n_3^2}=1\ . \tag{1.3}$$

In uniaxial liquid crystal along the *x*-axis, there is rotational symmetry which leads to $n_2 = n_3$, which commonly defined as n_o

$$n_o = n_2 = n_3\ , \tag{1.4}$$

the equation 1.4 defines ordinary refractive index, and equation 1.5 represents the extraordinary refractive index for a ray direction θ

$$n_e(\theta)^2 = \left(\frac{cos^2\,\theta}{n_1^2}+\frac{sin^2\,\theta}{n_3^2}\right)^{-1}. \tag{1.5}$$

The light ray along OP experiences two different refractive indices which represent the semi-axes of the ellipsoid perpendicular to OP as given by the above equations depending on polarization.

The ordinary index of refraction, n_o, fits well with Snell's law of refraction. The birefringence of a nematic liquid crystal is defined by the difference between n_e and n_o, $\Delta n = n_e - n_o$. The ordinary refractive index, $n_{o,}$ is observed for a linearly polarized light wave where the electric field vector vibrates perpendicular to the director (i.e. light travelling along the director). The extraordinary refractive index, n_e, is observed for a light wave where the electric field vector is parallel to the director. In

the birefringent system, described in Figure 1.7, n_1 is defined as n_e, and n_2 and n_3 are considered to be n_o. The optic axis is the direction of travel along which light experiences n_e, and is parallel to the director in an optically positive material. On the other hand, the optic axis is perpendicular to the director in an optically negative material. If n_2 and n_3 are larger than n_1, the material is optically negative, and if n_1 is larger than n_2 and n_3, the material is optically positive. Thus, optically positive birefringent materials have larger refractive index parallel to optic axis and $\Delta n > 0$, while an optically negative birefringent material has a larger refractive index perpendicular to the optic axis and its birefringence is negative. Figure 1.8 shows optically positive and negative indicatrix.

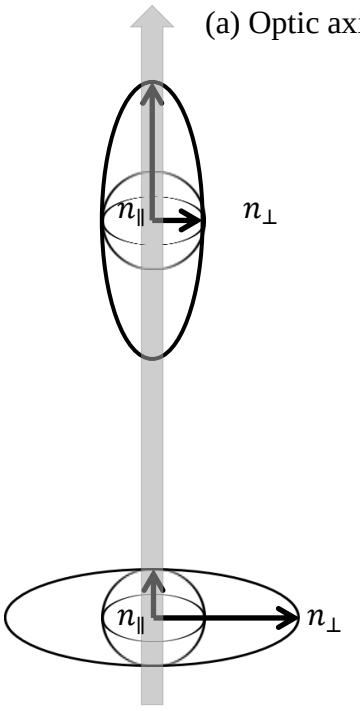

(b) Optically positive indicatrix ($n_\parallel > n_\perp$)
e.g. N phase, calamitic phase

(c) Optically negative indicatrix ($n_\parallel < n_\perp$)
e.g. N*phase, discotic phase

Figure 1.8 A uniaxial indicatrix with refractive indices $n_\parallel$, $n_\perp$. (a) is optic axis, (b) is optically positive indicatrix, (c) is optically negative indicatrix.

1.5 Introduction to Polarizing Microscopy

The polarizing microscopy is a widely used technique for observing the liquid crystal sample and allowing visualisation of its textures (the image formed through crossed polarizers) which allows identification of the phase and the determination of other properties such as alignment quality. This chapter introduces the function of the polarizing microscope when it deals with liquid crystal sample cells and several textures will be introduced as an exemplary investigations resulting from using the polarizing microscopy techniques for the liquid crystal mesogens.

1.5.1 Applications of Polarizing Microscopy

The principle use of polarizing microscopy is for observing birefringence in samples. This type of microscopy was developed for mineralogy and polarizing microscopy can distinguish between an isotropic material and an anisotropic material using two polarizers. [24-25] Polarizing microscopy can be combined with a temperature controller for heating and cooling the liquid crystal sample cell and also it is useful to do characterisation of newly synthesized mesogens. Polarizing microscopy can make a uniquely detailed visualisation of the samples compared with our naked eyes or a regular microscope. When polarizing microscope is coupled with differential scanning calorimetry and X-ray investigations, the device can be used for determination of phase transition temperatures, order of the transitions, and the actual structure of phase types. Also the polarizing microscope can be equipped with electro-

optics and mounted photodiodes to measure parameters such as tilt angle and threshold voltage. [26] This thesis focuses on observing micron-sized particles moving in a liquid crystal medium under the influence of an electric field applied by a using a function generator equipped with amplifier. Temperature is controlled using a temperature controller and this additional apparatus is connected to the stage holding the liquid crystal sample cell. The following section is going to introduce the interactions of light with liquid crystals, so that the observation of the textures of liquid crystal phases can be basically understood.

1.5.2 Schematic Structure of Polarizing Microscope

The polarizing microscope has two separate polarizers, the first one is for polarizing the incoming light source and the other one for polarizing the light that has passed through a sample on the stage. Figure 1.9 is the schematic diagram of polarizing microscope equipment with a side view.

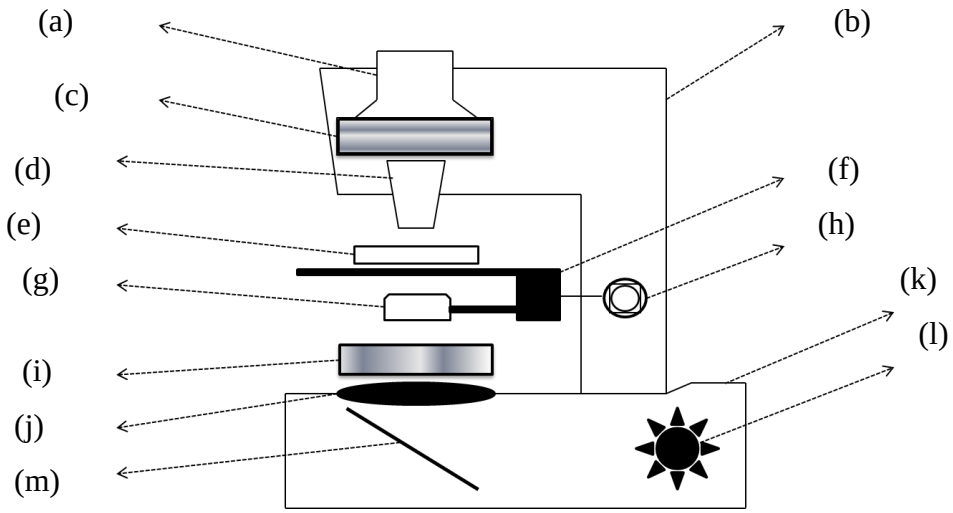

Figure 1.9 The schematic diagram of a polarizing microscope with crossed polarizers.

(a) ocular (b) upper body of the microscope (c) analyser (d) objective has low, medium and high magnifications (e) sample (f) stage is usually rotatable (g) condenser collects light and illuminates the sample uniformly (h) focus is a dial-button to regulate the height of the stage for focusing light onto sample (i) polarizer (j) lens (k) lower body of the microscope (l) light source (m) mirror reflects the light source.

The second polarizer is named as the analyser of the microscope and it is usually crossed (set up at 90°) with respect to the first polarizer, thus for an empty stage there is no light passing through between the polarizer and analyser when crossed. For observing the birefringence of liquid crystals, the sample is normally contained between two glass plates held a few micrometers apart and filled with the liquid crystal material. Light which has passed through a polarizer will reach the liquid crystal cell on the stage and the light experiences two different indices depending upon the polarization of light with respect to the director. Each parameter is related to the birefringence of the liquid crystal, and light will experience the extraordinary refractive index n_e , or the ordinary refractive index n_o depending upon the polarization of light. The light exiting through the sample can be linear, circular or elliptical polarized depending upon the phase shift between ordinary light ray and extraordinary light ray. [27]

1.5.3 Polarization of Light

A polarizing microscope has two polarizers, one is located below the sample and the other is above the sample. The light source emits white light as incident light;

the wave oscillates randomly in all directions and so is unpolarized. The incident light passes through the first polarizer in the first instance, and after this step the light wave is turned into a linearly polarized beam.

The critical first step of the polarization is performed commonly with a polarizing filter; a polarizer made of polymer molecules and plastic sheet. The filter was invented by Land in 1928 and registered the upgraded version of the filter as Polaroid to United States patent office. [28] On the plastic sheet the polymer molecules are located parallel to each other, with the long organic molecules can make a polymer grid. Unpolarized light wave travels through the polarizer, the electric field which is oscillating with the same direction of the polymer grid induces the conduction of electrons up and down the molecule. The electrons absorb energy from the light wave and subsequently the parallel component of the electric wave function is absorbed in the polarizer. On the other hand, the conduction electrons of the polymer molecules cannot move perpendicularly, so the perpendicular component of the electric wave function can pass out without significant absorption. The polarizer's axis is the polarization direction transmitted by the polarizer, with Figure 1.10 shows the diagram of a polarizing filter.

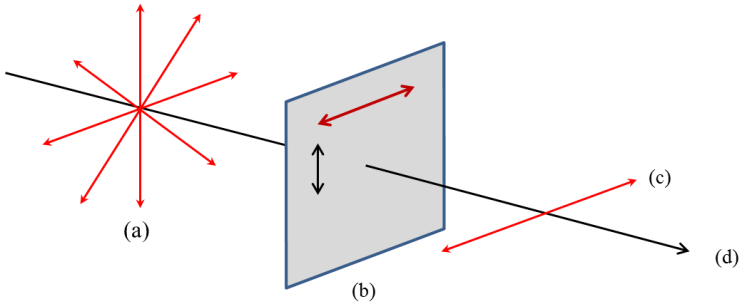

Figure 1.10 A diagram of a polarizing filter and light wave propagating perpendicular

to the polarizing filter domain. (a) An electric field of unpolarized light which is oscillating randomly in all directions. (b) Polarizer; the black coloured arrow line depicts the direction of polymer grid and the red coloured arrow line describes the polarizer's axis (c) Transmitted component of the electric wave which is perpendicular to the polymer molecules (d) Propagation direction of the light wave.

Light propagating through the first polarizer reaches the liquid crystal material contained in the sample cell and experiences the liquid crystal's optical anisotropy which was introduced in section 1.4.2.2. The linearly polarized light splits up into two components which experience the two different refractive indices, the ordinary ray n_o and the extraordinary ray n_e. The components have a phase shift after passing through the liquid crystal sample. Equation 1.6 shows that the phase difference depends on wavelength, birefringence and distance light travels as below. [29]

$$\delta = \kappa \Delta n d = \frac{2\pi}{\lambda}(n_e - n_o)\, d \quad , \tag{1.6}$$

where κ is a wave vector, λ is wavelength of the light, d is the thickness of the sample (between two substrates). Linear polarization of the light occurs when the δ = mπ, Circular polarized light passes through the sample when $\delta = \frac{1}{2}(2m+1)\pi$, with m as an integer. With other conditions of the phase shift, elliptically polarized light comes through. If we set the director at 45° to the polarization direction of incident light, equal intensity of light will be contained in the ordinary wave (experiencing refractive index n_o) and the extraordinary wave (experiencing refractive index n_e). The

wavelength of light is an important parameter for the output of a polarizing microscope, if the phase difference between the ordinary and extraordinary ray is a multiple of a wavelength, the light emerges linearly polarized in the same direction as the initial polarization of light incident upon the sample cell, and there will be no light transmitted. If a phase difference is a half of a wavelength, the light will be linearly polarized perpendicular to the incident light ray and will result in a full transmission through the second polarizer. [30] It is this, wavelength-dependence of the component transmitted by the analyser that causes the beautiful colours seen in birefringent samples between crossed polarizers. The colour depends on Δnd ; wavelengths satisfying $\Delta nd = \lambda, 2\lambda$ etc. do not pass the analyser and are subtracted from the white light spectrum.

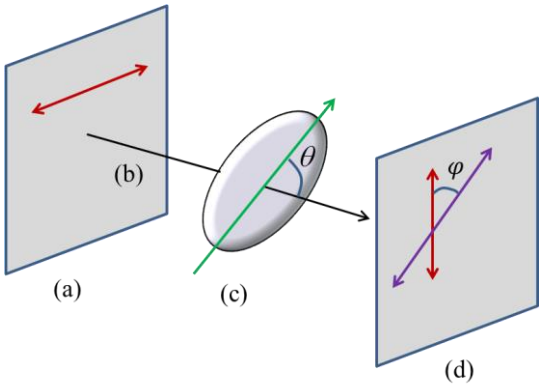

Figure 1.11 A geometric diagram of a birefringent liquid crystal material and light ray showing the polarization of light striking the polarizer and analyser. (a) a polarizer; the red arrow is a symbol of transmittance axis (b) the propagation of light; the direction of a light wave moves (c) a liquid crystal material's optical axis as depicted with a green arrow; θ is the angle between optic axis and propagation direction of the light wave (d) An analyser containing a transmittance axis symbolised by the red arrow, and the purple arrow shows a projection of the optic axis on the analyser plate; φ is the angle

between the liquid crystal's optic axis projected on the analyser domain and transmittance axis of the analyser.

Light exits the microscope *via* another polarizer aligned perpendicular to the first. No birefringence is observed if the polarizer is parallel or perpendicular to the director of liquid crystals, as all light will experience the same refractive index. If linearly polarized light is converted to elliptically polarized light, the light transmitted through the analyser is variable. The transmitted intensity through the medium can be expressed as equation 1.7. [29]

$$I = I_0 \, sin^2 2\varphi sin^2 \frac{\delta}{2} \quad , \tag{1.7}$$

where I_0 is incident light intensity is after polarizer, φ is angle between the birefringent plate (optic axis projection on the analyser) and analyser's transmittance axis.

For homeotropic orientational alignment of the uniaxial liquid crystal sample cell, the angle φ = 0°, thus Δn = 0 and the intensity of light is zero. When liquid crystal's director makes an angle of 45° with the polarizer, a maximum intensity is observed, as there will be equal light polarized along n_e and n_o. For uniform planar alignment the angle between optic axis and light propagation is π, thus $\Delta n = n_{\parallel} - n_{\perp}$ then I is depending on the $sin^2 2\varphi$. The maximum intensity of the transmitted light is accomplished when φ = 45°, and the minimum intensity of the light is for φ = 0° and φ = 90°. For example, a sample cell of a nematic liquid crystal phase viewed between

crossed polarisers only shows a dark state when the director lies parallel or perpendicular to the plane of polarisation of the incident light as all light will experience the same refractive index.

There is another characteristic optical property of liquid crystal is which is termed as an optical activity. Due to this property of chiral phases of liquid crystals, the polarization plane can change its direction clockwise or anti-clockwise depending upon the liquid crystal's activity. Figure 1.12 shows the concept of the rotatory function of the helical molecules in a liquid crystal phase; the right handedness liquid crystal phase turns the polarization plane anti-clockwise. [30]

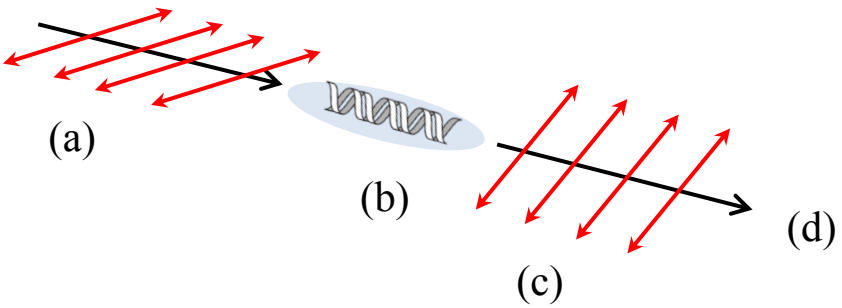

Figure 1.12 The optical active material. (a) incident plane polarized light (b) a chiral liquid crystal phase (c) exiting light of changed plane of polarization (d) propagation direction of light.

In summary, the polarizing microscopy is able to observe liquid crystal phases which exhibit optical anisotropy, and the intensity of light travelling through the liquid crystal medium and crossed polarizers can be seen as complicated domains filled with colours and zones of different intensities; which are termed textures. The following section will introduce the brief characteristic features of textures of a nematic phase

and a chiral nematic phase of liquid crystals in homogeneous or homeotropic alignment.

1.5.4 Observation of Textures of Liquid Crystal Phases

Using a polarizing microscope, it is possible to observe birefringence in a sample located between the polarizers as a result of liquid crystal optics. The interaction of light travelling through the polarizers with a liquid crystal sample cell in between gives rise to patterns of light caused by domains of different alignment which can be observed through the eyepiece. This section introduces several exemplary textures of liquid crystal phases observed with the polarizing microscope.

A nematic liquid crystal phase in-between two substrates is birefringent, with this phase appearing as a bright coloured texture because the nematic phase in general converts the incident linearly polarized light into elliptically polarized light, except for parallel and perpendicular conditions between the director and the polarizing axes of the polarizers. The colour observed in the texture is determined by the phase retardation of the ordinary and extraordinary waves in the material, with the level of transmission dependent upon the wavelength of light. Figure 1.13 and 1.14 show exemplary textures of nematic phases. [31-33]

The disclination is the result of strong changes of orientational order, with the continuous variation of the order parameter in an imperfect state, the thermodynamic distortion is termed a defect.

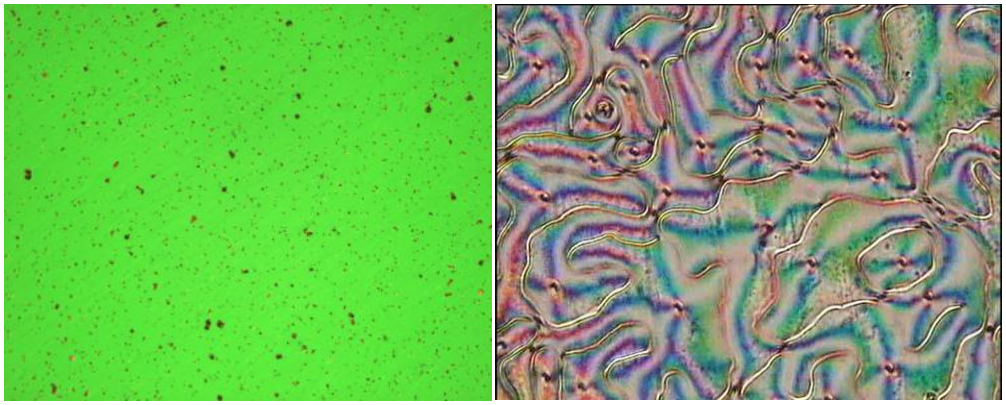

(a) (b)

Figure 1.13 Two nematic textures. Image (a) shows a well aligned E44 (Merk co.,) texture, with a homogenous colour with dark regions corresponding to particles used to separate the glass substrates (spacers). Image (b) shows surface disclination lines appearing like threads in a planar boundary condition. The disclination lines (180° turn of director in plane of substrates) in the texture are similar in appearance to threadlike textures. Threads are line singularities with π disclinations and end at the substrates, connected with brushes or make closed loops. For more information, see. [32] [Photo courtesy of Dr. H. Milton and Dr. I. Dierking]

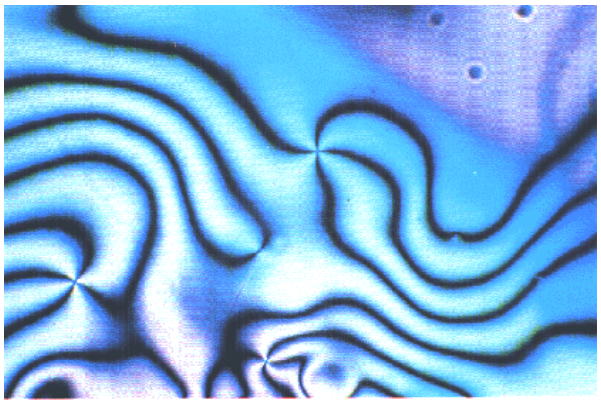

Figure 1.14 A nematic Schlieren texture. Two- and four-fold brushes can be observed, leading into singularities. The curved dark brushes gather to point

singularities; topological defect with values s = ± (number of brushes/4). [Photo courtesy of Dr.S. Lagerwall & B. Stebler]

The black brushes are the region in which the director is parallel or perpendicular to the plane of polarization of light coming into the liquid crystal sample, in this case the polarization of light is not changed, thus the light cannot pass through by analyser and a black area is observed through the polarizing microscope.

A chiral nematic liquid crystal phase located between two crossed polarizers shows bright colours. The incident linearly polarized light is rotated by the optical activity of the chiral nematic phase. The rotation of the axis of the incident light ray of linearly polarized state is highest when the wavelength of the light is similar to the pitch of the chiral nematic phase. [30] Figure 1.15 and 1.16 are characteristic textures of a chiral nematic liquid crystal phase.

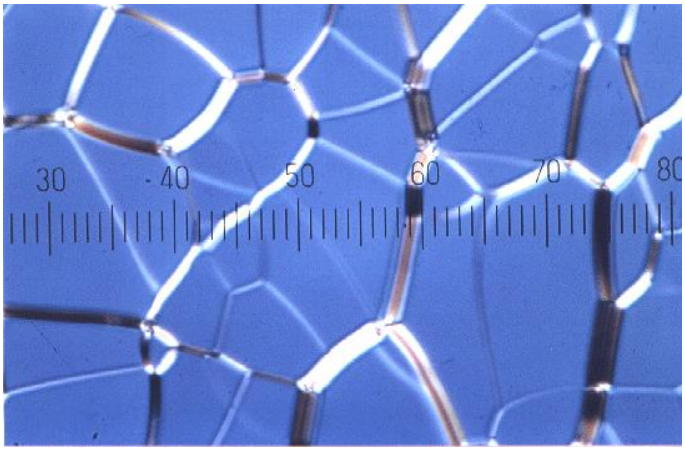

Figure 1.15 A cholesteric oily-streaks Grandjean texture. The helical axis of the chiral nematic phase is oriented perpendicular to the substrate plane except the area of defects named oily-streaks defects. [Photo courtesy of Dr. I. Dierking]

As shown above in Figure 1.15, the homogeneous planar cholesteric structure shows uniform texture with the colour depending on the pitch and/or phase retardation. Within the chiral nematic liquid crystal cell, different types of irregularities are induced and manifest themselves in the appearance of defects; oily streaks.

Another chiral nematic structure arises from homeotropic boundary conditions and reveals the periodicity of the helical structure. The director is oriented perpendicular to the substrates and the helical axis is in the plane of the substrates. The appearance of such textures depends on the ratio of thickness/pitch.

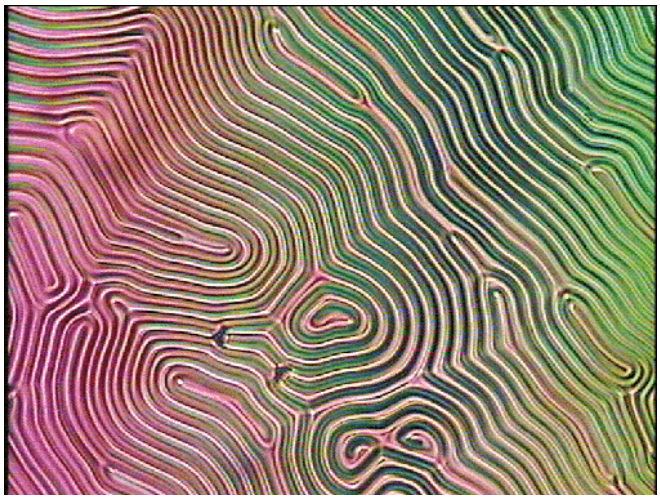

Figure 1.16 A fingerprint texture of a chiral nematic phase. The helical axis located in the plane of the substrate. The line pattern is due to the helical structure of the liquid crystal phase. [Photo courtesy of Dr. I. Dierking]

1.6 Summary

In this chapter, the simplest liquid crystal structures and ordering in space were introduced, as the characteristic anisotropy in liquid crystal gives rise to their

fundamental physical properties like dielectric anisotropy and optical anisotropy. To observe liquid crystal phases, their interaction with light, textures, the dynamics and electro optic properties, it is essential to make a specimen of liquid crystal with substrates, known as a liquid crystal cell. The aligned liquid crystal in homogeneous or homeotropic conditions give rise to critical optics when observation is performed with polarizing microscopes. This brief introduction of basic concepts of liquid crystal physics is useful to understand the experimental work. The next chapter presents a scientific literature review and builds towards the central theme of this thesis; particle motions in liquid crystals.

1.7 References

[1] R. Virchow, *Ueber ein eigenthümliches Verhalten albuminöser Flüssigkeiten bei Zusatz von Salzen*. Archiv für pathologische Anatomie und Physiologie und für klinische Medicin, 1854, Volume 6, Issue 4, pp.572-580.

[2] F. Reinitzer, *Beiträge zur Kenntniss des Cholesterins*. Monatshefte für Chemie und verwandte Teile anderer Wissenschaften, 1888, Volume 9, Issue 1, pp.421-441.

[3] P. J. Flory, *Phase equilibria in solutions of rod-like particles*. Proceedings of the Royal Society A, 1956, Volume 234, Number 1196, pp.73-89.

[4] P. J. Collings, M. Hird, Introduction to liquid crystals. 1997, Taylor & Francis Ltd.

[5] I. Dierking, Textures of liquid crystals. 2003, WILEY-VCH GmbH & Co.KGaA

[6] B. Bahadur, Liquid crystals applications and uses.Volume l. 1990, World Scientific Publishing Co.Ptd.Ltd.

[7] S. Kumar, Liquid Crystals. 2001, Cambridge university press.

[8] P. G. de Gennes, The physics of Liquid Crystal. 1974, Oxford university press.

[9] P. H. Hermans & P. Platzek, *Beiträge zur Kenntnis des Deformationsmechanismus und der Feinstruktur der Hydratzellulose - IX*. Über die theoretische Beziehung zwischen Quellungsanisotropie und Eigendoppelbrechung orientierter Fäden, Kolloid-Zeitschrift. 1939, Volume 88, Issue 1, pp.68-72.

[10] L. Pasteur, *Memoire sur la relation qui exister entre la forme crystalline st la somposition chimique, et sur la cause de la polarisation rotatoire*. Comptes rendus hebdomadaires des séances de l'Académie des Sciences. 1848, Volume 26, pp.535-539.

[11] J. A. Le Bel, *Sur les relations qui existent entre les formules atomiques des corps organiques et le pouvoir rotatoire de leurs dissolutions*. Bulletin de la Société Chimique de France, 1874, Volume 22, pp.337-347.

[12] J. H. van't Hoff, *A suggestion looking to the extension into space of the structural formulas at present used in chemistry, and a note upon the relation between the optical activity and the chemical constitution of organic compounds*. Archives neerlandaises des sciences exactes et naturelles, 1874, Volume 9, pp.445-454.

[13] W. T. Kelvin, *Baltimore lectures on molecular dynamics and the wave theory of light*. 1904, London, C.J. Clay and Sons; Baltimore, Publication agency of the Johns Hopkins University.

[14] H. Kitzerow and C. Bahr, Chirality in Liquid Crystals. 2001, Springer.

[15] J. E. Bigelow and R. A. Kashnow, *Poincaré sphere analysis of liquid crystal optics.* Applied Optics, 1977, Volume 16, Issue 8, pp.2090-2096.

[16] P. Jägemalm, On the optics and Surface Physics of Liquid Crystals. 1999, CHALMERS Göteborg University.

[17] K. Hiltrop and H. Stegemeyer, *Contact angles and alignment of liquid crystals on lecithin monolayers*. Molecular Crystals and Liquid Crystals, 1978, Volume 49, Issue 2, pp.61-65.

[18] H. Mada, *Study on the surface alignment of nematic liquid crystals: temperature dependence of pretilt angles*. Molecular Crystals and Liquid Crystals, 1978, Volume 51, Issue 1-2, 1979, pp.43-56.

[19] Y. B. Kim *et al*, *Atomic Force Microscopy of Rubbed Polyimide Aligning Films for Liquid Crystal Displays*. Molecular Crystals and Liquid Crystals, 1995, Volume 262, Issue 1, pp.89-98.

[20] J. M. Greary, J. W. Goodby *et al*, *The mechanism of polymer alignment of liquid-crystal materials*. Journal of applied physics, 1987, Volume 62, Issue 10, pp.4100-4108.

[21] L. M. Blinov and V. G. Chigrinov, Electrooptic Effects in Liquid Crystal Materials. 1996, Springer.

[22] W. H. de Jeua and Th. W. Lathouwersa, *Nematic Phenyl Benzoates in Electric Fields: I. Static and Dynamic Properties of the Dielectric Permittivity*. Molecular Crystals and Liquid Crystals, 1974, Volume 26, Issue 3-4, pp.225-234.

[23] D. A. Dunmur, Physical Origin of Liquid Crystal Optical Properties. The optics of Thermotropic Liquid Crystals, 1998, Taylor & Francis Ltd. pp.5-40.

[24] W. J. Patzelt, *Two new polarizing microscopes*. Praktische Metallographie/ Practical Metallography, 1997, Volume 34, Issue 12, December, pp.632-638.

[25] W. J. Patzelt, *New microscope for materials sciences*. Praktische Metallographie/ Practical Metallography, 1997, Volume 34, Issue 11, November, pp.583-587.

[26] S. Kumar, Liquid Crystals. 2001, Cambridge university press.

[27] N. H. Hartshorne, 1974, The Microscopy of Liquid Crystals, Microscope Publications Ltd.

[28] E. H. LAND, Light polarizing material. Filed June 2nd, 1936, Serial No. 83,040 26 Claims, Patented July 19, 1938, No.2,123,902.

[29] I. Dierking, Textures of liquid crystals. 2003, WILEY-VCH GmbH & Co.KGaA.

[30] T. Scharf, POLARIZED LIGHT IN LIQUID CRYSTALS AND POLYMERS. 2007, John Wiley & Sons, Inc.

[31] M. Kleman *et al*, *Surface disclination lines in 4-methoxy-benzylidene-4'-n-butylaniline (MBBA)*. Solid state communications, 1973, Volume 12, Issue no.6 pp.581 -584.

[32] A. Saupe, *Disclinations and Properties of the Director field in Nematic and Cholesteric Liquid Crystals*. Molecular Crystals and Liquid Crystals, 1973, Volume 21, pp.211-238.

[33] R. B. Meyer, *Surface polarity induced domains in liquid crystals*. Solid State Communications, 1973, Volume 13, Issue 7, pp.989-992.

Chapter 2
Introduction to Colloidal Systems of Liquid Crystals and Literature Review

After the discovery and description of solutions of insoluble substances (silver chloride, sulphur, Prussian blue) by Selmi, and following the investigation of colloidal gold Sol by Faraday, the pseudo solutions were termed as ‘colloidal’ (from the Greek “kolla”, which means "glue") by Graham in 1861. The Scottish chemist, Graham emphasised that these colloidal systems had shown slow diffusion rates and no sediments under normal gravity, thus the particles were considered to be larger than 1 nm and smaller than 1 μm. In his work, gelatin appeared to be like a colloidal system, and it was proposed that these substances were defined as ‘colloids’. To describe their peculiar forms of aggregation such systems become a ‘colloidal condition of matter’. [1-2] In the 20th century there were numerous developments in physics and chemistry in the field of colloids performed experimentally and theoretically, also a number of advances in understanding colloids and formulating colloidal systems.

This chapter is going to introduce basic principles of colloid science and review articles about several types of colloidal systems of liquid crystal materials, in the cases where the liquid crystal acts as either the discontinuous phases or the continuous phase. The following section will describe colloidal systems and their composition in detail.

2.1 Traditional Types of Colloidal Systems

2.1.1 Definition of Colloidal Systems

A colloidal system consists of a dispersed phase (or a discontinuous phase) distributed uniformly as the form of a finely divided state into a dispersion medium (or a continuous phase). Nowadays in colloid science, the colloids' size is not only restricted dimensionally from 1 nm to 1 μm and the 'glue-like' substances, thus the etymological meaning of 'colloidal' has become irrelevant. Generally, colloids consist of particles substantially larger than atoms or ordinary molecules, but are usually too small to be visible to the unaided eye. More broadly, colloids can describe any substance, including thin films and fibers, having at least one dimension in this general size range, which encompasses about 1 nm ~ 1 μm. [3]

The scientific study of colloids started from the early 19th century. In the late 1820s, a British botanist Brown discovered, using a microscope, that minute particles suspended in a liquid (a suspension of pollen grains in water) experience a permanent motion, with the particle equally likely to move in any direction. This motion appeared due to the irregular collision of colloidal particles by the molecules of the surrounding fluid; termed 'Brownian motion'. Selmi, an Italian chemist, demonstrated that salts and colloidal materials such as silver chloride, sulphur or Prussian blue would coalesce and showed there was a difference in their precipitating power (instability of the dispersed material). The Scottish chemist Graham's work on the colloidal state and its characteristic properties (low diffusivity, the absence of crystallinity, and the lack of

ordinary chemical relations) resulted from the large size of the constituent particles, and was published during the 1860s, and he is regarded as the founder of modern colloid science. In the year of 1905 to 1906, Einstein and Smoluchowski independently gave the first quantitative theory of Brownian motion; which was defined by motion of the particle in a medium to be equality likely in all directions. This quantitative theory was confirmed by Perrin and Svedberg. [4-5]

2.1.2 Dispersed Phases and Dispersion Media

Colloidal systems may exist as dispersions of one substance in another, with the following combinations observed - liquid in gas (i.e. liquid aerosol), solid in gas (i.e. solid aerosol), liquid in liquid (i.e. emulsion), solid in liquid (i.e. sols or colloidal suspensions), solid highly concentrated in liquid (i.e. paste), solid in solid (i.e. solid suspension or dispersion), gas in liquid (i.e. foam), gas in solid (i.e. solid foam) and Xerogels; microporous oxide, porous glass, zeolites etc. All of these systems are named as ‘disperse systems’. Another typical colloid system includes ‘macromolecular colloids’ where macromolecules are dispersed in a solvent (i.e. gels). ‘Association colloids’ are also a type of colloidal system where micelles (the aggregation of surfactant molecules appears above a certain concentration in solution) are dispersed in a solvent. Some examples of colloidal systems around us are fog or mist as a liquid aerosol, industrial smoke as a solid aerosol, milk or butter or pharmaceutical/cosmetic creams as a emulsion, colour paint as a colloidal suspension, mud as a paste, pearl as a

solid suspension, stained glass as a ‘disperse system’, soap foam as a foam, jelly or glue as gels in the boundary of ‘macromolecular colloids’, and finally muscles are ‘biocolloids’ where proteins are dispersed in thin films of lecithin. An ‘association colloid’ is where nucleation does not arise from the formation of colloidal dispersions by growth from the molecular state, but from a self-assembling process, such as micelles in a detergent solutions and vesicles in biological structures such as cell membranes. These association colloids are called as ‘self-assembly systems’.

The previously mentioned systems are known as ‘simple colloids’, although beyond the simple colloidal system there are ‘multiple colloid’ systems consisting of these co-existing phases, such as mineral flotation of minerals in water and air, and double emulsions of oil in water in water. [3]

As shown above with the various types of systems, the dimension of dispersions is not restricted between 1 nm – 1 μm; the traditional dimension in colloid science, thus larger particles can be a dispersed phase in colloidal systems. All colloidal systems can be either generated or eliminated by nature as well as by industrial and technological processes. The colloids prepared in living organisms by biological processes are of critical importance to their lives. Those produced with inorganic compounds in the atmosphere in our planet are crucial in terms of the environment.

2.1.3 Stability and Kinetic Properties of Colloids

A colloidal system has higher free energy than that of the corresponding bulk state, but the disperse system is in a metastable state (with a sufficiently high free energy barrier compared with *kT* in a case of colloidal system of dispersed particles in a dispersion medium) and may remain in that state for a very long time as the energy barrier acts to prevent the elimination of the state of colloidal system. The free energy barrier keeps the particles apart to make the system colloidally stable. The main contribution of the total free energy of interactions between two colloid particles are shown as the most general equation for the total energy difference ΔG. [3]

$$\Delta G = \Delta G^{att}(van\ der\ Waals) + \Delta G^{rep}(short\ range) + \Delta G^{rep}(electrostatic) + \Delta G^{rep}(steric) + \Delta G(other\ effects) \quad (2.1)$$

Where '^{att}' and '^{rep}' imply attractive and repulsive contribution.

In the colloidal system, particles experience movement within the dispersion medium and in some cases in the direction of an applied electric field to the system. The kinetic properties are Brownian motion (a single particle's zigzag random movement), diffusion (particles motion down a concentration gradient), osmotic phenomena (molecules flow from a location of higher chemical potential to a region of lower potential). There are phenomena of particles sinking when they are denser than dispersion medium which is called sedimentation and rising toward the surface of the system is called creaming in gravitational field. When an electric field is applied to the colloidal system, the charged particles tend to move and there can be related phenomena; electro-osmosis and streaming potential. [3-6]

Liquid crystal colloids are important in order to understand in terms of display technology, and in particular, certain phenomena such as Brownian motion for fundamental scientific experiments and electrophoresis. For the next section, colloidal system using liquid crystal will be reviewed.

2.2 Colloidal Systems of Liquid Crystals

The traditional colloidal system deals with isotropic materials, but in the case of dealing with the anisotropic liquid crystals, this interesting system shows the huge potential for the application areas in the industries of electronics, food, drugs, cosmetics and biotechnology. In isotropic solvents, the spatial aggregation of colloids is controlled by a fine balance between the attractive dispersion forces and the Coulomb, steric, and other repulsive forces. The nature of colloidal interactions in nematic liquid crystals is quite different. Colloidal systems of liquid crystals are orientationally ordered complex fluids, in which dispersed phases can be aligned into a certain direction. Because of their anisotropy, the orientation of nematic liquid crystals can be manipulated by external electric or magnetic fields, or even by anisotropic surfaces, which is an important issue in liquid crystal display technology. This thesis is concerned with colloidal particles dispersed in liquid crystalline medium. In particular, the influence of electric fields on the particles is the main topic of study. Colloidal liquid crystal systems have very different properties from ionic colloids, and this section reviews the work that has been carried out on these relatively new and exciting

systems. The following review is an introduction to the articles where the physics and chemistry of the system has been investigated with extensive interest in systems where liquid crystals behave as a dispersed phase or as a dispersion medium within the system.

2.2.1 Liquid Crystal Colloids Without External Field Manipulation

Liquid crystals used as dispersion medium for colloidal particles provide novel ways of control over the spatial organisation of colloidal systems. Liquid crystals can mediate forces between dispersed particles into the liquid crystal media in the colloidal systems. In 1997, Poulin *et al.* investigated and reported the behaviour of dispersed water droplets (1 to 5 μm in diameter) in a nematic liquid crystal medium with its interface stabilised by small amount of surfactant. A nematic drop containing a single water droplet produced a specific pattern which was a result of the rotation of the nematic anisotropy axis through a full 360° about the central water droplet; a topological defect called a hedgehog as shown in Figure 2.1-C. This is a feature of a distorted four-arm star by the nematic medium. The four-arm star structure was recognised as a clue of the novel colloidal interaction in their works. The components showed the interactions included a short-range repulsion and a long-range dipolar attraction and forces arising from the orientational elastic energy of the nematic dispersion medium and formation of the topological defects around the dispersed particles. This resulted in the formation of anisotropic chainlike structures (as in Figure

2.1-A) of the colloidal particles by the attractive interaction. Also the system resulted in the separation between droplets (as in Figure 2.1-B) with a significant fraction of their diameter by the shorter range repulsion. Both of the phenomena exist for the stabilisation of the colloidal system.

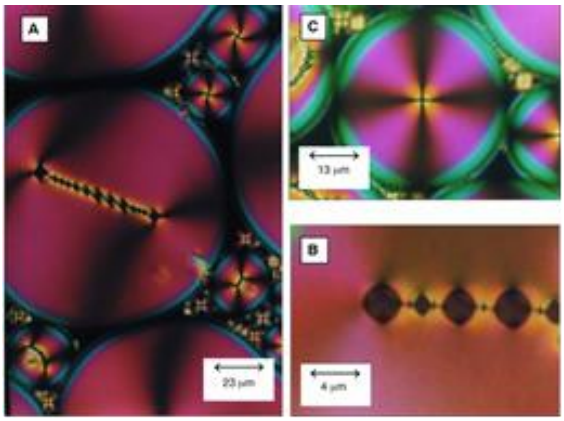

Figure. 2.1 [P. Poulin, H. Stark, T. C. Lubensky, and D. A. Weitz, "Novel Colloidal Interactions in Anisotropic Fluids". *Science*, 21 March, 1997, Volume 275, No.5307, pp.1770-1773.] (A) Microscope image of a nematic multiple emulsion taken under crossed polarizers. (B) A chain of water droplets under high magnification. (C) A nematic drop containing a single water droplet.

Using the Frank free energy equation, with consideration of local alignment of the anisotropic liquid crystal medium in the colloidal system, Poulin *et al.* calculated the energy E_D of the droplet-defect dipole as a function of the separation R (distance between the defect and the droplet centre), and then calculated the equilibrium separation R_0.

$$E_D \sim \left[\frac{K}{(R-a)^2}\right]\left[AR^3 - \left(\frac{4\pi}{3}\right)a^3\right] , \qquad (2.2)$$

where *K* is elastic constant, *A* is a number of order unity, *R* is the separation, *a* is the diameter of the dispersed particle. The energy was growing linearly at large *R* (much larger than *a*), increased as *R* approached *a*, and the lowest E_D was found at R_0. For their second investigation, the role of how surface energy affected the behaviour of colloidal particles in a liquid crystal medium, the total topological charge Q (determined by boundary conditions on **n**) [7] in a nematic liquid crystal has been considered. In a parallel boundary condition at infinity, the force Q to become zero, but under a normal or homeotropic boundary conditions on a closed surface of the sphere, the force Q becomes 1. The single water drop in a closed nematic drop showed a radial hedgehog at a water drop. In the drop-chaining region, the water droplets which were added to another created a hyperbolic hedgehog in the nematic host medium to satisfy the force Q remained as 1 for a formation of a global constraint within the nematic medium. The effective dipole-dipole potential accounts for the attractive interaction and leads to the formation of chains constraint in the liquid crystal medium was confirmed their experimental observation.

$$U_{\alpha\beta} = 4\pi K p_\alpha^z p_\beta^z \frac{1-3\cos^2\theta}{R^3} \quad , \tag{2.3}$$

where θ the angle between *R* and *z* axis, p_α^z is dipole moment of defect α along the *z* axis. The effective dipole-dipole potential is minimised when p_α^z and p_β^z are same sign (this means that p_α and p_β are pointing same direction), so the chaining process was a preferred behaviour in the colloidal system. Their conclusion is that water droplets create defects in the anisotropic host fluid (a dispersion medium; nematic liquid crystal material) that prevent close contact between the water droplets (dispersed material;

colloidal particles as liquid state). Finally, they measured the increasing separation distance (between the water droplets) within the drop-chaining when the size of the drop increased, depicted for the preference of the dipole moment aligning along the director **n**. [7]

Loudet *et al.* report that a binary mixture consisting of an isotropic fluid and a liquid crystal self-organises into highly ordered arrays of monodisperse colloidal droplet chains which minimise the free energy. The self-assembly by topological defects could be applied to other systems with similar symmetry. The size and spatial organization of the droplets are controlled by the orientational elasticity of the liquid-crystal phase, and the defects are usually caused by droplets exceeding a critical size. [8]

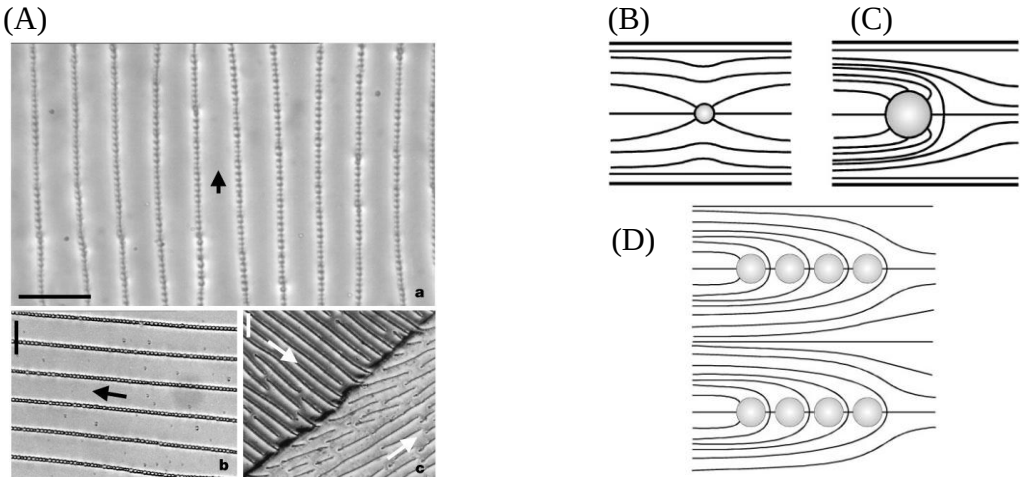

Figure 2.2 [J-C. Loudet, P. Barois & P. Poulin, "Colloidal ordering from phase separation in a liquid- crystalline continuous phase". *Nature*, 5 October, 2000, Volume 407, pp.611-613.] (A) Highly ordered arrays made of monodisperse droplets form. (a) System composition: liquid crystal, 98.0 wt%; silicone oil, 2.0 wt%. Black arrow

denotes direction of polymer rubbing on the device substrate. Scale bar, 50 μm. (b) System composition: liquid crystal, 98.4 wt%; silicone oil, 1.6 wt%. Black arrow denotes direction of polymer rubbing. Scale bar, 35 μm. (c) Chains aligned in different directions (picture of system between crossed polarizers). They are obtained by rubbing different regions of the substrate in different directions. System composition: liquid crystal, 98.4 wt%; silicone oil, 1.6 wt%. White arrows denotes direction of polymer rubbing. Scale bar, 60 μm.

(B) As time passes, the droplet size becomes larger. The black lines represent the axis of preferential orientation of the liquid-crystal molecules. For small particles, the liquid crystal is slightly distorted, and its alignment at the surface of the particle may adopt different orientations. (C) For large particles, the alignment is normal to the particle surface. This induces the formation of a companion defect located near the particle. The global structure has dipolar symmetry. (D) The distortions for an assembly of dipolar droplets that form parallel chains. The defect between neighboring droplets inhibits the coalescence.

When a single particle with a specifically defined planar surface anchoring is introduced to the colloidal system, the liquid crystals tend to align along the surface of this particle. For this liquid crystal action, the liquid crystals are frustrated, as they are aligned locally along the surface of particle, and homogeneously oriented far away from the particle. This frustration arises when it not possible to form a uniformly aligned nematic liquid crystal, and results in a strong elastic distortion of the liquid

crystal around the particle. For a particle with normal surface anchoring conditions, dipolar and quadrupolar nematic colloids have been observed. Muševič *et al.* used a system of a spherical particles dispersed in a nematic liquid crystal medium, and it was observed that dipolar and quadrupolar colloids in a thin layer of a nematic liquid crystal had colloidal particles confined to a few micrometer-thick layer of a nematic liquid crystal, which forms two-dimensional crystal structures bound by topological defects. [9]

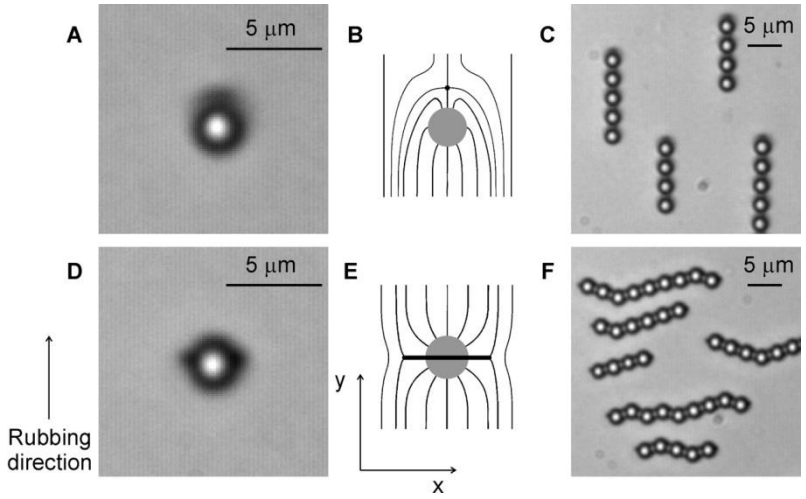

Figure. 2.3 [I. Muševič, M. Škarabot, U. Tkalec, M. Ravnik, and S. Žumer, "Two-Dimensional Nematic Colloidal Crystals Self-Assembled by Topological Defects", *Science*, 18 August, 2006, Volume 313, No.5789, pp.954-958.] (A) Micrograph of a d = 2.32 μm silica sphere in an h = 5 μm layer of 5CB with a hyperbolic hedgehog defect (black spot on top). (B) The nematic order around the colloid has the symmetry of an electric dipole. (C) Dipoles spontaneously form dipolar (ferroelectric) chains along the rubbing direction. (D) The same type of colloid in a thin (h = 2.5 μm) 5CB layer. The two black spots on the right and left side of the colloid represent the Saturn ring. (E)

The nematic order has in this case the symmetry of an electric quadrupole. (F) Quadrupoles spontaneously form kinked chains perpendicular to the direction of rubbing.

In chiral nematic liquid crystals, self-organisation of solid particles was investigated by Hijnen *et al.* using fluorescein isothiocyanate (FITC)-labelled melamin particles in a short pitch liquid crystal medium. Molecular alignment in a cholesteric (chiral nematic) liquid crystal can be described using two vectors: the director for local alignment **n** and the helical axis **z**. The director is always perpendicular to **z** and describes a helix with a characteristic pitch length (p).

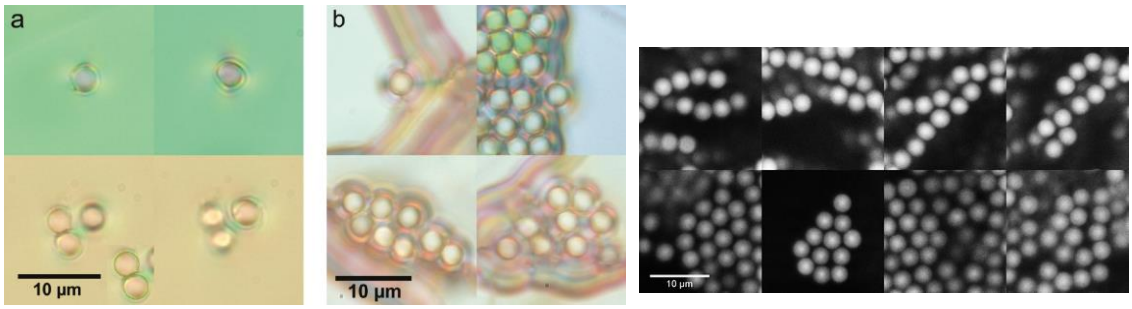

Figure 2.4-1 [N. Hijnen, T. A. Wood, D. Wilson, and P. S. Clegg, "Self-Organization of Particles with Planar Surface Anchoring in a Cholesteric Liquid Crystal". *Langmuir*, 21 JULY, 2010, Volume 26, Issue 16, pp.13502–13510.] High-magnification birefringence images of melamine particles (d = 3 μm) in a cholesteric liquid crystal. (a) Images (p = 1.5 μm) taken at a sample thickness of ~5 μm in the top row and images taken at a sample thickness of ~10 μm in the bottom row. The bottom-row images are of the same three particles but with a different choice of focal plane. The

particles can be seen to be touching. (b) Images (p = 0.4 μm) taken at a sample thickness of ~5 μm and at higher magnification in the top row and images taken at a sample thickness of ~15 μm in the bottom row. (c) Confocal images at high magnification of melamine particles (10 vol. %) in the nematic (top row) and the cholesteric (bottom row) with p = 0.4 μm.

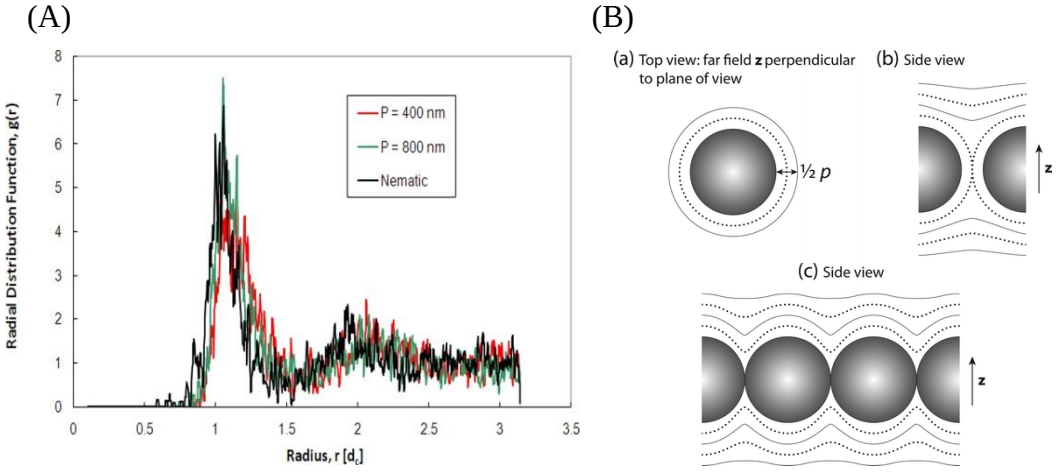

Figure 2.4-2 [N. Hijnen, T. A. Wood, D. Wilson, and P. S. Clegg, "Self-Organization of Particles with Planar Surface Anchoring in a Cholesteric Liquid Crystal". *Langmuir*, 21 JULY, 2010, Volume 26, Issue 16, pp.13502–13510.] (A) Radial distribution functions of the melamine (d = 3 μm) particles in a nematic liquid crystal and cholesteric liquid crystals of different pitch lengths obtained from the analysis of confocal images of particles in planes. (B) Cartoons showing the proposed organisation of the cholesteric liquid crystal around the particles. (a) Top view of the onionlike arrangement. (b) Helical order between two particles viewed from the side; $\lambda^{-1/2}$ lines may form in the gap. (c) Plane of particles in contact as viewed from the side.

The particle surface promotes planar alignment of the chiral nematic liquid crystal at some pitch lengths and the cholesteric liquid crystal structure, ‘wraps around’ the particles as shown in Figure 2.4-2 (B)-(c). The 2-D array of particles is referred to as a ‘plate’ structure as reported by Hijnen *et al*. As the pitch of the cholesteric helix is increased, the size of the plate decreases, with this phenomenon attributed to a decrease in the layer compression modulus. However, it is likely that the mechanism is not simply as they suggest as a layer compression modulus does not strictly occur in the chiral nematic phase. Increasing the pitch induces the particle-particle separation due to the wrapping of particles in cholesteric ‘layers’. [10]

In addition to particle-particle interactions, defect-particle interactions can appear to stabilise the colloidal system. Pires *et al.* investigated the particle-hedgehog systems in a nematic liquid crystal medium and observed a defect-particle interaction.

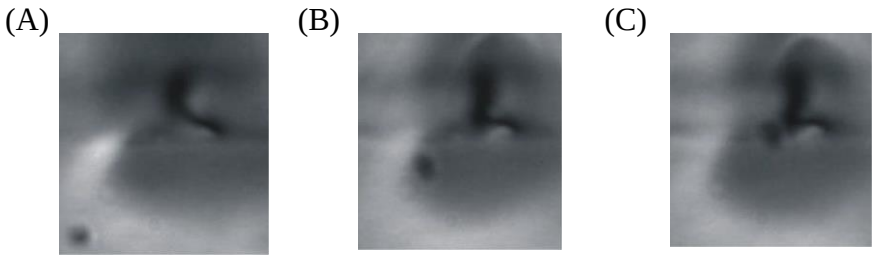

Figure 2.5 [D. Pires, J. B. Fleury, and Y. Galerne, “Colloid Particles in the Interaction Field of a Disclination Line in a Nematic Phase”. *PHYSICAL REVIEW LETTERS*, 15, June, 2007, Volume 98, pp.247801.] (A), (B), (C) Photographs (width 50 μm) taken before the bead is captured by the disclination line at times t = -240 s, -56 s, -2 s, respectively. The particle is indicated with round black spot, and the line shows

disclination line. Note that the line is slightly distorted by the attraction exerted by the particle.

Similarly with particle-particle interactions in colloidal system of liquid crystals, the interaction between a particle and a disclination has an electrostatic analogue, the splay replacing the electric field, thus the disclination line attracts the beads in a self-assembling process as appeared above. [11]

Related with the above reviewed articles, there are far more related works both theoretical and experimental. [12-20] Colloidal particles (dispersed phase) experience new particle-particle interactions when dispersed in a liquid crystal material (dispersion phase). These resulting interactions arise from each particle's anchoring which distorts the ordering of the liquid crystal medium at the expense of elastic energy. The form of the distortion is also related to boundary conditions of the particle's surface; the strength and orientation of molecular anchoring at the surface. A pair of particles can minimise the elastic energy cost by adopting a preferred separation with some fixed orientation with respect to the far-field ordering direction of the liquid crystal medium. When the liquid crystal medium exhibits homeotropic anchoring at the surface of the dispersed particle, a hyperbolic hedgehog defect can form and the long-range interaction has a dipolar character. In the case of planar surface anchoring and weak homeotropic anchoring, long-range interactions result in a quadrupolar character. In addition to particle-particle interactions, there can be an attraction between a particle and a line defect (disclination) in a nematic liquid crystal. Particles

with surfaces of planar anchoring in a chiral nematic medium are suggested to be ‘wrapped up’ with the liquid crystal’s cholesteric layers (better described as a periodic structure) to form 2D plates in the cholesteric phase; this is qualitatively different from the chains formed in the nematic phase. In the case of an interaction between a defect and a particle, the topological defects and distortions around the particles generate elastic forces that govern the stability and the ordering of the suspension. The particle surface properties impose the boundary conditions of the liquid crystal and the resultant far field distortions.

The previous papers describing colloidal particles dispersed in a liquid crystal phase reveal that interactions between particles determine the stabilisation of systems with self-assembly or self-organisation, without an external applied field into the system. The colloidal self-assembly stabilised systems have broad application areas, such as functional devices performing energy, electron, or ion exchange or transfer processes to form the core of molecular and supramolecular photonics, electronics, and ionics. [21-24]

2.2.2 Liquid Crystal Colloids With Manipulations

Translational or rotational movements of dispersed particles within the dispersion medium of colloidal systems using liquid crystals are of intensive interest for fundamental and industrial applications. The application area is of a wide range, with more information later in this section. One of the most interesting methods of producing a manipulation force in a colloidal system of liquid crystal is by optical

trapping techniques, with the most common being electric field application. This section is going to firstly introduce optical trapping, and then secondly, the effects of applying an electric fields to the system.

2.2.2.1 Laser Manipulation

A laser is a light emitting device through optical amplification by the stimulated emission of electromagnetic radiation, with the term ‘Laser’ an acronym for Light Amplification by Stimulated Emission of Radiation. The first laser to be developed was a ruby laser, with a flash lamp pulsing white light with a high intensity to pump a ruby (chromium atoms) to make a population inversion of the atoms which makes more excited atoms than ground state atoms. This makes a very fast initiation for outputting a pulse with high peak power. Liquid crystal droplets dispersed in an isotropic fluid medium can be manipulated with the technique of laser trapping. This technique is especially important in medicine and biology, such as laser-assisted in vitro fertilisation, nanosurgery, biomechanics of molecular motor proteins, microrheology. [25-30] Juodkazis *et al.* demonstrated optical switching by optical manipulation of nematic liquid crystal droplets with circularly polarised light. The rotation of the liquid crystal enables fast switching of submillisecond, which can act as an optical switch. [31]

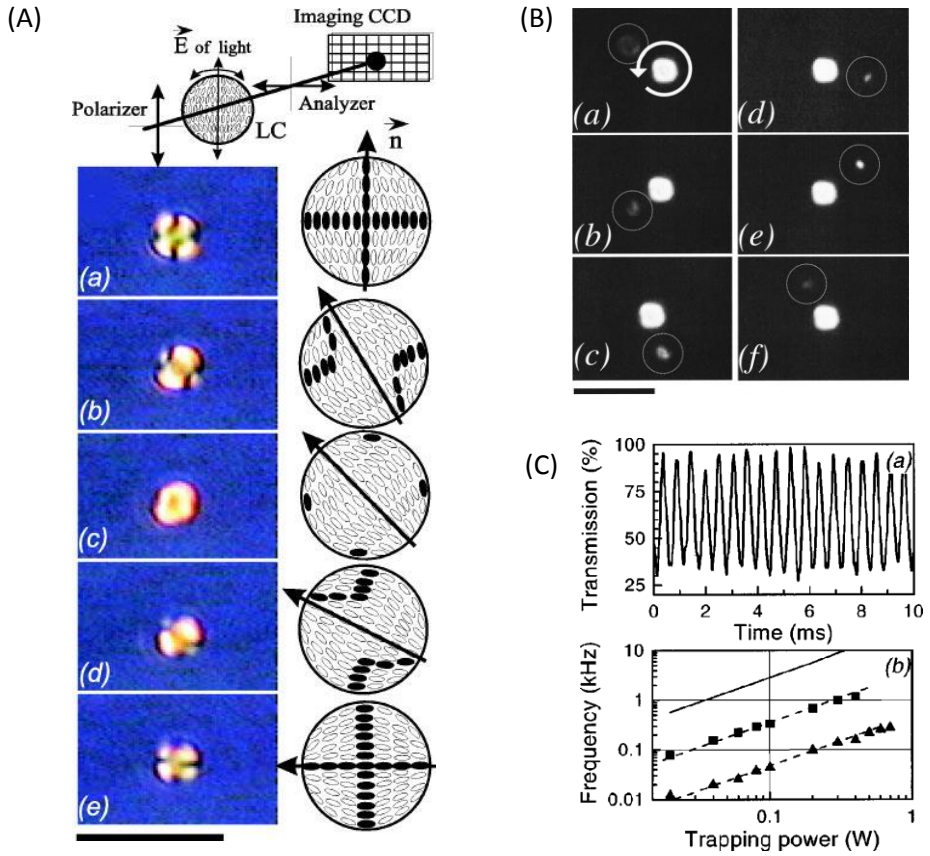

Figure 2.6 [S. Juodkazis, M. Shikata, T. Takahashi, S. Matsuo and H. Misawa, "Fast optical switching by a laser-manipulated microdroplet of liquid crystal". *APPLIED PHYSICS LETTERS*, 14 JUNE, 1999, VOLUME 74, NUMBER 24, pp.3627-3629.] (A) Angularly controlled orientation of a LC (liquid crystal) droplet by plane-polarized irradiation. The images made by light passed through a polarizer–droplet–analyser bear the signature of polar alignment of LC molecules (schematically shown on the right), which scatter the passing light. The regions, which are marked by black ellipses in a schematic drawing of the LC droplet, to those where the passing light is not scattered (less transmitive regions on the video frames). By polarization control of the incident beam, the LC droplet was accordingly aligned to the polarization plane of the incident beam, as shown in the five video frames (a)~(e). The polarization was controlled by a

λ/2 plate (scale bar: 10 μm). (B) Spinning of an LC droplet by circularly left polarized light (marked by arrow). The spinning of a nematic LC droplet can be recognized by viscous orbiting of smaller particle (enclosed in circle) on consecutive snap shots (a)~(f) made with 30 ms separation. The rotation speed of the droplet itself was higher than the 30 Hz resolution of the video recorder (scale bar: 10μm). (C) An optical switching as transmission changes of the rotating LC droplet (the diameter of the droplet was 1.8 μm; the irradiation power was 700 mW). The switching time of 280 μs was determined between the highest and the lowest transmission, and corresponded to the droplet's rotation by a π/4 angle. (b) The power dependencies of rotation frequency for the droplets of 1 μm (squares) and 2.3 μm (triangles) in diameter. The theoretical limit of rotation frequency for the 1 μm diameter droplet (solid line) was calculated by Equation of $\Gamma = -8\pi\eta(a/2)^3\omega$ as the transfer of all light spin $\Gamma_{max} = (P/\hbar\omega)\cdot\hbar$ into the rotation, where P is the irradiation power.

Gleeson *et al.* [32] showed that optical angular momentum of circularly polarized light can be transferred from the laser to a nematic liquid crystal droplet, and then subsequently reported linearly polarized light illumination can initiate a rotation of chiral liquid crystal droplet dispersed in water. Sanderson and Gleeson *et al.* [33-34] confirmed laser manipulation as a tool for studying microrheology of liquid crystals; effective viscosities are measured by inducing movement of a colloidal particle in a liquid crystal medium using linearly polarised light for the trapping and manipulation of micrometre-sized polystyrene particles in a liquid crystal medium of planar aligned nematic liquid crystal.

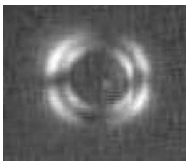

Figure 2.7 [H. F. Gleeson, T. A. Wood, and M. R. Dickinson, "Laser manipulation in liquid crystals: an approach to microfluidics and micromachines". *Philosophical Transactions of the Royal Society A*, 2006, Volume 364, Number 1847, pp.2789-2805.] Photograph of a 6μm diameter polystyrene particle dispersed in MLC-6648 (Merk) and viewed between crossed polarizers, showing the symmetric transmission pattern (approx. 1000×).

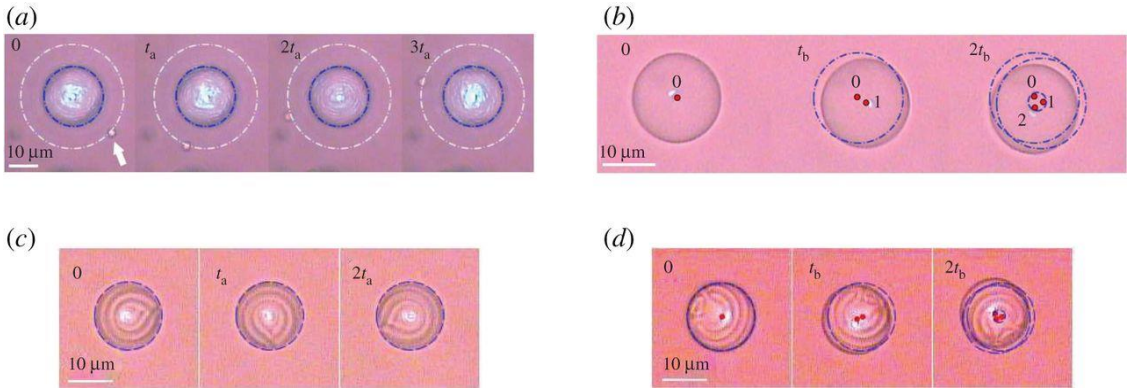

Figure 2.8 [J. L. Sanders, Y. Yang, M. R. Dickinson, and H. F. Gleeson, "Pushing, pulling and twisting liquid crystal systems: exploring new directions with laser manipulation". *Philosophical Transactions of the Royal Society A*, 2013, Volume 371, Number 1988, pp.20120265.] Time evolution showing the continuous rotation of nematic and chiral nematic LC droplets in circularly and elliptically polarized optical tweezers. (*a*) A nematic bipolar droplet rotates about its centre, where a nearby small droplet can be seen orbiting owing to their hydrodynamic interaction. (*b*) The centre of the radial nematic droplet orbits as a circle. (*c*) A Frank–Pryce droplet (cholesteric LC droplets with parallel surface anchoring. [34]) rotates about its centre. (*d*) The centre of a variational Frank–Pryce droplet orbits as a circle in company with its spin rotation.

Using laser tweezers, three-dimensional colloidal crystals of liquid crystal can be assembled. The geometrically regular 3D micro-structures from dielectric objects are called ‘photonic crystals’ and have attracted enormous interest because of their abilities to guide and control light at a microscale. The dispersion relation for light with a frequency of oscillation in the forbidden gap cannot propagate inside the crystal, light of a certain frequency falling on such a crystal is reflected from the crystal, and if the light is reflected for all incident angles, then the band gap is a complete photonic band gap. The photonic band structure was introduced by Yablonovich and Gmitter in 1989. [35] There has been immense interest since the invention of photonic crystals in the science and technology of the crystal and there are various approaches to the question of how to produce such crystals. The fabrication of photonic crystals has been approached using a variety of techniques, such as directed colloidal crystallization on patterned surfaces, using a micromechanical laser, optoelectronic tweezers, colloidal self-assembly via DNA hybridization, microstructures produced by using conventional microelectronic photolithography. [36-40] Muševič *et al.*, researched on the investigation of the composition of the 2D and 3D dimensional structures of liquid crystal colloids; photonic crystals. [41]

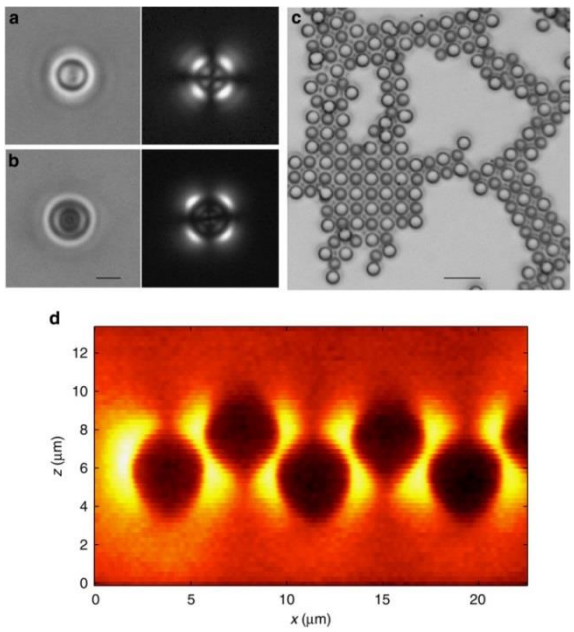

Figure 2.9-1 [A. Nych, U. Ognysta, M. Škarabot, M. Ravnik, S. Žumer, and I. Muševič, Assembly and control of 3D nematic dipolar colloidal crystals. *Nature Communications*, 2012, Volume 4, Article number: 1489.] Laser-tweezers assembly of a 3D dipolar colloidal crystal observed under crossed polarizers. (a,b) Microscopic images of 2.32 μm dipolar silica microspheres in the homeotropic cell filled with 5CB nematic liquid crystal. In (a), the topological point defect is above the microsphere, in (b), the defect is below it. Left panels are taken without polarizers, right panels are taken between crossed polarizers. Scale bar, 2 μm. (c) Quasi-2D checkerboard structure formed by 4.32 μm silica particles in ~10 μm-thick homeotropic cell filled with ZLI-2806. The lattice was observed with completely open condenser aperture diaphragm enhancing the 'checkerboard'-like look of the crystal. No polarizers were used. Scale bar, 10 μm. (d) A vertical cross-section of a quasi-2D checkerboard colloidal crystal of 4 μm colloidal particles, obtained from confocal microscope imaging of a structure like in (c). The alternating arrangement of the microspheres with

topological defects above and below them is clearly seen. The defects are not resolved in this image, they are located at the points where the two bright lobes that encircle each particle come together.

Figure 2.9-2 [Laser-tweezers assembly of a 3D dipolar colloidal crystal observed under crossed polarizers by I. Muševič *et al*. *Nature Communications*, 2012, Volume 4, Article number: 1489.] (a) Three isolated colloidal particles of 4 μm diameter in the

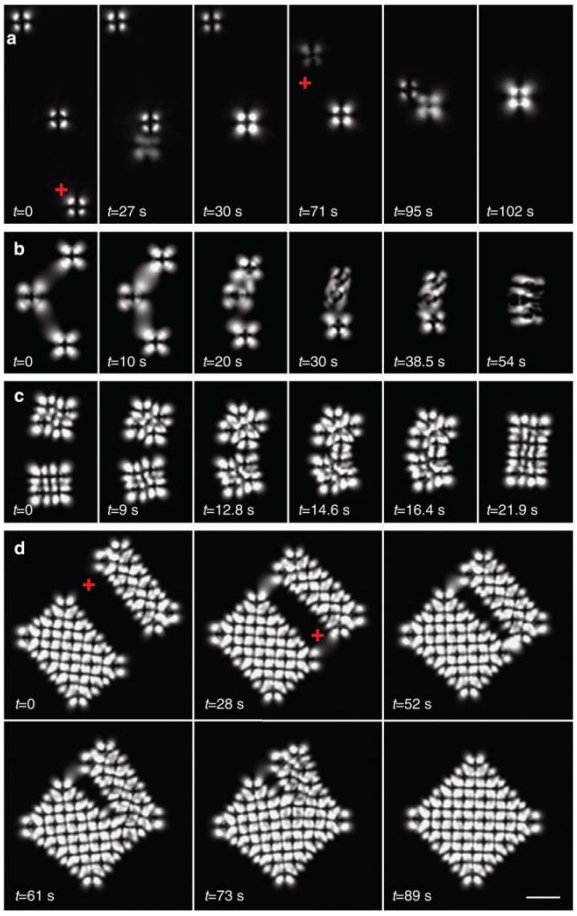

ZLI-2806-filled homeotropic cell of ~25 μm thickness appear as bright objects with a dark cross in the centre. Using laser tweezers, one particle is brought close to the other and they spontaneously form a chain of two particles in a direction perpendicular to the plane of the image. The pair appears like a single but larger and brighter particle (3rd image from the left). The third particle is brought to the couple and it spontaneously forms a dipolar colloidal chain of three particles on top of each other. (b) Three chains, each made of three dipolar particles, are brought close to each other and they start to assemble into a frustrated colloidal trio. Note the tilting of the chains. (c) Two colloidal blocks of 2 × 2 × 3 particles self-assemble into 2 × 4 ×

3 blocks. (d) Colloidal blocks of 2 × 6 × 3 and 4 × 6 × 3 particles assemble into the final 6 × 6 × 3 dipolar colloidal crystal. The assembly at the initial stage was guided by the laser tweezers until blocks started to attract themselves. Scale bar, 10 μm. In all images, the small red cross is the optical trap, used to direct the colloidal assembly.

Figure 2.9-3 [Structure of a 3D dipolar nematic colloidal crystal by I. Muševič *et al.* *Nature Communications*, 2012, Volume 4, Article number: 1489.] (a) Fluorescent confocal polarizing microscopy images of two horizontal cross-sections of a 3D, 6 × 6 × 3 dipolar colloidal crystal, assembled from 4 μm diameter colloidal particles in the homeotropic aligned nematic liquid crystal ZLI-2806. The images were acquired by refocusing along the *z*-axis direction by 2.6 μm . Scale bar, 5 μm. (b) The 3D representation of the fluorescent confocal polarizing microscopy image of a 6 × 6 × 3 3D dipolar colloidal crystal. Here, the fluorescence intensity was inverted to show the in-plane arrangement of the particles in the XY, YZ and XZ planes. Scale bar, 5 μm. (c) Numerical simulation of a 3D dipolar nematic

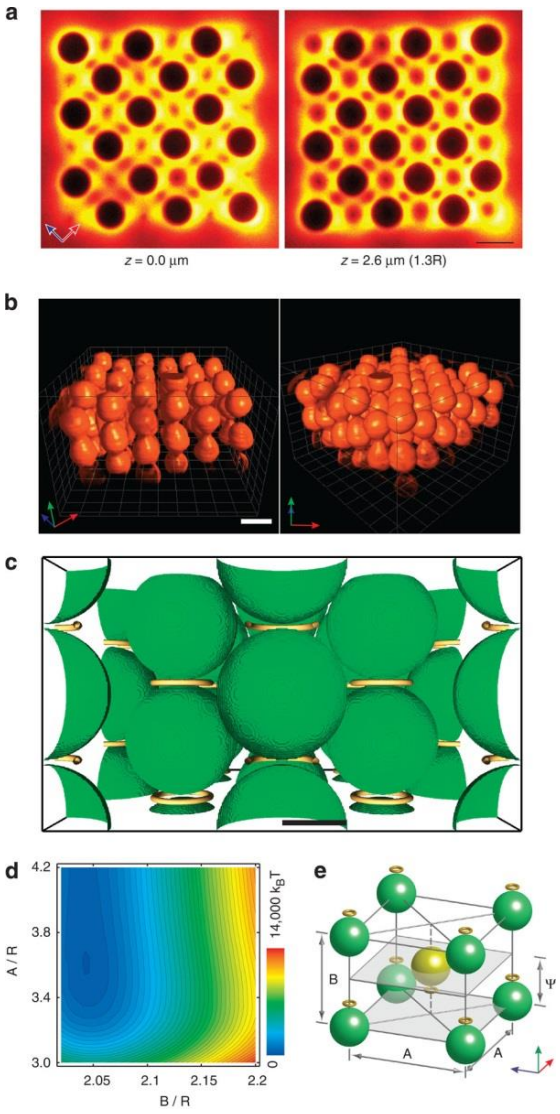

colloidal crystal. Point topological defect opened into small loops, somewhat larger as observed in experiments, and are visualized as iso-surfaces of fixed nematic degree of order *S*. Scale bar, 1 μm. (d) Free energy of one colloidal crystal unit cell as a function of the lattice constants A and B in units of particle radius R. (e) Schematic drawing of the crystal structure showing the tetragonal Bravais lattice with basis.

2.2.2.2 Electric Field Manipulation

Electric field application to various kinds of liquid crystal systems is one of the most common tools for the manipulation of liquid crystal directors or colloids in liquid crystal media. [42-48] However, there are rather a few examples of experimental stories in this area, which can be thought of as still in its infancy. Two key examples are of the work by Dierking *et al.* and Lavrentovich. [49-50]

Dierking *et al.* performed the first quantitative characterisation of micro-sized inorganic particle migration in a thermotropic liquid crystal, using the simplest anisotropic fluid; a nematic phase. The motion of a particle was observed under an applied electric field and the dependence on amplitude, frequency, ion dopant and surface charge was investigated. The experiment found out a stability regime in amplitude-frequency space for the different types of translational motion observed for a single dispersed microsphere for triangular, sinusoidal, and square wave field application. The surface charge of the particles may be the driving force for the microsphere migration as the Figure 2.10-1~3 show their experimental results. A

schematic diagram of the experimental cell is shown in Figure 2.10-1, the ITO electrodes transfer the electricity to the liquid crystal cell imposing the colloidal particle in the LC medium.

Figure 2.10-1 [I. Dierking, G. Biddulph, and K. Matthews, "Electromigration of microspheres in nematic liquid crystals". *PHYSICAL REVIEW E*, 2006, Volume 73, pp.011702.] (a) Side view of the employed Hele-Shaw cell with cell gap d =10 μm. At zero electric field the nematic director **n** is approximately parallel to the bounding substrates. Particle motion is observed in the plane perpendicular to the direction of the applied electric field. (b) Top view of the cell as observed in the polarized microscopic experiments. At zero applied field the director **n** is uniformly oriented along a preferred direction. Particle motion is observed parallel to this direction and perpendicular to the applied ac electric field direction.

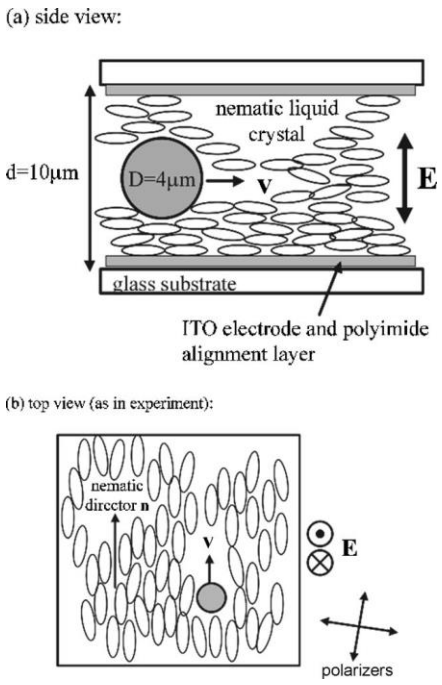

(A) (B)

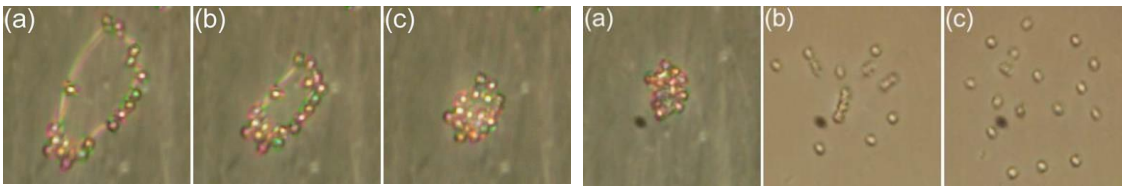

Figure 2.10-2 [Schematic illustration of the experimental conditions by I. Dierking *et al.* 2006. *PHYSICAL REVIEW E*, 2006, Volume 73, pp.011702.] (A) Exemplary time

series of the collection of microspheres towards a cluster of particles by a collapsing defect loop in the nematic phase at zero applied electric field. (a) $t - t_0 = 6$ s, (b) $t - t_0 = 3$ s, (c) $t - t_0 = 0$ s. The value of $t - t_0$ describes the time to defect annihilation. The displayed image size is 120 ×120 μm^2. (B) Exemplary time series showing the repulsion of particles from a cluster during electric application at amplitude E = 8 $V\mu m^{-1}$ and frequency f = 13 Hz. (a) t = 0 s, (b) t = 2 s, and (c) t = 4 s. The displayed image size is 120 ×120 μm^2.

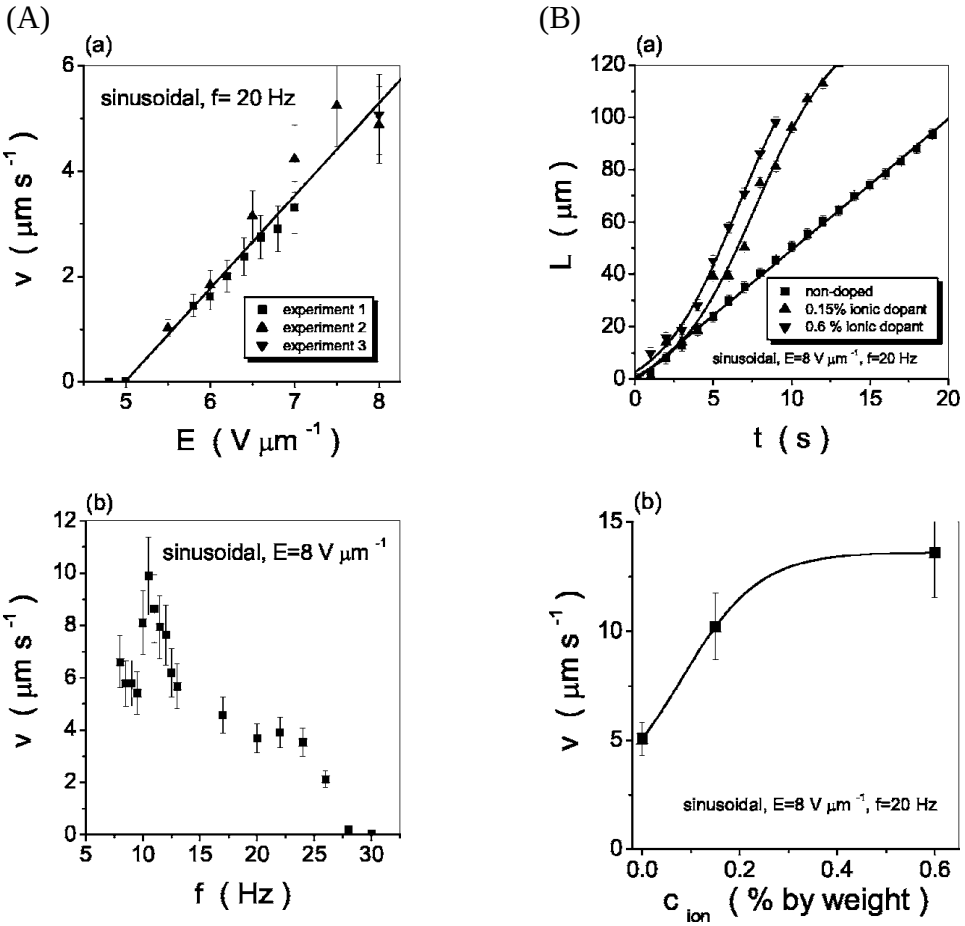

Figure 2.10-3 [Displacement and Velocity dependence by I. Dierking *et al.*2006. *PHYSICAL REVIEW E*, 2006, Volume 73, pp.011702.] (A-a) Velocity dependence of

a single microsphere as a function of applied sinusoidal field amplitude *E*. The particle velocity v increases linearly above a threshold field of E_{th} = 5 Vμm^{-1}, as depicted for several independent measurement series. (A-b) The frequency dependence of the particle velocity exhibits a maximum and microsphere motion ceases for increasing frequency of the applied electric field. Note that an equivalent behaviour is also observed for other applied wave forms, with the velocity maximum shifted towards higher frequencies for the square wave field. (B-a) Particle displacement L as a function of time for different ionic dopant concentrations. At short times t < 5 s, microsphere motion appears to be nonlinear for the doped samples. (B-b) For the linear regime, t > 5 s, the particle velocity increases with increasing ionic dopant concentration and approaches saturation at approximately C_{ion} = 0.4% by weight.

As a conclusion, the micro-sphere motion is directed along the nematic director, and proportional to the applied field amplitude. The regime of linear migration and the particle's linear motion velocity can be increased by the addition of ionic dopant. The velocity of two- and three-particle microsphere clusters is roughly proportional to the number of particles indicating that surface charges adsorbed on the particles may be the driving force for the movement in the boundary of the linear migration regime. Dierking *et al.* focused on the importance of the study of the dynamics of micron-sized particle migration in a fluid environment as the study can offer the possibilities for the determination of viscosities on a local, non-macroscopic scale useful in microrheology.

The motion of single, micron-sized glass spheres in a ferroelectric liquid crystal was investigated systematically by Dierking *et al.* When an electric field was applied to micro-sized spheres which are dispersed in a ferroelectric smectic liquid crystal, the particle translated along the smectic layer plane. The spheres translational velocity was independent of amplitude but increases linearly with frequency of the applied electric field and temperature increased in the system of micro-sized spheres in the ferroelectric smectic liquid crystal medium. Figure 2.11-1~3 will review their work as follows.

Figure 2.11-1 [I. Dierking, P. Cass, K. Syres, R. Cresswell, and S. Morton, Electromigration of microspheres in ferroelectric smectic liquid crystals. *PHYSICAL REVIEW E, 2007, Volume 76, pp.021707*.] Schematic illustration of the experimental geometry. (a) Side view of the cell where smectic layers are oriented in the "bookshelf-geometry" between two substrates with planar boundary conditions, separated by a distance of 10 μm. Particles of diameter D = 3−4 μm are dispersed within the ferroelectric liquid crystal matrix. Electric fields are applied perpendicular to the substrate plane. (b) Top view of the cell, indicating the two director orientations of the FLC in response to the applied electric ac field. The observed microsphere translation occurs along the smectic layer plane.

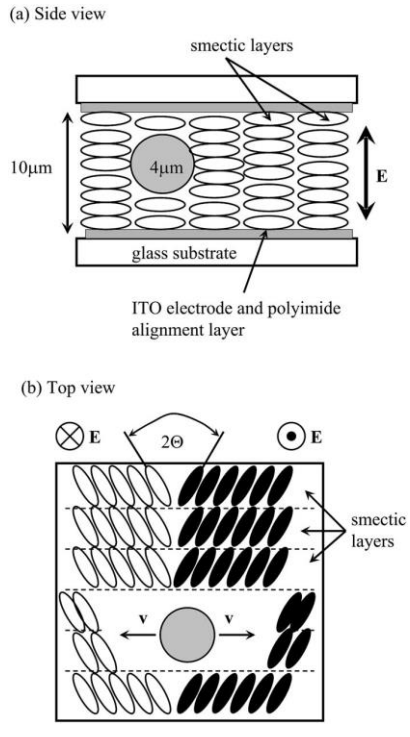

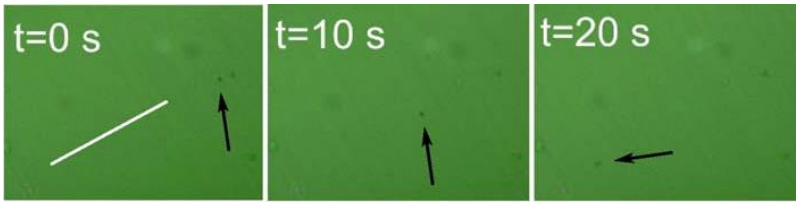

Figure 2.11-2 [Exemplary time series of texture photographs during particle translations by I. Dierking *et al. PHYSICAL REVIEW E, 2007, Volume 76, pp.021707*.] The black arrows indicate the position of an isolated D = 3μm microsphere. Particle motion is linear in time and proceeds within the smectic layer plane, which is indicated by the white line in the left part of the figure. Displayed image size is 130 μm×100 μm.

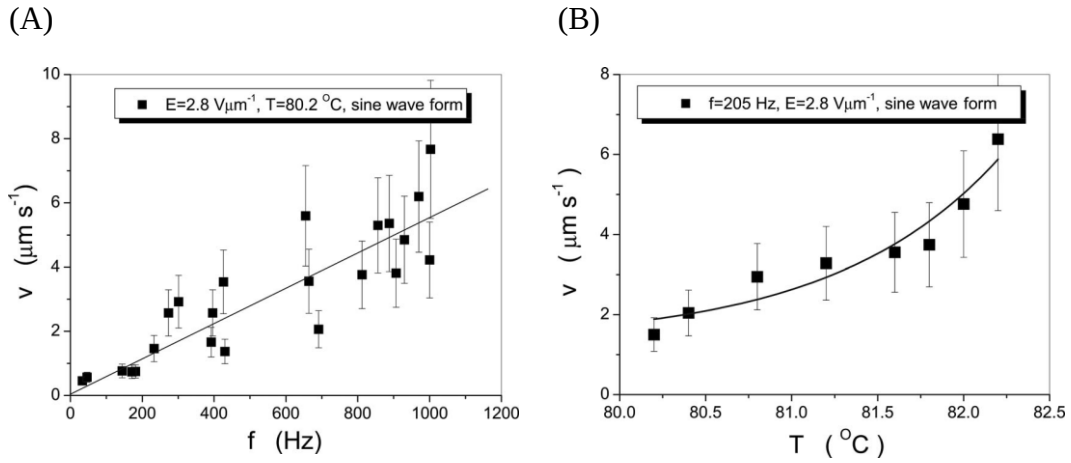

Figure 2.11-3 [The microsphere velocity by I. Dierking *et al. PHYSICAL REVIEW E, 2007, Volume 76, pp.021707.*] (A) Frequency dependence of the microsphere velocity for the D = 4 μm particles. Despite relatively large scattering, the data clearly indicates a (linear) increase of the particle velocity with frequency of the applied electric field. (B) Temperature dependence of the D = 4 μm microsphere velocity at a fixed electric field amplitude of E = 2.8 Vμm^{-1} and frequency f = 205 Hz. The observed increase in

microsphere velocity can be attributed to the decrease in liquid crystal viscosity by increasing the temperature.

As a result, the dispersed spherical particles exhibit linear translational motions along the smectic layer plane within certain parameter regimes of electric field amplitude and frequency, and related to saturated director switching in the ferroelectric SmC* phase. The velocity of micro-sized spheres (at a constant field amplitude and frequency) increased as temperature increased due to the decrease of the viscosity of the liquid crystal medium. The motions of micro-sized spheres was caused by flow effects, possibly due to mass pumping.

Lazo and Lavrentovich observed that the electrophoresis in a nematic liquid crystal medium resulting in two types of nonlinearity when investigating the relationship between particle velocity and electric field. Figure 2.12 (A) is the system used in their work.

(A)

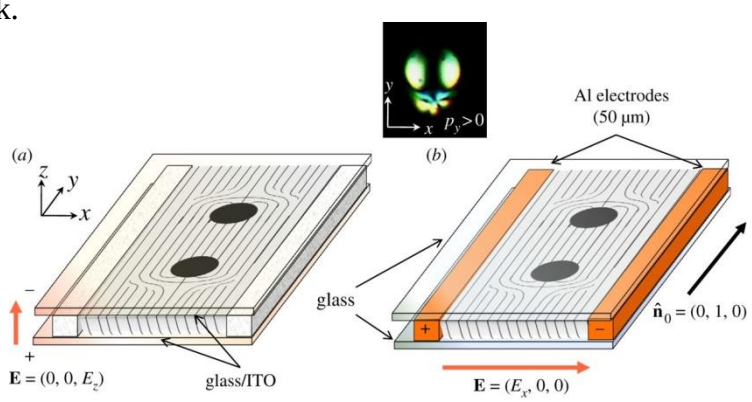

Figure 2.12 [I. Lazo and O. D. Lavrentovich, "Liquid-crystal-enabled electrophoresis of spheres in a nematic medium with negative dielectric anisotropy". *Philosophical Transactions of the Royal Society A*, 2013, Volume 371, No.1988, pp.20120255.]

(A) Scheme of electrophoretic experiment for spheres showing opposite polarities of p_y in an LC with $\Delta\varepsilon < 0$ aligned along $\mathbf{n}_0 = (0, 1, 0)$. (a) Out-of-plane configuration with the electric field $\mathbf{E} = (0, 0, E_z)$. (b) In-plane configuration with the electric field $\mathbf{E} = (E_x, 0, 0)$. The inset shows a polarizing microscope texture of a spherical particle with a hyperbolic hedgehog near its bottom.

(B)

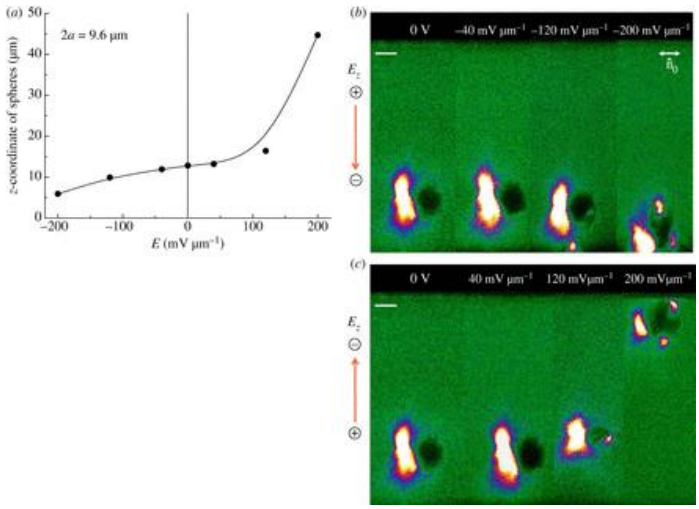

(B) Electrically controlled levitation of $2a = 9.6$ μm spherical particles in MLC7026-000. (a) z-Position of microspheres in the bulk as a function of the electric field. Fluorescent confocal polarizing microscopy textures of a vertical cross section of the nematic cell with a colloidal sphere (b) for negative E_z and (c) for positive E_z. The white scale bar corresponds to 5 μm.

In the work of Lazo *et al.*, the velocity component parallel to the applied electric field grows linearly with the field, but when the field is high enough, it also shows a cubic dependence. The most interesting is the second type of nonlinear electrophoresis that causes the sphere to move perpendicularly to the applied field described in the above work.

2.3 Summary

The composites of liquid crystals and colloidal particles may show complicated structures, controlled by the minimisation of energy of the colloidal system achieved by elastic distortions of the anisotropic medium at around the dispersed particles and by topological defects at the colloidal surfaces. Colloidal systems have been investigated by a few authors, in particular, attention has been paid to the behaviour of the various structures that can be formed in colloidal liquid crystal systems and there are many construction methods available. The possible industrial applications of these systems cover the areas of biomedical sensors, micro-laser devices and electric-display devices.

This thesis is particularly aimed at examining the influence of electric fields on micro-sized colloidal particles in liquid crystals. It can be seen that there is rather little research in this area.

2.4 References

[1] T. Graham, On Liquid Transpiration in Relation to Chemical Composition. Philosophical Transactions of the Royal Society of London, 1861, Volume 151, pp.373-386.

[2] T. Graham, *On Liquid Diffusion applied to Analysis.* Journal of the Chemical Society, 1862, Volume 15, Issue 0, pp.216-270.

[3] D. H. Everett, Basic principles of colloid science. 1988, The Royal Society of Chemistry.

[4] A. Einstein, *Zur Theorie der Brownschen Bewegung*. ('*On the theory of the Brownian movement.'*) Annalen der Physik, 1906, Volume 324, Issue 2, pp.371-381. ; M. von Smoluchowski, *Zur kinetischen Theorie der Brownschen Molekularbewegung und der Suspensionen*. ('A kinetic theory of Brownian molecular movement and suspension.') Annalen der Physik, 1906, Volume 326, Issue 14, pp.756-780.

[5] J. Perrin, *Mouvement brownien et réalité moléculaire*. Ann. Chimie et Physique, 1909, Volume 8, Issue 18, pp.1-114. ; T. Svedberg, *The Brownien Movements*. Ion, 1909, Volume 1, pp.373-402.

[6] I. Morrison & S. Ross, Colloidal Dispersions. 2002, A John Wiley & Son, Inc., Publication.

[7] P. Poulin *et al.*, *Novel Colloidal Interactions in Anisotropic Fluids*. Science, 1997, Volume 275, No.5307, pp.1770-1773; H.-R. Trebin, *The topology of non-uniform media in condensed matter physics.* 1982, ADVANCES in PHYSICS, Volume 31, Number 3, 195-254.

[8] J. C. Loudet *et al*., *Colloidal ordering from phase separation in a liquid-crystalline continuous phase*. Nature, 2000, Volume 407, pp.611-613.

[9] I. Muševič *et al*., *Two-Dimensional Nematic Colloidal Crystals Self-Assembled by Topological Defects*, Science, 2006, Volume 313, No.5789, pp.954-958.

[10] N. Hijnen *et al*., *Self-Organization of Particles with Planar Surface Anchoring in a Cholesteric Liquid Crystal*. Langmuir, 2010, Volume 26, Issue 16, pp.13502–13510.

[11] D. Pires *et al*., *Colloid Particles in the Interaction Field of a Disclination Line in a Nematic Phase*. PHYSICAL REVIEW LETTERS, 2007, Volume 98, pp.247801.

[12] O. Mondain-Monval *et al*., *Weak surface energy in nematic dispersions: Saturn ring defects and quadrupolar interactions*. THE EUROPEAN PHYSICAL JOURNAL B, 1999, Volume 12, pp.167-170.

[13] E. M. Terentjev, *Disclination loops, standing alone and around solid particles, in nematic liquid crystals.* PHYSICAL REVIEW E, 1995, Volume 51, No.2, pp.1330-1338.

[14] C. M. Noël *et al*., *Measurement of Elastic Forces between Iron Colloidal Particles in a Nematic Liquid Crystal.* PHYSICAL REVIEW LETTERS, 2006, Volume 96, pp.217801.

[15] M. Vilfan *et al*., *Confinement Effect on Interparticle Potential in Nematic Colloids*. PHYSICAL REVIEW LETTERS, 2008, Volume 101, pp.237801.

[16] I. Muševič *et al*., *2D Interactions and Binary Crystals of Dipolar and Quadrupolar Nematic Colloids*. PHYSICAL REVIEW LETTERS, 2008, Volume 100, p.217803.

[17] M. Skarabot *et al*., *Hierarchical self-assembly of nematic colloidal superstructures.* PHYSICAL REVIEW E, Volume 77, pp.061706.

[18] Y. Gu et al., *Observation of Saturn-Ring Defects around Solid Microspheres in Nematic Liquid Crystals.* PHYSICAL REVIEW LETTERS, 2000, Volume 85, No.22, pp.4719-4722.

[19] T. Araki *et al*., *Colloidal Aggregation in a Nematic Liquid Crystal: Topological Arrest of Particles by a Single-Stroke Disclination Line.* PHYSICAL REVIEW LETTERS, 2006, Volume 97, pp.127801

[20] T. C. Lubensky, *Topological defects and interactions in nematic emulsions*. PHYSICAL REVIEW E, 1998, Volume 57, No.1, pp.610-625.

[21] J-M. Lehn, *Toward Self-Organization and Complex Matter.* Science, 2002, Volume 295, pp.2400

[22] P. L. Roach *et al*., *Structure of isopenicillin N synthase complexedwith substrate and themechanism of penicillin formation.* Nature, 1997, Volume 387, pp.827-830.

[23] W. A. Wolkert, *Colloidal Hard-Sphere Crystal Growth Frustrated by Large Spherical Impurities.* Science, 2005, Volume 309, No.5738, pp.1231-1233.

[24] A. van Blaaderen *et al*., *Template-directed colloidal crystallization.* Nature, 1997, Volume 385, pp.321-324.

[25] H. Kojima, M. Kikumoto, H. Sakakibara, and K. Oiwa, *Mechanical Properties of a Single-Headed Processive Motor, Inner-Arm Dynein Subspecies-c of Chlamydomonas Studied at the Single Molecule Level*. Journal of Biological Physics, 2002, Volume 28, Issue 3, pp.335-345.

[26] K. König, H. Liang, M. W. Berns, and B. J. Tromberg, *Cell damage in near-infrared multimode optical traps as a result of multiphoton absorption.* Optics Letters. 1996, Volume 21, Issue 14, pp.1090–1092.

[27] K. König, *Robert Feulgen Prize Lecture; Laser tweezers and multiphoton microscopes in life sciences.* Histochemistry and cell biology, 2000, Volume 114, Issue 2, pp.79 -92.

[28] U. Bockelmann, Ph. Thomen, B. Essevaz-Roulet, V. Viasnoff, and F. Heslot, *Unzipping DNA with optical tweezers: high sequence sensitivity and force flips.* Biophysical journal, 2002, Volume 82, Issue 3, pp.1537-1553.

[29] H. Kojima, E. Muto, H. Higuchi, and T. Yanagida, *Mechanics of single kinesin molecules measured by optical trapping nanometry.* Biophysical journal, 1997, Volume 73, Issue 4, pp.2012-2022.

[30] S. Henderson, S. Mitchell, and P. Bartlett, *Propagation of Hydrodynamic Interactions in Colloidal Suspensions.* PHYSICAL REVIEW LETTERS, 2002, Volume 88, Number 8, pp.088302.

[31] S. Juodkazis *et al., Fast optical switching by a laser-manipulated microdroplet of liquid crystal.* APPLIED PHYSICS LETTERS, 1999, Volume 74, No.24, pp.3627-3629.

[32] T. A.Wood, H. F. Gleeson, M. R. Dickinson, and A. J. Wright, *Mechanisms of optical angular momentum transfer to nematic liquid crystalline droplets.* 2004, Applied Physics Letters, Volume 84, pp.4292–4294.

[33] H. F. Gleeson, T. A. Wood and M. R. Dickinson, *Laser manipulation in liquid crystals: an approach to microfluidics and micromachines.* Philosophical Transactions of the Royal Society A, 2006, Volume 364, Number 1847, pp.2789-2805.

[34] J. L. Sanders, Y. Yang, M. Dickinson, and H. F. Gleeson, *Pushing, pulling and twisting liquid crystal systems: exploring new directions with laser manipulation.* Philosophical Transactions of the Royal Society A, 2013, Volume 371, Number 1988, pp.20120265. ; J. Bezić and S. Žumer, *Structures of the cholesteric liquid crystal droplets with parallel surface anchoring.* 1992, Liquid Crystals, Volume 11, Number 4, pp.593-619.

[35] E. Yablonovich and T. J. Gmitter, *Photonic band structure: the face-centered-cubic case.* Physical Review Letters, 1989, Volume 63, pp.1950–1953.

[36] A. van Blaaderen, R. Ruel, and P. Wiltzius, *Template-directed colloidal crystallization*. Nature, 1997, Volume 385, pp.321–324.

[37] K. Aoki, HT. Miyazaki, H. Hirayama, K. Inoshita, T. Baba, K. Sakoda, N. Shinya, and Y. Aoyagi. *Microassembly of semiconductor three-dimensional photonic crystals*. Nature Material, 2003, Volume 2, pp.117–121.

[38] PY. Chiou, AT. Ohta, and MC. Wu. *Massively parallel manipulation of single cells and*

microparticles using optical images. Nature, 2005, Volume 436, pp.370–372.

[39] C. A. Mirkin, R. L. Letsinger, R. C. Mucic, and J. J. Storhoff, *A DNA-based method for rationally assembling nanoparticles into macroscopic materials.* Nature, 1996, Volume 382, pp.607–609.

[40] D. Liang and J. E. Bowers, *Recent progress in lasers on silicon*. Nature Photonics, 2010, Volume 4, pp.511–517.

[41] A. Nych, U. Ognysta, M. Škarabot, M. Ravnik, S. Žumer, and I. Muševič, *Assembly and control of 3D nematic dipolar colloidal crystals.* Nature Communications, 2012, Volume 4, Article number: 1489.

[42] Y. Mieda and K. Furutani, *Microsphere Manipulation using ferroelectric liquid crystals.* PHYSICAL REVIEW LETTERS, 2005, Volume 95, pp.177801.

[43] G. Liao, I. I. Smalyukh, J. R. Kelly, O.D. Lavrentovich, and A. Jákli, *Electrorotation of colloidal particles in liquid crystals*. PHYSICAL REVIEW E, 2005, Volume 72, pp.031704.

[44] A. Jákli, B. Senyuk, G.Liao, and O.D. Lavrentovich, *Colloidal micromotor in smectic A liquid crystal driven by DC electric field.* Soft Matter, 2008, Volume 4, pp.2471-2474.

[45] O. P. Pishnyak, S. Tang, J. R. Kelly, S. V. Shiyanovskii, and O.D. Lavrentovich, *Leviation, Lift, and bidirectional Motion of Colloidal Particles in an electrically driven Nematic Liquid Crystal*. PHYSICAL REVIEW E, 2007, Volume 99, pp.127802.

[46] T. Togo, K. Nakayama, M. Ozaki, and K. Yoshino, *Electric field-induced migration of SiO_2 particles in smectic liquid crystal.* Japanese journal of applied physics , 1997, Volume 36, pp.L1520-L1522

[47] K. Nakayama, M. Ozaki, and K. Yoshino, *Properties of Liquid Crystals in Photonic Crystal, Synthetic Opal*. Molecular Crystals and Liquid Crystals Science and Technology. Section A, 1999, Volume 329, Issue 1, pp. 433-440.

[48] Y. Shimoda, M. Ozaki, and K. Yoshino, *Electric field tuning of a stop band in a reflection spectrum of synthetic opal infiltrated with nematic liquid crystal.* Applied physics letters, 2001, Volume 79, Issue 22, pp.3627-3629.

[49] I. Dierking, G. Biddulph, and K. Matthews, *Electromigration of microspheres in nematic liquid crystals.* PHYSICAL REVIEW E, 2006, Volume 73, pp.011702. ; I. Dierking, P. Cass, K. Syres, R. Cresswell, and S. Morton, *Electromigration of microspheres in ferroelectric smectic liquid crystals.* PHYSICAL REVIEW E, 2007, Volume 76, pp.021707.

[50] I. Lazo and O. D. Lavrentovich, *Liquid-crystal-enabled electrophoresis of spheres in a nematic medium with negative dielectric anisotropy*. Philosophical Transactions of the Royal Society A, 2013, Volume 371, No.1988, pp.20120255.

Chapter 3

Experimental Details

3.1 Introduction

Chapters 1 and 2 gave an introduction to the areas of liquid crystals and colloids, with the final part of Chapter 2 describing the emerging area of colloidal liquid crystals. This thesis is aimed at measuring and understanding the electric-field induced motion of micron-sized particles suspended in various liquid crystal phases. The sample preparation and cell design is described in Section 3.2. The apparatus required to make measurements on the samples is described in Section 3.3. Finally, the image analysis needed to quantify the motion of the particles is described in Section 3.4.

3.2 Sample Preparation and Cell Design

3.2.1 Liquid Crystal Materials

Two types of liquid crystalline materials were used in this thesis, nematic and chiral nematic systems. The materials are summarized in Table 3.1 which gives their

name, transition temperatures and any important comments about their properties that are relevant to the experiments carried out.

Material name	Important features
(S, S)-EPHDBPE (Sigma –Aldrich.)	Chiral nematic material with an inversion point in the helical twist between 82.5˚C and 83.0˚C. (C 57 S_1 57.2 S_C^* 78.1 N* 95.7 I , [1])
Nematic 1 (CHISSO Corp.)	Positive dielectric anisotropy nematic material, $\Delta\varepsilon = 10.4$ at room temperature.
Nematic 2 (Merk Advanced Technologies Ltd.)	Negative dielectric anisotropy nematic material, $\Delta\varepsilon = -3.4$ at room temperature

Table 3.1 Information about the liquid crystalline materials used in this thesis.

3.2.2 Micron-Sized Particles

Two types of particles were used in the experiments described in this thesis. The studies of electric-field induced motion of particles in the chiral nematic phase described in Chapter 4 were made using spherical silica particles of diameter 2.5 μm.

The dielectric constant of silicon dioxide is 3.8-3.8 [2] The same particles were used in Chapter 5, which examines unusual electric-field induced particle motion in the isotropic phase of (S, S)-EPHDBPE.

The experiments on nematic systems were designed to study geometries that were not previously accessed. As mentioned in the previous chapter, there are several papers that describe studies of spherical particles in nematic materials. The work in this thesis describes the motion of elongated particles in 4 distinct nematic geometries. The elongated particles were supplied by Dr.Dierking. [3]

3.2.3 Liquid Crystal Cell Preparation

The sample cells used in these experiments were made from Indium-Tin-Oxide (ITO) coated glass plates. The cells are provided by Dr.Dierking for chapter 4 and 5, and by Dr.Chang for chapter 6. The ITO coating acts as the electrodes of the device, applying an electric field perpendicular to the device substrates. Both of the electrode areas were treated with a polyimide alignment agent, with parallel rubbing on both surfaces to get planar (homogeneous) alignment. In the case of homeotropic alignment, the surfaces were treated with specific chemicals (invented for the special purpose, name protected) by Dr. Chang. The thickness of the cell was maintained by means of a spacer and varied from ~ 6 μm to ~ 10 μm in practice. Figure 3.1 shows a schematic illustration of the composition of a sample cell.

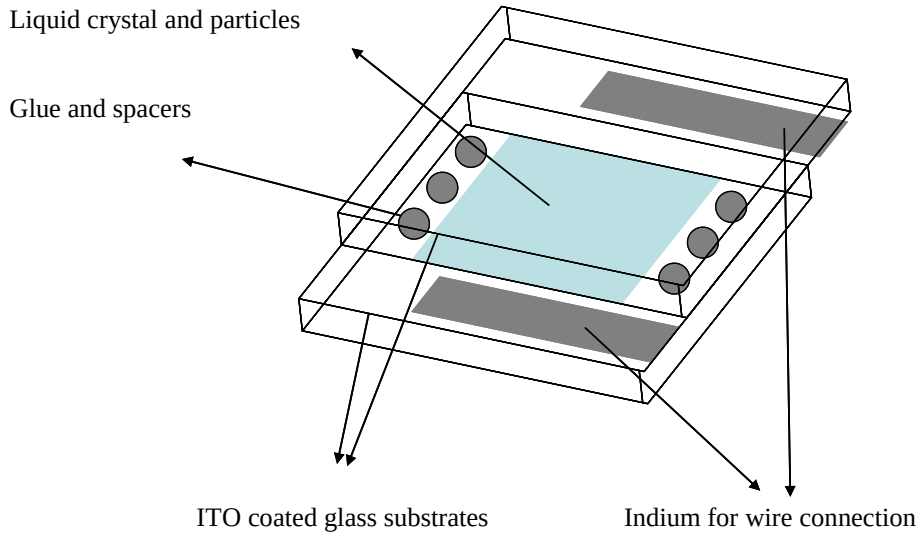

Figure 3.1 The schematic illustration of composition of a sample cell.

The cells were filled by placing a small amount of micron-sized particles at the open edge on one of the glass plates, then adding the liquid crystal material. Capillary action ensured that the cell filled with a combination of the liquid crystal and the particles. The cell was kept on a hot plate above the clearing temperature of the liquid crystal for the filling process with the materials. The concentration of particles in the liquid crystal was not controlled directly using this method, but it was successful in providing sample cells that had a few particles in the area under study. Too many particles would cause chains to form, as described in Chapter 2.

3.3 Apparatus

The investigation of the motions of the micron-sized particles was carried out using a polarizing microscope fitted with a video camera. Polarizing microscopy is a well-known technique for studying liquid crystals. [4] An introduction to polarizing microscopy was presented in Section 1.5.3, and the application to the different liquid crystal phases, allowing them to be identified by their different textures was summarized in section 1.5.4. Polarizing microscopy allowed the liquid crystal samples in this work to be checked for excellent alignment, as well as allowing the micron-sized particles to be visualized. It was also used to identify the phase transitions in the liquid crystal samples used.

The apparatus used is shown schematically in Figure 3.2. The liquid crystal sample is held in a Linkam hot stage that allows the temperature to be changed between room temperature and + 300˚C, and held with a relative accuracy of ± 0.1˚C. The polarizing microscope is equipped with a uEye video camera (uEye Gigabit Ethernet UI-5460-C) linked to a computer. The video camera allowed images of the liquid crystal sample to be collected with a time resolution 0.0175 sec. The pictures obtained have a spatial resolution limited by the pixel size which is 0.278 μm. These parameters are important in determining the resolution with which particle motion can be determined, the two important parameters being displacement and velocity.

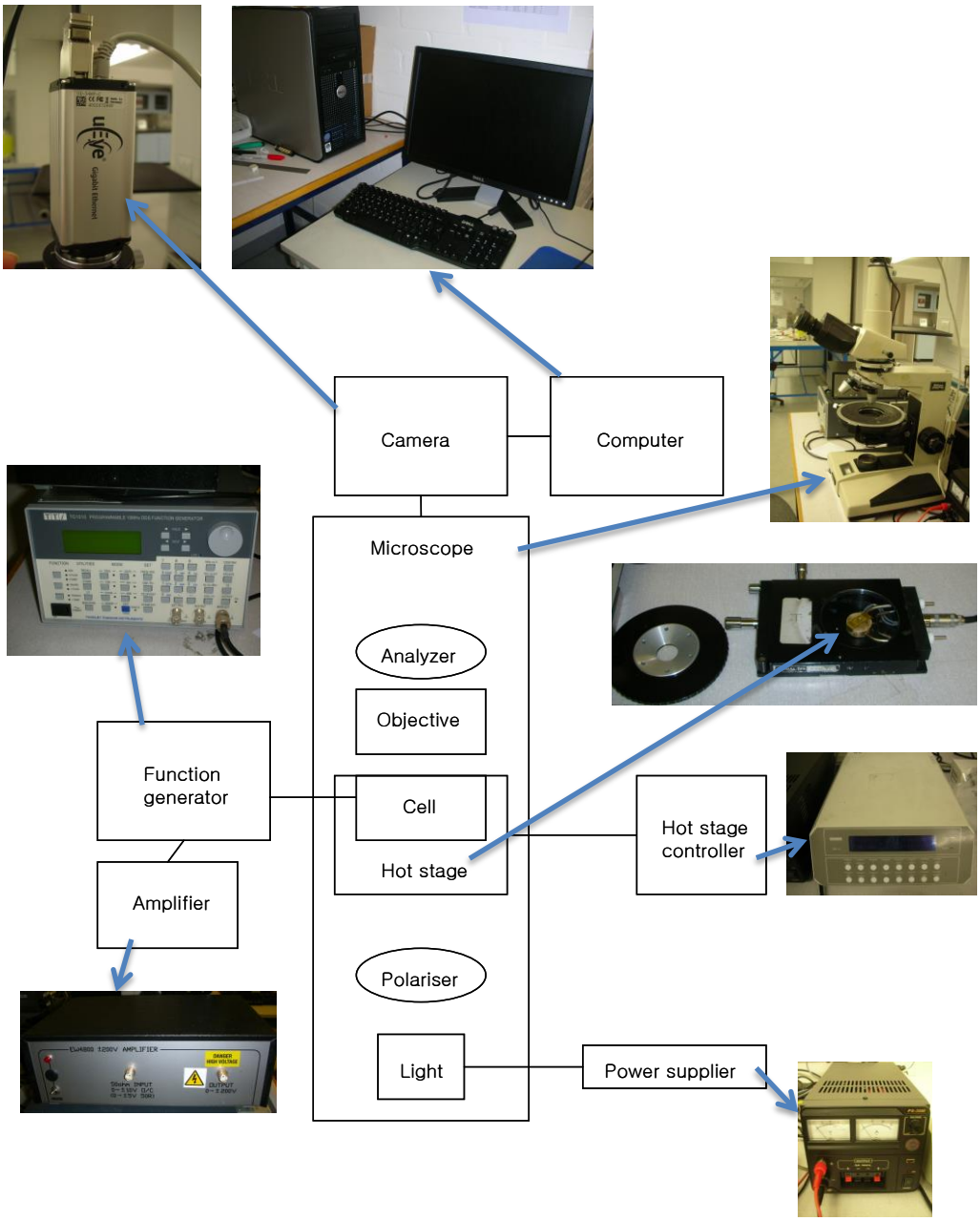

Figure 3.2 Schematic of the experimental set up for observation of particles in liquid crystals.

The electric field that was applied to the sample was generated by a function generator connected to an amplifier. The electric field applied to the cell was in the frequency range from 2Hz to 1000Hz and the amplitude varied from 0 to $30V_{pp}$. At a fixed field amplitude, the motion of the particles was traced in steps of 2-5Hz over frequency ranges of interest. The observed direction of motion of the particles was perpendicular to the direction of the electric field (in the plane of the sample cell).

3.4 Data Analysis

A motion picture was made up of frames which had been taken by the uEye digital camera connected to the polarizing microscope. The 'uEye player' software saved each frame of the motion picture and then the movement of the particle was traced by 'IMAGETOOL3.0' software in the pixel domain. The distance in pixels was then converted into μm units.

The linear velocities of the micron sized particles were calculated from the ratio of the real distance (μm) to time period (seconds) of the movement. The angular velocities of the micron sized spheres were derived from the ratio of the oriented angle (degree or radians) to the time period (seconds). The uncertainties in the measurement were calculated from the degree of inaccuracy involved in defining the centre of the particle with a mouse click in using IMAGETOOL3.0, together with ± 1 pixel (0.278 μm) to locate the centre of the moving particles saved in each video frame. Another

contribution to the uncertainty came from fitting the slope of distance or angle versus time.

Figure 3.3 shows one of the traces of linear translation of a microsphere in a liquid crystal under an applied ac electric field. The plot of distance as a function of time yields the linear velocity (μms^{-1}).

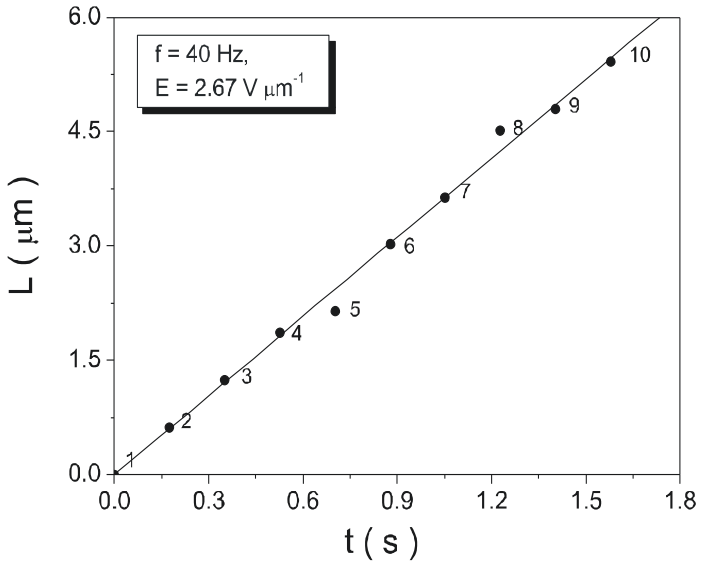

Figure 3.3 Exemplary linear displacement of the particle as a function of time.

Circular motion of a micron-sized spherical particle is shown in figure 3.4. The time interval between each position is 0.018 seconds. The data in figure 3.4 are used to generate Figure 3.5 which is a plot of angle as a function of time. The slope of figure 3.5 gives the angular velocity, ($^{\circ}$ s^{-1}).

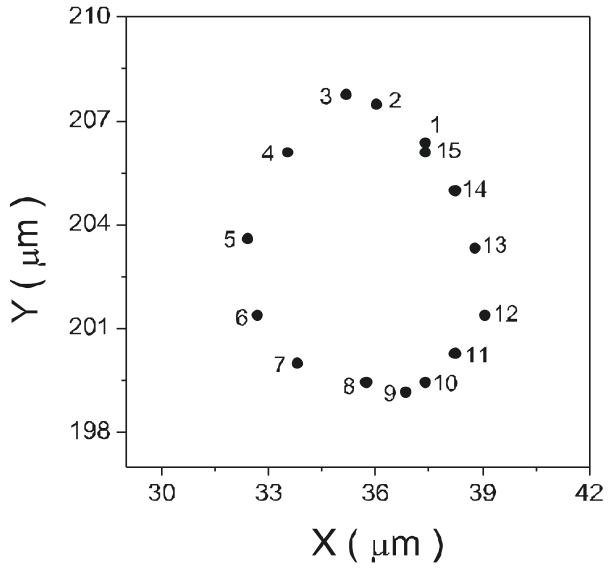

Figure 3.4 Exemplary trace of the circular motion of a spherical particle in an applied electric field.

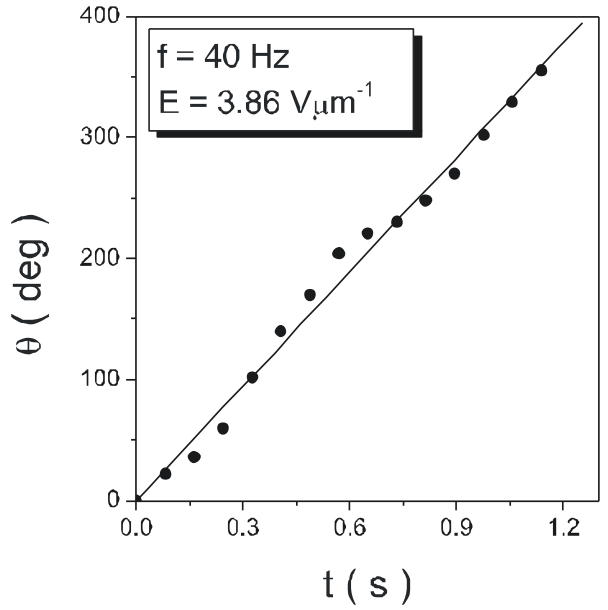

Figure 3.5 The plot of angle moved for a particle as a function of time.

3.5 Summary

This chapter has summarized the experimental methods used in the thesis. Samples of micron-sized particles suspended in chosen liquid crystals are fabricated into cells that allow an electric field to be applied perpendicular to the cell substrates. Polarizing microscopy is used to examine the quality of the alignment as well as to determine the field-frequency regime in which certain types of particle motion can be observed. In cases where linear or circular motion is observed, image analysis is used to determine the linear or angular velocity of the particle. The following experimental chapters use these techniques to study the motion of spherical particles in chiral nematic and isotropic liquid crystals and of elongated particles in nematic systems with different geometries.

3.6 References

[1] I. Dierking, F. Giedelmann, P. Zugenmaier, W. Kuczynskit, S. T. Lagerwall and B. Stebler, *Investigations of the structure of a cholesteric phase with a temperature induced helix inversion and of the succeeding S_c* phase in thin liquid crystal cells.* Liquid Crystals,1993, Volume 13, No.1, pp.45-55.

[2] H. R. Duff, D. C. Gilmer. *High Dielectric Constant Materials,* Springer-Verlag, Berlin, Heidelberg (2005)].

[3] The product information by Nippon Electric Glass Co., Ltd. On the web site as http://www.neg.co.jp/EN/product/LCD.html

[4] I. Dierking, Textures of liquid crystals. 2003, WILEY-VCH GmbH & Co.

Chapter 4

Motions of Spherical Particles in the Chiral Nematic Liquid Crystal Phase

The chiral nematic phase is thermodynamically almost equivalent to the nematic liquid crystal phase, but the chiral nematic phase has a handedness associated with the chirality in the molecules. The handedness in chiral nematic liquid crystals is generated from the director which is twisted into a helix. The spatial scale of the background deformation is normally much larger than the molecular size, and the scale can be recognized as the pitch length of the helix. These helical liquid crystals can undergo additional deformation caused by external fields and surface interactions. Further, a molecular tendency to form smectic layers or a double twisted state can influence the physical properties of the phase in the low or high temperature regimes of the phase. [1] The chiral nematic phase was the first investigated liquid crystal in history, and has been a great subject in physics. Due to their characteristic optical properties, weak or strong twist deformations, and twisted disclinations, the complexity of these helical structures has been attracting intensive interest for decades. Those interests have meant that helical structures of liquid crystals have had impact in areas that range from electronic display devices in industrial developments to the fundamental bio-medical research related to the elasticity of DNA. [2-7]

The experiments in this chapter used chiral nematic liquid crystals which can offer interesting uniform textures in which to investigate the dynamics of micron-sized spherical particles in a chiral phase, under the application of electric fields.

4.1 Motivation

Electrophoretic mobility has been investigated in different kinds of fluids, in which variables include electrolytes, rheology, modification of the geometry of electrodes and specimen cells, the types of external fields, or the character of inclusions (particles). [8-9] Liquid crystals are interesting as systems for colloidal dispersions or suspensions because of their characteristic structures, possessing directors, which can introduce novel forces in those systems as mentioned in the previous chapters of introduction.

When an electric field is applied to colloidal suspensions, linear motions of micron-sized spherical particles are observed along the directors of nematic phases, and in smectic phases linear motions appear along the layers; such observations (2-dimensional or 3-dimensional) were introduced in the previous chapter. Škarabot *et al.* investigated the transport of colloidal particles in nematic liquid crystals in a specimen cell using electric field. [10] Mieda *et al.* reported a 2-dimensional micromanipulation of a negatively charged particle in the nematic phase, controlled with the polarity switch and the duty-ratio of the rectangular-wave voltage which made the liquid

crystal flow. [11] Pishnyak *et al*. investigated the bi-directional levitation of spherical particles in nematic liquid crystal phases under the application of an electric field. [12] West *et al.* measured the drag effect at the nematic-isotropic liquid crystal interface and a pumping effect of the colloidal system (particles in liquid crystals). [13] Takahashi et al. improved the response speed of the mobile fine particle display cells in the nematic liquid crystal system. [14] Yamamoto *et al.* used an electric field to provide dynamic control of a particle-doped lamellar phase for self-assembly of bio-matter. [15] Most work has been carried out on nematic host phases, but Togo *et al.* reported their observation of circular displacement of micron-sized silica particles in a chiral nematic phase under the electric field. [16] The chiral nematic phase is locally very similar to the nematic phase but the direction of the preferred orientation of the molecules (the director) is periodic in space. (The spatial period is $\mathbf{P}/2$ as $\mathbf{n} = -\mathbf{n}$.) Another feature of the chiral nematic phases is their defects; oily streaks are the most common topological defect in chiral nematic liquid crystals, and these can be stabilised by including micron-sized colloidal particles within the network to make gel-like systems. [17]

As summarised above, the dynamics of small particles has been investigated primarily in nematic liquid crystals or smectic liquid crystals; the nematic director is found to influence the motion of particles while the smectic layers offer a channel for the particle motion when the electric field is applied. For chiral nematic liquid crystals, however, the spiral structure can be expected to have an effect on the motions of particles, perhaps inducing circular motion related to the handedness of the chiral material. In this chapter, the motions of particles in liquid crystals are studied using the

chiral nematic materials as the dispersion medium of the particle-liquid crystal composite. This investigation is aiming to deduce whether the dispersed particles can offer microscopic visualization of the chiral nematic phase, or indeed new modes of particle motion in liquid crystals.

4.2 Experimental Results

To investigate the 2-dimensional movement of spherical particles, it is important to have a sample without defects. Thus, the chiral nematic liquid crystal that forms a helicoidal structure between two glass plates, showing the simplest domain, with homogeneous boundary conditions, i.e. the Grandjean planar texture is used in this chapter. The selected material is ((S,S)-EPHDBPE) with phase transition temperatures of C 57℃ S_1 57.2℃ S_c* 78.1℃ N* 95.7℃ I. Below 57℃ the material is in a crystalline solid state, between 57℃ and 95.7℃ the smectic and chiral nematic phases appear, then above 95.7℃ the liquid crystal phase is transformed into an isotropic liquid state. The material is of particular interest as it has an inversion point of the helical pitch, at a temperature between 82.5℃ and 83℃. (from a left handed to a right handed helicoidal structure.) Table 5.1 shows the pitch length of the liquid crystal material as a function of temperature. Minus values depict a left handed helix. [18] Choosing a material with an inversion point allows an investigation of both the magnitude and the influence of the handedness of the pitch on the particle motion. The

temperature in the chiral nematic material ((S,S)-EPHDBPE) selected to describe features of particle motion in detail is 90.3 ℃ ± 0.3℃ because at this temperature the fewest defects in the planar texture are observed. Further, the threshold voltage to the field-induced finger print texture which occurs (above E = 10Vμm^{-1}) is sufficiently high that is does not interfere with the study of particle motion. This Grandjean planar texture gives a nice domain for the observation of the movement of particles.

Temperature (℃)	82.4	82.6	89.9	90. 1	90.9	92.0
Pitch length (μm)	-27. 5	64.8	1.4	1.7	1.5	1.5

Table 4.1 The temperature dependence of the cholesteric pitch. [Dierking *et al*., Liquid Crystals, 1993, Volume 13, No.1, pp.45-55.]

4.2.1 The Stability Regime of the Silica Sphere in the Chiral Nematic Phase

The experiment has been carried out with the homogeneous boundary conditions for the liquid crystal material, using two glass substrates. The thickness between the two substrates is 6 μm, and the diameter of spherical silica particles is 2.5

μm. The geometry of the specimen cell is called a sandwich cell, and the electric field is applied perpendicularly to the substrates.

The types of particle motion observed in this chapter are depicted in Figure 4.1, which is for experiments carried out at 90.3℃. All the motions disappear above the frequency of 400 Hz. Between 200 and 400 Hz, only random motion appears clearly. Below 10 Hz, above 1 $V\mu m^{-1}$, there is also only random motion. As the frequency increases from 10 Hz, linear motion and circular motion appear. Between the frequencies of 10 and 70 Hz, linear motion appears between 1.5 and 4 $V\mu m^{-1.}$ With higher amplitude fields, circular motion dominates in the broad frequency region f = 10 ~ 200 Hz. (There are dotted lines to guide sights in every regime graphs.)

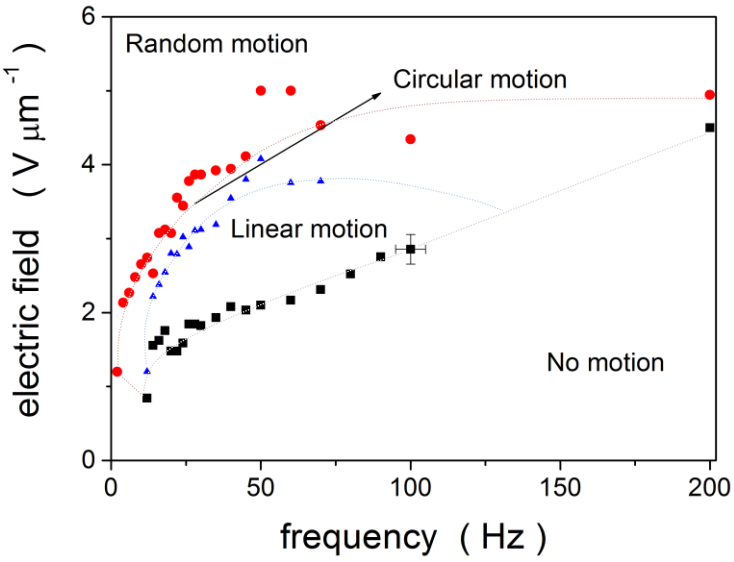

Figure 4.1 The stability regime of the motions of the silica spheres in the chiral nematic phase at 90.3℃. Four types of motions, random motion – circular motion – linear – no motion are included. The red circles are showing the boundary of the

'Random motion' (chaotic flying movement) regime and the 'Circular motion' (circle shaped motions) regime. There is a 'Linear motion' regime between the blue triangles and the black squares. The black squares are the boundary between the 'Linear motion' (1-dimensional line shape motion) and the 'No motion' (zero movement) regime observed on varying the amplitude and frequency of the applied electric field.

As will be discussed later, experiments are not possible at certain temperatures where oily streak textures dominate or the planar texture is not stable. At lower temperatures in the left handed chiral nematic phase (~ 81℃), the planar texture immediately disappears with the applied electric field, even with a very low field ~ 0.5 $V\mu m^{-1}$. At intermediate temperatures (83 ~ 85℃), there is a phase inversion, and the planar texture is not clear because the undulation and the pitch jump are predominant simultaneously in the liquid crystal domain on application of an electric field. At high temperatures (87 ~ 90℃), the pitch jump occurs very obviously and the interface of the different domains disturb the observation of particle motion. Those temperature ranges are therefore not included in the discussion of the temperature dependence of the particle motions. The planar texture becomes most clear above 90℃, then at the 90.3℃, the circular motion and linear motion of particles appears clearly visible using polarizing microscopy.

Using the graph showing the different regimes (Figure 4.1), an analysis of the circular motion and linear motion of the spherical silica particles and their temperature dependence is described in the following sections.

4.2.2 The Circular Motion of the Silica Sphere in the Chiral Nematic Phase

The circular motion appears clearly between the frequency region of f = 10 ~ 100 Hz. Within the circular motion regime of Figure 4.1, a typical trajectory of a circular motion of the silica spheres in the chiral nematic phase can be observed. The exemplary trajectory is Figure 4.2, and the diameter of the circular motion is ~7 μm.

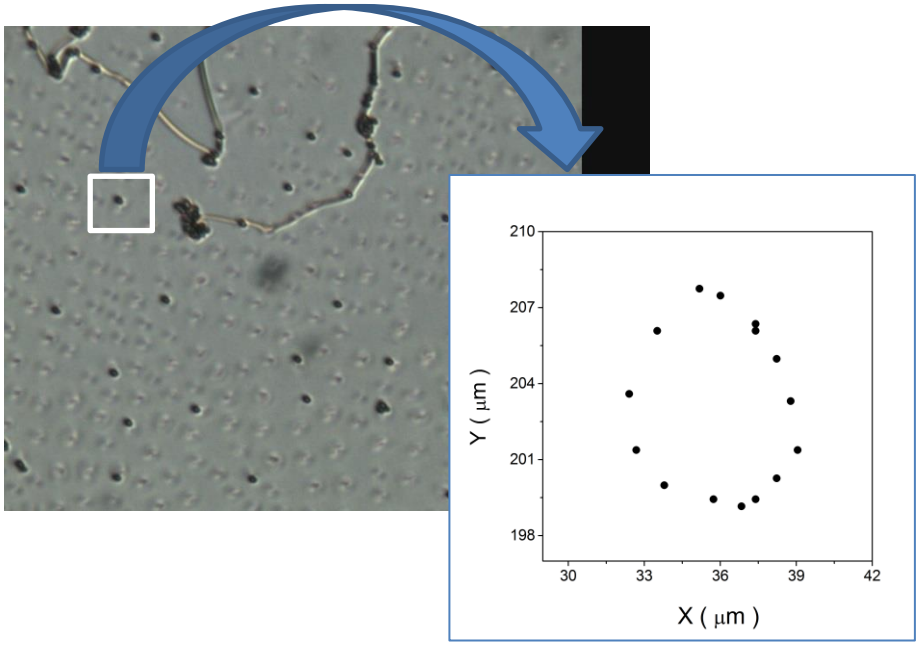

Figure 4.2 An exemplary circular trajectory of the micron-sized silica sphere at 90.3℃. The applied electric field has the value of E = 3.86 Vμm^{-1} and f = 40 Hz.

The direction of the circular motion is random; no dependence of the direction on the handedness of the chiral nematic phase is observed.

4.2.2.1 The Frequency Dependency of the Circular Motion of a Silica Sphere in the Chiral Nematic Phase

With the trajectory of the particles derived from the observation the circular motions, the motion's angular velocity can be calculated. Figure 4.3 is the angular velocity of the particle as a function of frequency. The angular velocity, ω, of the particle motion, increases as the frequency increases within the circular motion regime. The angular velocity of the particle is in the range of 200 ~ 600 ^{o} s^{-1} (3.49 ~ 10.47 rads s^{-1}). Above a frequency of approximately 50 Hz, although circular motion disappears, the velocity is not zero because the motion has not ceased, rather a regime of linear motion of the particle has started.

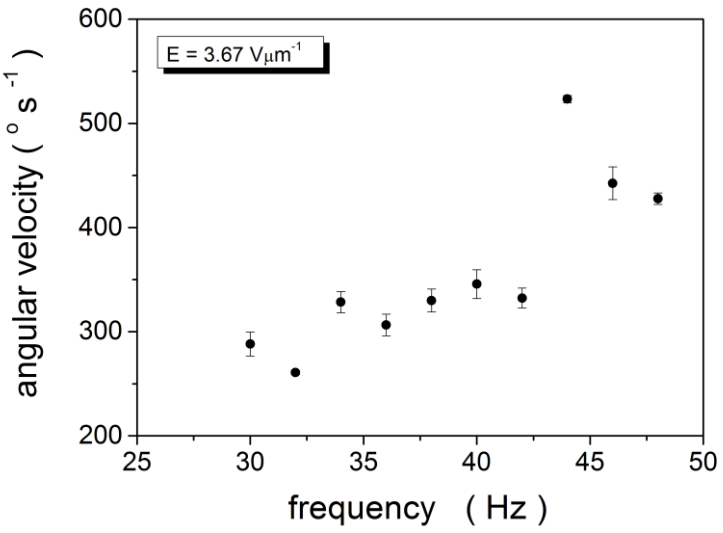

Figure 4.3 The angular velocity of the micron-sized silica sphere as a function of frequency of the applied electric field. The applied electric field is E = 3.67 Vμm^{-1}.

4.2.2.2 The Electric Field Dependency of the Circular Motion of a Silica Sphere

Within the regime of circular motion, the midpoint of the regime is chosen as a typical value for the amplitude of the electric field. At the frequency of 40 Hz, the dependence of angular velocity on the field is shown in Figure 4.4. The velocity increases as the amplitude of the electric field increases. The angular velocity of the particle is in the range of values 150 ~ 600 ^{o} s^{-1} (2.62 ~ 10.47 rads s^{-1}). The electric field necessary for the circular motion is above E = 3.3 Vμm^{-1} at f = 40 Hz. The fitting of the data will be discussed later in section 4.3.1.1

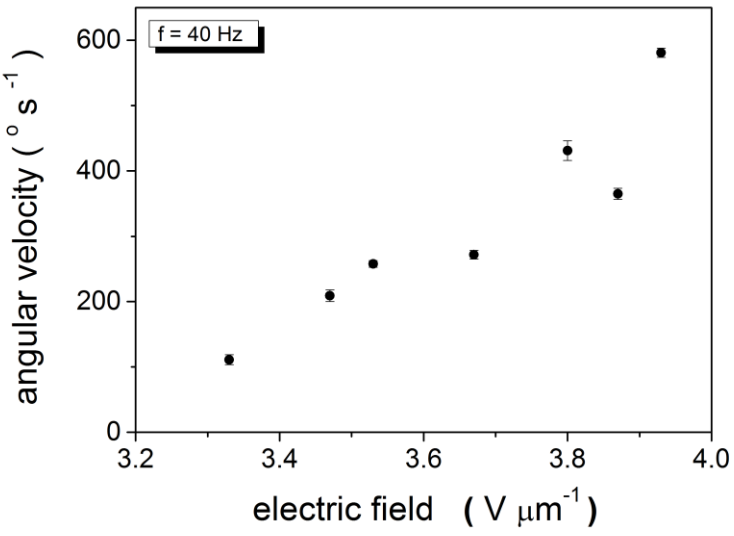

Figure 4.4 The angular velocity of the micron-sized silica sphere as a function of the applied electric field. At a frequency f = 40 Hz.

4.2.3 The Linear Motion of the Silica Sphere in the Chiral Nematic Phase

The chiral nematic liquid crystals possess a helical structure, anchored between the two glass plates and the circular motions appear as described in section 4.2.2. While the linear motion of the particles in the chiral nematic liquid crystal phase is not expected, it is exhibited within the regime. Figure 4.1 shows the regime of the linear motion in the frequency region between f = 10 ~ 100 Hz, E = 1.5 ~ 4 Vμm^{-1}. The trajectories of silica particles exhibiting linear motion show both frequency dependence and amplitude dependence, discussed later. Figure 4.5 is an exemplary trajectory of the linear displacement of a spherical particle.

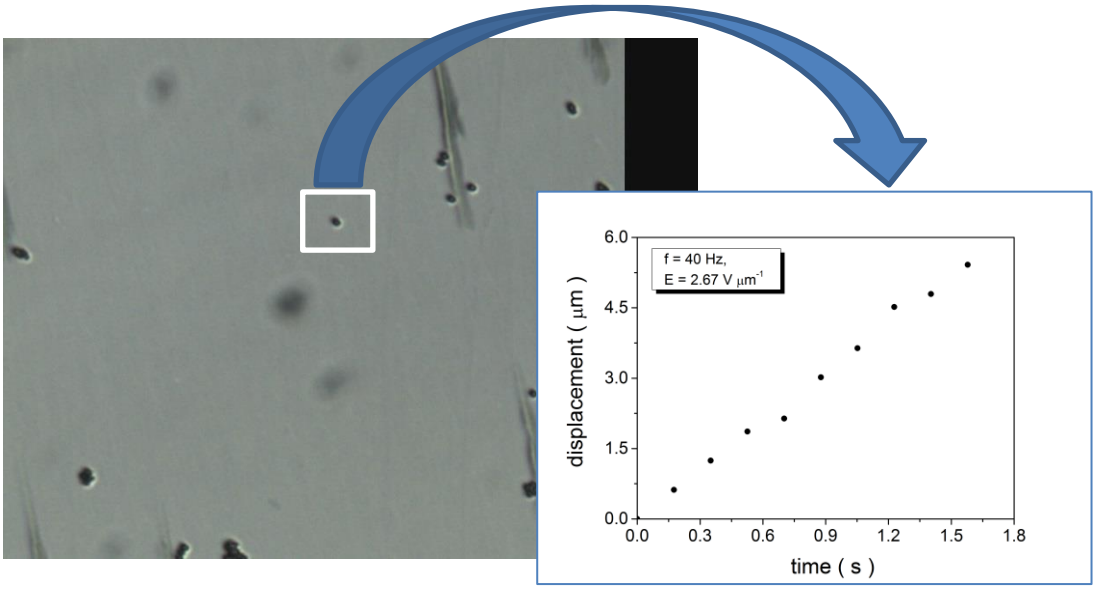

Figure 4.5 An exemplary linear trajectory of the micron-sized silica sphere at 90.3℃. The applied electric field has a value of E = 2.67 Vμm^{-1} and f = 40 Hz.

The direction of the displacement of moving particles does not possesses any preferred direction of the linear motion (e.g. there is no apparent influence of the rubbing direction), therefore the linear motion is analysed by the displacement as a function of time only.

4.2.3.1 The Frequency Dependency of the Linear Motion of a Silica Sphere in the Chiral Nematic Phase

Figure 4.6 depicts the linear velocity of the particle as a function of the frequency of the applied field. The velocity v, of the particle's linear motion decreases as the frequency increases within the linear motion regime. The range of the velocity of the particles undergoing linear motion is 1.5 ~ 4.5 μms^{-1}. Above 70 Hz, not only the linear motion but also other motions disappear, and the velocity becomes zero.

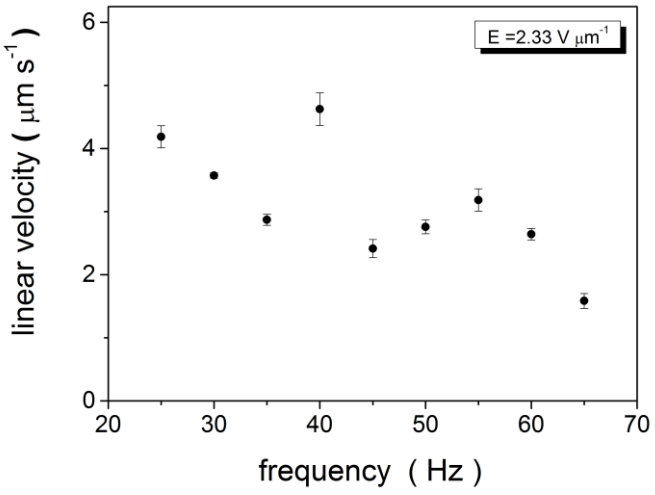

Figure 4.6 The linear velocity of the micron-sized silica sphere as a function of

frequency of the applied electric field. The applied electric field is E = 2.33 Vμm^{-1}.

4.2.3.2 The Electric Field Dependency of the Linear Motion of a Silica Sphere in the Chiral Nematic Phase

Figure 4.7 shows the linear velocity of the particle as a function of the amplitude of the electric field. The linear velocity of the particle increases as the electric field increases and shows an approximately linear dependence. Within the regime of this specific condition, the linear velocity of the particles has the range of 1.5 ~ 6.5 μm s^{-1} with a threshold field of around 1.8 Vμm^{-1}. When E is lower than the threshold, the particle seems to have a tiny vibration in random directions, without displacement in the perpendicular direction to the applied electric field. The fitting of the data will be discussed later in section 4.3.1.4.

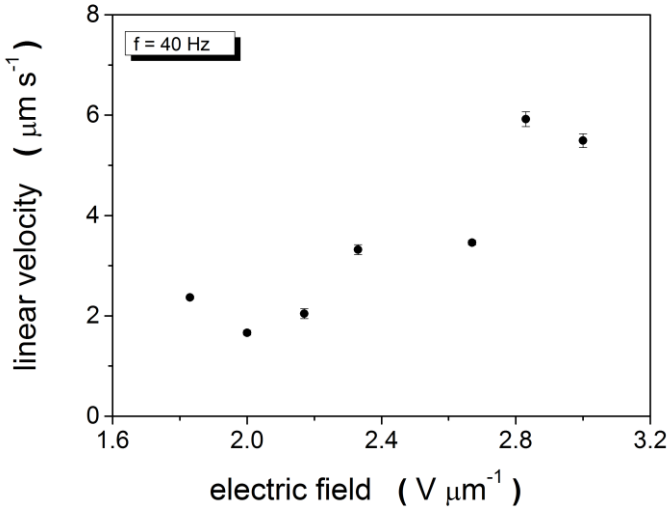

Figure 4.7 The linear velocity of the micron-sized silica sphere as a function of amplitude of the applied electric field. The frequency of the field is f = 40 Hz.

4.2.4 The Temperature Dependence of the Motion of the Spherical Particle the Chiral Nematic Phase

The chiral nematic phase has a phase inversion temperature, where the helical pitch becomes infinite. The planar textures without defects are required so that the particle's motion can follow a clear trajectory of the movement in the domain. The texture exhibited by the chiral nematic material is strongly dependent on temperature. Figure 4.8 indicates the temperature regions where phase inversion and oily streaks occur in the sample studied. Field-induced motion of the particles would only be clearly observed at temperature where the texture is planar. The circular motion of the spherical particles has temperature dependence, while the linear motion has no serious dependence on temperature. Figure 4.8 shows that the angular velocity associated with the circular motion in the planar regimes becomes slower in the higher temperature range. The dashed lines indicate large texture changes in the sample, either from planar to oily streak or pitch inversion, or in purely planar regimes, where a pitch jump occurs. Around the inversion temperature (**PhI**), the circular motions were not observable. The textures with oily streaks or undulation which are sensitive to the electric field (**Un**) are also not available to observe the motions of particles.

At lower temperatures with the left handed chiral nematic phase (~ 81℃), the planar texture immediately disappears even with a very low field (~ 0.5 $V\mu m^{-1}$), thus the motions of particles cannot be observed. In the temperature range of 81 ~ 83.5℃, and 86 ~ 87℃, the particles' motions are nearly all random, and are only seen for a

much smaller regime of field amplitude-frequency space. To compare the motions as a function of temperature, the frequency and amplitude were chosen E = 3.33 Vμm^{-1} and f = 20 Hz. The circular motion at 90.3℃ clearly had a critical field, to be discussed in more detail in section 4.3.1.1. In comparing the angular velocity as a function of temperature, ideally, data at the same value of E/E_c would be used. Unfortunately, however, it was not always possible to obtain sufficiently detailed data of the circular motion for this, for instead, data are compared at the same value of E. Above 90℃, especially 90.3 ± 0.2℃, the oily streaks are disappearing easily, also there is nearly no interface appearance occurred by pitch jumps in the temperature range. The angular velocity decreases from 580~80 ° s^{-1} (10.1 ~ 1.4 rads s^{-1}) as temperature increases as shown in Figure 4.8.

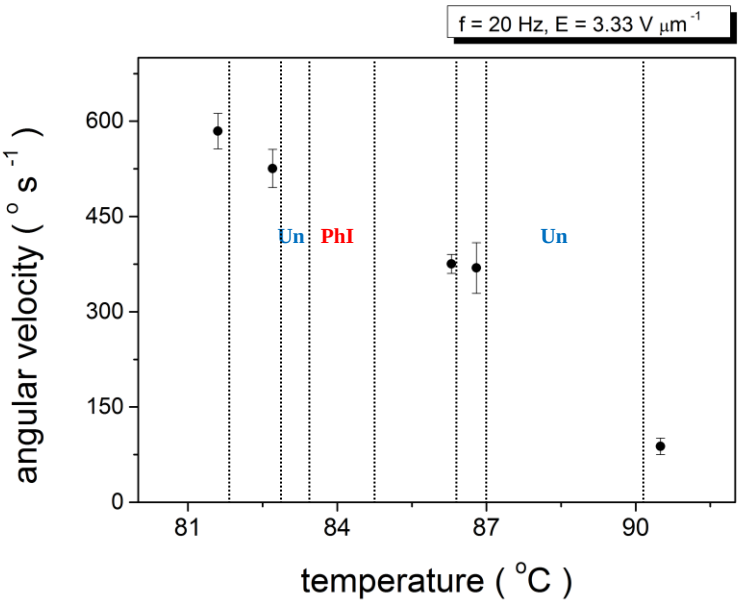

Figure 4.8 The angular velocity of the micron-sized silica sphere as a function of temperature. The applied electric field is E = 3.33 Vμm^{-1} and the frequency of the field is f = 40 Hz.

Where circular motion was observed, there was no relationship between the direction and the handedness of the helix, indeed the direction was arbitrary from experiment to experiment.

4.3 Discussion of the Results

In order to give a full description of the results reported in section 4.2, it is important to describe the properties of the chiral nematic phase, especially the dependence of pitch on temperature, in detail. This chapter will start with inspection of the liquid crystal material.

4.3.1 Chiral Nematic Phase and Geometry of the Sample

The chiral nematic liquid crystal material shows a phase inversion temperature which introduces the change of handedness and the appearance of a planar domain texture with a different helical pitch length. There have been many kinds of chiral nematic liquid crystals made by mixing chiral dopants with liquid crystals, but the material used in this thesis is a single compound exhibiting both chiral nematic and tilted smectic liquid crystal phases, shown in Figure 4.9. Walba *et al*. synthesized and reported the design of the chemical process and an investigation of the Smectic C* phase of the material. [19] Example textures are shown in Figure 4.10.

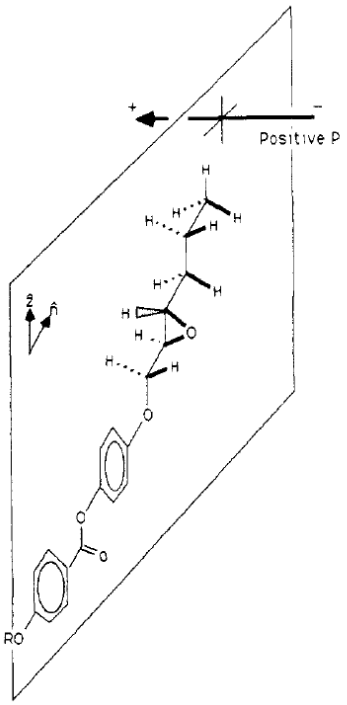

Figure 4.9 The synthesized single compound possessing a helix inversion temperature. [Taken from D. M. Walba *et al*., *Design and Synthesis of New Ferroelectric Liquid Crystals. 2. Liquid Crystals Containing a Nonracemic 2,3-Epoxy Alcohol Unit*. Journal of American Chemical Society. 1986, Volume 108, 7424-7425]

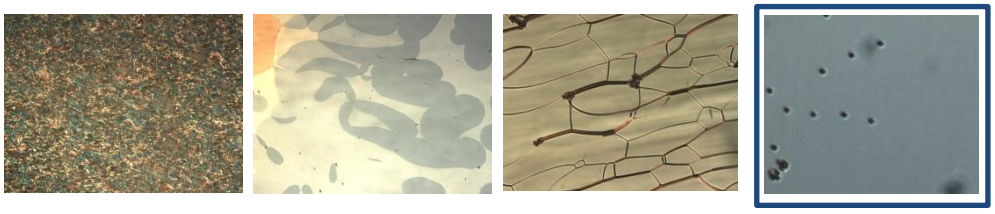

(a) C at 60℃ (b) N* at 81.5℃ (c) N* at 87.2℃ (d) N* at 90.3℃

Figure 4.10 The textures of (S,S,)-EPHDBPE at certain temperatures with particle inclusions. (a) crystalline state of the material. (b) chiral nematic texture with pitch jumps (c) chiral nematic phase with oily streaks. (d) Grandjean planar texture without defects which is the best texture for the experimental work in this chapter.

In this thesis, the experiment is performed with homogeneous boundary conditions. The cell geometry results in several regimes with Grandjean planar textures as the temperature is modified and above 90℃, the planar texture appears without cholesteric defects (oily streaks). The lower temperature Grandjean planar texture is easily distorted with low electric fields, therefore the higher temperature offers a stable planar texture for the investigation of the particle motions. The square wave form with symmetry 50% is used as it causes the least undulation of the liquid crystals' planar domain and causes the perpendicular direction of the movement of particles with respect to the applied electric field in the liquid crystal sandwich cell. Dierking *et al.* measured the pitch of the material which is depicted in the Figure 4.10. [18]

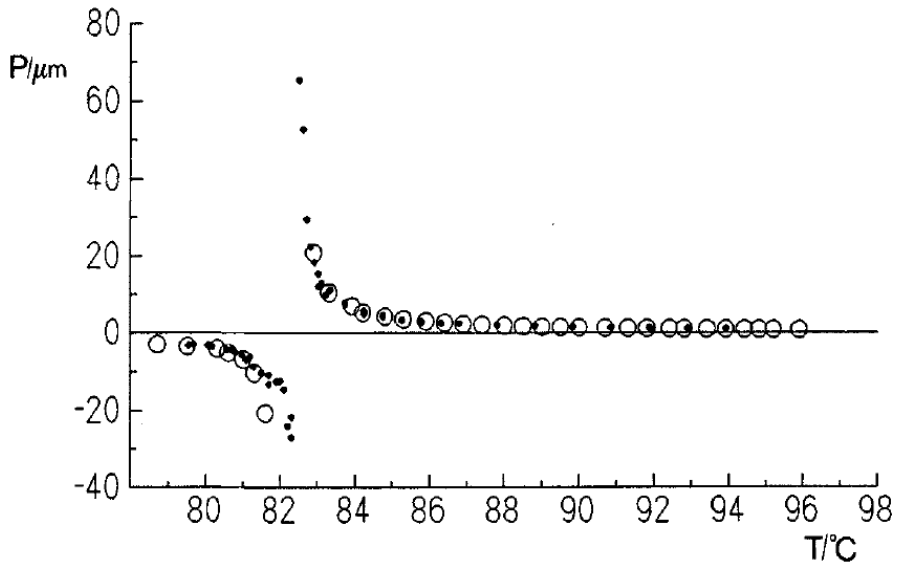

Figure 4.11 The pitch length of the chiral nematic phase as a function of temperature. The black circles are the experimental value of length. The graph shows a helix

inversion temperature around 82.5℃. [Taken from Dierking *et al*., Liquid Crystals, *Investigations of the structure of a cholesteric phase with a temperature induced helix inversion and of the succeeding S_c* phase in thin liquid crystal cells.* 1993, Volume 13, No. 1, pp.45-55.]

The chiral nematic phase constructs 4×2π twists within the 6μm cell gap at 90.3℃, and the ratio of particle diameter (2.5 μm) is approximately half of the cell gap. Using the square wave form of the electric field, the manipulation of particles can be promoted toward the direction of the 2-dimensional movement which is parallel to the substrates and perpendicular to the applied electric field. Figure 4.12 is a schematic diagram of specimen cell, showing approximately how both the particle dimension and the pitch are constrained by the substrates.

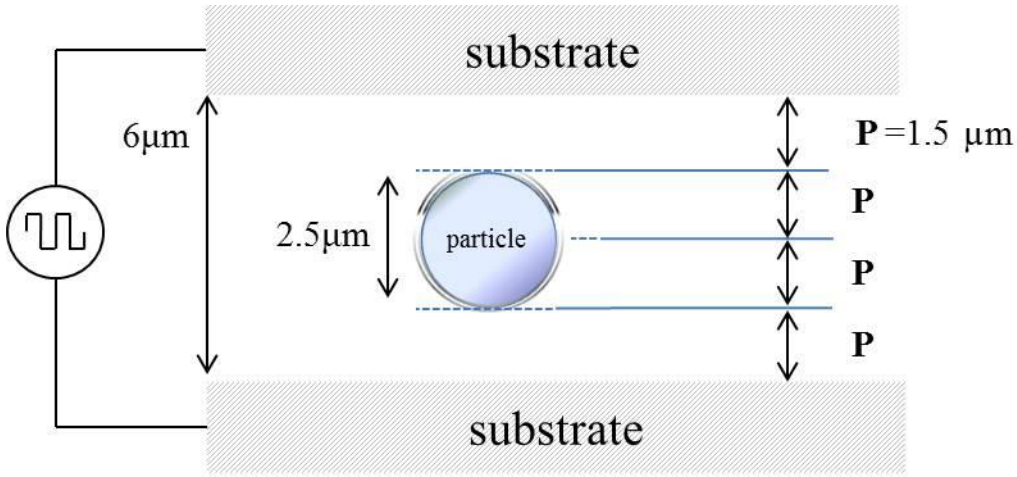

Figure 4.12 Schematic diagram of a sample cell with a side view when particle motion is observed at 90.3℃. There are the homogeneous boundary conditions for

liquid crystal alignment on the substrates, and a planar boundary condition around the silica particle.

4.3.2 Chiral Nematic Phase and Motions of Particles

As shown in figure 4.1, the movement of the particles is complicated (to observe the motion types, and appearing their motion types). In the regime, wherever movement occurs, the random motion appears over the widest range with respect to the electric field amplitude and frequency. The random motion is the displacement of the particles with largely different distances as a function of time, and the direction of the movement changes quickly. There is no relationship of the angles between the directions of the movement within time domain and no regular displacement, therefore the motions are called ‘Random’. This irregular movement of the particles in the higher field with too fast to track with our observation system. The dynamics of the random motions were not measured in this experiment, where study was focused on circular motions and linear motions. The following sections will discuss the dependence of both motions on electric field.

4.3.2.1 Dependence of Angular Velocity on Field Amplitude

The silica particles show that their angular velocities increase as the amplitude of electric field increases (Figure 4.2.) and also increases with frequency (Figure 4.4.).

The amplitude of the electric field has an effect on the circular motion. In this experiment, the dispersion medium (the liquid crystal material) and dispersed solid (the silica sphere) satisfy the condition required for a stable Quincke rotation. [20] The detailed investigation of the circular motion has been performed an observation in the optimum (planar) domain for the trajectory of particle motions. The circular displacement is a 2-dimensional motion which is perpendicular to the applied electric field, induced by the symmetry of electric field with alternating voltage (a square wave form) and cell geometry (the particle diameter is nearly a half of the cell gap). The direction of the movement is not related to the handedness of the chiral liquid crystal phase in this experiment. Similar circular motion in the chiral nematic phase has been repeated only by one other group [16], though they did not attempt to analyse features of the circular motion. Although Quincke rotation applies to particles rotating on their axis, and the particles in the liquid crystal satisfy the relevant conditions, such an analysis is now considered with respect to the circular motion. Thus, the circular motion is analysed by:

$$\omega = \frac{1}{\tau_{MW}} \sqrt{\frac{E^2}{E_{cr}^2} - 1} \ , \tag{4.1}$$

where τ_{MW} is the Maxwell-Wagner interfacial polarization relaxation time, E is electric field, E_{cr} is critical voltage for moving of the particles in the chiral nematic phase. At f = 40 Hz, the circular motion of particle exhibits the angular velocity as a function of amplitude of the field as shown in Figure 4.4. The data of Figure 4.4 is fit to Equation 4.1 using the rearranged Equation 4.2:

$$\omega^2 = \left(\frac{1}{\tau_{MW}}\right)^2 \left(\frac{E^2}{E_{cr}^2} - 1\right). \quad (4.2)$$

Figure 4.13 shows the data fit to equation, and the fit calculates the E_{cr} = 3.1 ± 0.1 Vμm^{-1} and τ_{MW} = 3.91 ± 0.14 s. The critical field is in nice agreement with the experimental value that there were no circular motions induced by fields below around 3 Vμm^{-1}. The charge relaxation time fits well with the experimental work of chiral nematic phase and particle system in this chapter, because there are 3 ~ 4 seconds of initiation time which is needed to start the circular motions after the application of the electric field.

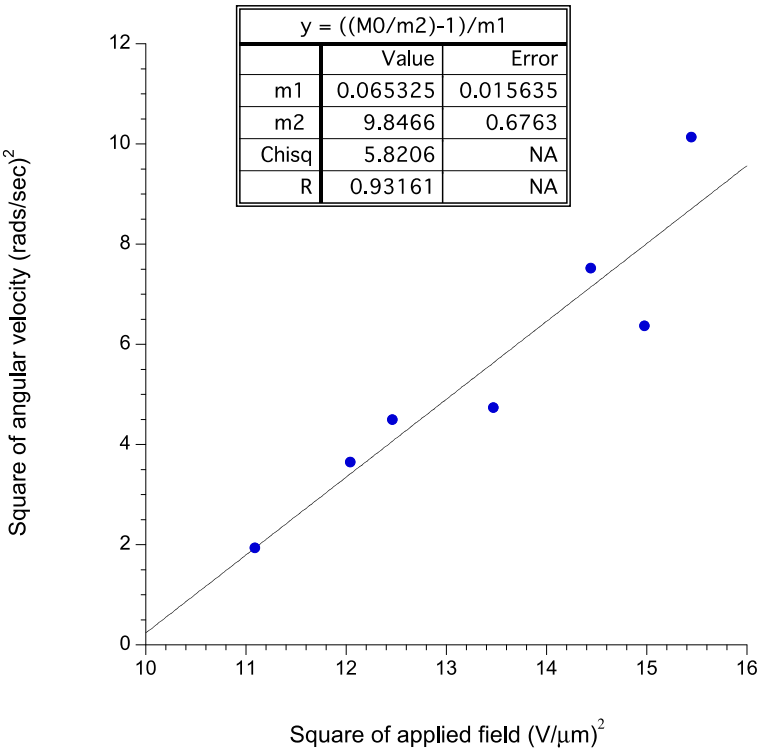

Figure 4.13 The data plot of the square of the critical field versus the square of angular velocity. The straight line shows the fit to equation 4.2 which gives the values of E_{cr} and τ_{MW} indicated in the text. y = ω^2, M0 = E^2, m2 = E_{cr}^2 , m1 = τ_{MW}^2 .

4.3.2.2 Frequency Dependence of Motions in Chiral Nematic Phase

The angular velocity of circular motion increases with the frequency of the electric field, however the regime of the circular motions are stable below 100 Hz, while the linear motions of the particles fade in the frequency region between 75 ~ 100 Hz. The maximum frequency where the motions stop can be used for the calculation of an ion diffusion coefficient using Schwarz's formula [21] :

$$f_{max} = \frac{1}{\tau_{\mathrm{DEL}}} , \tag{4.3}$$

$$\tau_{\mathrm{DEL}} = \frac{r^2}{2D} , \tag{4.4}$$

where r is the radius of the particle, τ_{DEL} is delay time, D is ion diffusion coefficient. [21] In this chiral nematic phase, the ion diffusion coefficient is found to be ~ 7.8 × $10^{-11}m^2s^{-1}$ using equation 4.3 and 4.4. This value is much smaller than the ion diffusion coefficient found by a similar calculation in the isotropic phase (D_{iso} ~ 3.1 × $10^{-11}m^2s^{-1}$) which will be discussed its calculation in chapter 5.

The ratio of $D_{110℃\ of\ Iso}$ / $D_{90.3℃\ of\ N*}$ is generally related to the viscosity of the material at the specific temperatures by Stoke-Einstein relation, [22] where the ratio calculated by:

$$\left(\frac{D^0\eta^o}{T}\right)_{T_1} = \left(\frac{D^0\eta^o}{T}\right)_{T_2} \quad , \tag{4.5}$$

where η is viscosity, T is absolute temperature. Using equation 4.5, the ratio of $D_{110℃\ of\ Iso}$ / $D_{90.3℃\ of\ N*}$ can be calculated by:

$$\left(\frac{D^o_{110℃}}{D^o_{90.3℃}}\right)_{LC} = \frac{\eta^o{}_{90.3℃}}{\eta^o{}_{110℃}} \times \frac{273.15+110}{273.15+90.3} \quad . \tag{4.6}$$

Equation 4.6 shows that the viscosity of the chiral nematic phase is approximately 3.8 times higher than its isotropic phase, the isotropic phase. The fact that the chiral nematic phase has a 4 times smaller D than the isotropic phase is because the chiral nematic phase is an ordered fluid. Typical values of D in nematic liquid crystals is ~10^{-11} m^2 s^{-1}, so the chiral nematic phase has 7 times higher value of $D_{\text{nematic phase}}$. There are very few measurements of D in the chiral nematic phase, but figure calculated here is reasonable as it might be expected that the helical structure results in a lower ionic diffusion than the more simply ordered nematic phase.

4.3.2.3 Dependence of Angular Velocity on Temperature

The most important object of this chapter is to measure the dynamics of circular motions of particles to find out whether the motion is related to the handedness of the chiral nematic phase or not. The investigation of the circular motions has been performed in the best domain for the trajectory of particle motions. The direction of the circular motion was observed for several different experiments, but there was no-handedness dependency. Therefore the expected effect of the chiral nematic material's alignment in-between the cell has been revealed to have no effect on the motions of the spherical inclusions in this system. Togo *et al.* investigated a similar system (but longer pitch than cell gap) and concluded that the effect of the anisotropy of the molecular alignment on the particle action was hardly shown. [16]

Figure 4.8 shows the angular velocities are higher at lower temperatures for a given electric field. The electric field application is focused on finding the common regime of circular motion of the particles. It was not easy to find several planar domains where circular motions are observed without strong undulation or defects or perturbation. There are only a few temperature regions with such reasonable domains for observing circular motions. As the temperature increases, the fluid's viscosity decreases, therefore it might be expected that the angular velocity increases, but the opposite is observed. Thus the angular velocity changes are not related to the liquid crystal's viscosity. Further, the ion diffusion coefficient ratio of the chiral nematic phase is smaller than the isotropic phase by a factor of ~ 4, and is also ~ 7 times higher than the nematic phase ~7. Thus, the chiral nematic material could be a good dispersion medium which has a short charge separation time so that the dispersed

particles can be moved with lower energy companied with fast speed in the dispersion system. These characteristics have great potential for applications.

As a final comment in this section, it is worth noting that in this system, a larger *D* than in the nematic phase means that the finite time needed to induce an electric dipole is shorter. Consequently, the critical maximum frequency (above which particle motion ceases) is larger than in nematic systems. Therefore, chiral nematic materials show broader regions of interest (field amplitude-frequency space) where particle motion can be observed, making them interesting materials for future study.

Although the angular velocities of particles at each planar domain in different temperatures do not depend on viscosity, of it could depend on the stability of the planar textures in this experimental condition. The perturbations appearing in the planar domains interfere very much in several cases, when the temperature region reaches the helix inversion temperature, and when oily streaks predominant to the textures increase. Even planar textures which are stable within certain temperature ranges, experience undulation of the planar domain with the application of electric field. Helfrich investigated the deformation about a 2-dimensional undulation in the plane parallel to the cell surface. The threshold voltage of the undulation of the planar domain is proportional to the twisting power. [23-24]

The twisting power of the liquid crystal material becomes higher as temperature increases from 80℃ to 94℃ in this material. [18] Figure 4.14 shows that the pitch^{-1} values are ~ 0.6 μm^{-1} at 90.3℃, ~ 0.3 μm^{-1} at 87℃, ~ -0.3 μm^{-1} at 81℃.

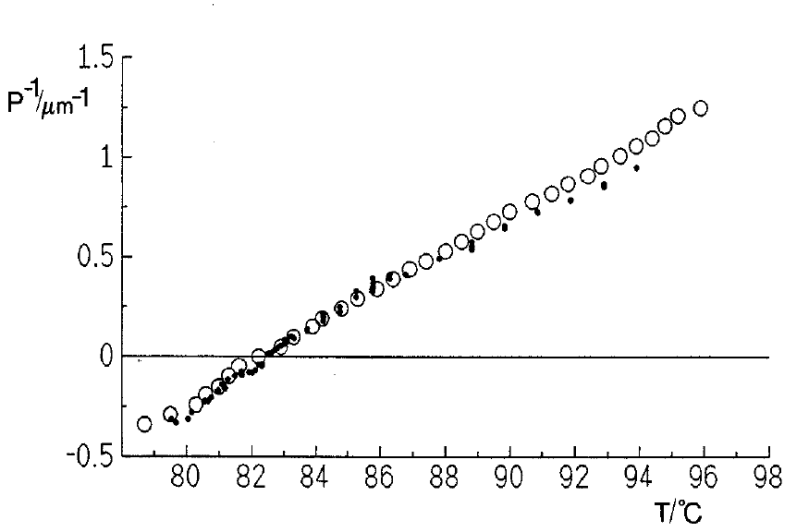

Figure 4.14 The twisting power of the liquid crystal material as a function of temperature. The black circles are experimental values by the Cano-Grandjean method and the white circles are values calculated from the colour change observation. [18] The experimental results are both fit well showing helix inversion as temperature changes. (The negative values indicate a left handed and the positive values indicate a right handed helicoidal structure.) The zero point is where the pitch length is infinite (∞) at the inversion temperature (~ 82.5 ℃) . [Taken from Dierking *et al.*, *Investigations of the structure of a cholesteric phase with a temperature induced helix inversion and of the succeeding S_c* phase in thin liquid crystal cells.* Liquid Crystals, 1993, Volume 13, No. 1, pp.45-55.]

Chiral nematic liquid crystals show higher perturbation field in their shorter pitch [24-26]. In the observation of our system, the system shows bigger perturbation field (Helfrich Threshold) as shorter pitch area as well. The threshold with circle shape periodic perturbation in our system is just below the critical field ($\boldsymbol{E}_c$) where a circular

motion of a particle starts at 90.5℃. Our longer pitch regimes of planar textures show less undulation (higher Helfrich threshold field) as Helfrich, and Hurault explained in their works, thus the particle's circular motion results in higher angular velocity without undulation disturbance. Nevertheless, at the lower temperature the lower twisting power regimes show easy pitch jumps due to the applied electric fields, thus the particle motion is disturbed by the undulation. So, as Figure 4.8 shows, as temperature increases the particle motion shows a smaller angular velocity. 81℃ and 87℃, **P** = 3 ~ 4 μm, **P** ~ d (as d = 2.5 μm) might disturb the planar structure. 90.3℃, **P** = 1.3 μm, **P** ~ not d (d = 2.5 μm) at least 2 turns up and down of the particle in the sample cell. The twisting periodicity might be effect on the particle motions with less freedom.

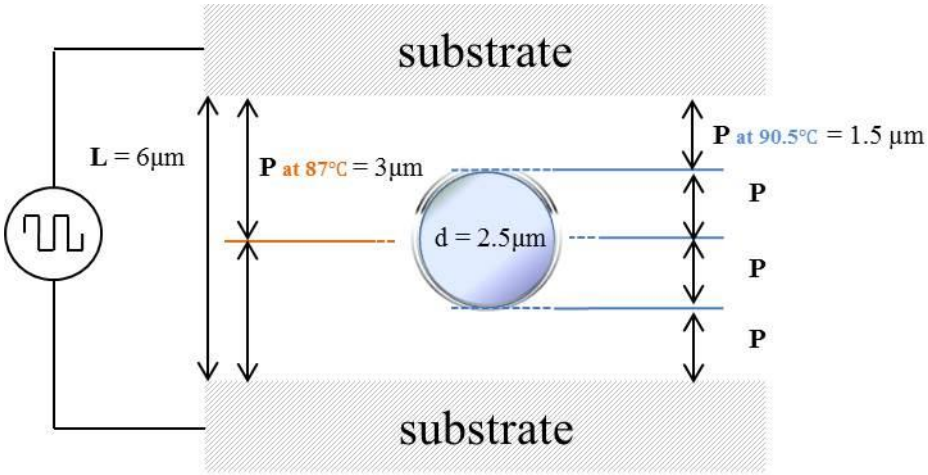

Figure 4.15 The schematic diagram of the sample cell with a side view which shows pitch at longer pitch regime (an example at 87℃) and shorter pitch regime at 90.5℃. In a case of 87℃, the helical pitch can be 2π turns far away from the spherical particle, but around the particle the liquid crystal's helical structure cannot be periodic(without

2π turns), while in higher temperature there could be spatial periodicity with 2π turns up and down of the particle inclusion. **L** is cell gap, the substrate is ITO coated glass plate.

The diameter of the circular motion is found to be nearly same as the cell gap, the undulation of the chiral nematic phase might drag the particles to move. The out typical domains are not showing the Williams domains, but circular shape undulation when we see from above, therefore the newly circular dragging flow using a new theoretical model would be a future work for chiral nematic liquid crystals with spherical particles.

4.3.2.4 Velocity of Linear Motion

The silica spherical particles in the chiral nematic phase show that their linear velocities increase as the amplitude of electric field increases (Figure 4.7), and there is no specific dependence on frequency of the field (Figure 4.6). The field induced linear motions of spheres have been observed in several nematic liquid crystal systems, smectic liquid crystal phases. Dierking *et al*, observed electrophoretic mobility which is perpendicular to electric field [27-28], Ryzhkov *et al*., calculated the electrophoretic mobility using the equation with cubic term. [29]

In this chapter, the chiral nematic phase shows Grandjean Planar texture without undulation in the regime of linear motion of the particle, so the critical field

which moves a particle with a linear displacement is lower than the critical field of undulation. The linear displacement movement has no preferred direction but the amplitude of the applied electric field drives the linear motion faster as in the nematic phase Dierking *et al*. and Ryzhkov *et al*., reported. The experimental data is fitted using the traditional linear electrophoretic mobility under the applied electric field ***E*** with our E_{cr} and nonlinear electrophoretic mobility with cubic term to find better fitting.

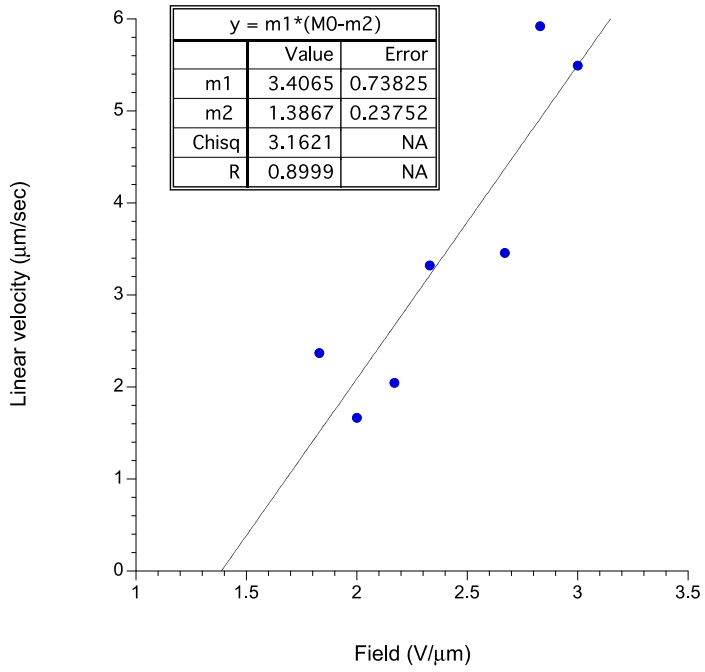

Figure 4.16 The data plot of amplitude of electric field versus linear velocity. The straight line shows the fit to an equation $v = a(E-E_{cr})$, gives the values of E_{cr} indicated on the figure (~1.4 V/µm). y = v, M0 = E, m2 = E_{cr} .

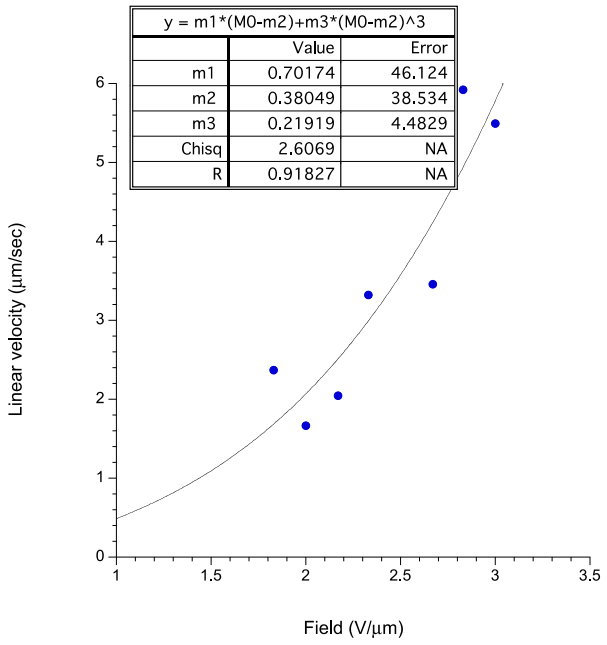

Figure 4.17 The data plot of amplitude of electric field versus linear velocity. The straight line shows the fit to an equation $\nu = a(E-E_{cr}) + b(E-E_{cr})^3$, gives the values of E_c indicated on the figure (~0.4 V/µm). y = ν, M0 = *E*, m2 = E_{cr} .

The experimental data of spherical particle's linear motion fit well to both equations. However, cubic term included in the equation gives an unreasonable value for the critical field E_{cr} , but without cubic term, the critical field is much closer to our observation. Therefore, using the electrophoretic mobility equation the linear velocity observed in this chapter can be expressed by electrophoresis. (Figure 4.16)

4.4 Conclusions

In this chapter, the detailed investigation of spherical silica particles results in circular and linear motions in the chiral nematic liquid crystal phase. The circular motion has no dependence of direction on the handedness of the chiral nematic phase. Field dependence of the angular velocity can be analysed by Quincke rotation. Critical frequency allows an estimate of ion diffusion coefficient which is physically reasonable. The unusual temperature dependence of the circular motion cannot be explained with the relation to viscosity, but undulation. Linear motion of the particle starts above E_{cr} . Where linear motion occurs, it has similar features to nematic and other electrophoretic systems, but the constrained geometry of the thin cell gap results in electrophoretic mobility without cubic term.

The motions become faster with amplitude of electric field. Frequency did not have such a strong effect on the motion but the maximum frequency occurs as ion diffusion may have an effect on the liquid crystal-particle composite system.

The behaviour appears to depend very strongly on the balance of different length scale, i.e. pitch length, particle diameter and cell thickness. These give a good idea for future work.

4.5 References

[1] Heinz-Siegfried Kitzerow and Christian Bahr, Chirality in Liquid Crystals. 2001, Springer-Verlag New York, Inc.

[2] M. Goh, M. Kyotani, K. Akagi, *Highly twisted helical polyacetylene with morphology free from the bundle of fibrils synthesized in chiral nematic liquid crystal reaction field.* Journal of the American Chemical Society, 2007, Volume 129, Number 27, pp. 8519–8527.

[3] S. Chen, L. Chen, *Flow effect in the chiral-homeotropic liquid-crystal cell.* Applied Physics Letters, 1999, Volume 75, Number 22, pp.3491-3493.

[4] G. Petriashvili, K. Japaridze, L. Devadze, C. Zurabishvili, N. Sepashvili, N. Ponjavidze, M. P. De Santo, M. A. Matranga, R. Hamdi, F. Ciuchi, R. Barberi, *Paper like cholesteric interferential mirror.* Optics Express, Volume 21, Issue 18, 2013, pp. 20821-20830.

[5] J. Guo, J. Zhang, Q. Zhang, N. Jianga, and J. Wei, *Fabrication of cholesteric liquid crystal microcapsulates by interfacial polymerization and potential as photonic materials.* Royal Society of Chemistry Advances, 2013, Volume 3, Issue 44, pp.21620-21627.

[6] J. L. Sikorav, J. Pelta, and F. Livolant, *A liquid crystalline phase in spermidine-condensed DNA.* Biophysical Journal, Volume 67, Issue 4, October 1994, pp.1387–1392.

[7] A. Leforestier and F. Livolant, *Supramolecular ordering of DNA in the cholesteric liquid crystalline phase: an ultrastructural study*. Biophysical Journal, 1993, Volume 65, Issue 1, pp.56–72.

[8] A. T. Andrews, Electrophoresis: theory, techniques, and biochemical and clinical applications. 1986, Oxford University Press.

[9] I. D. Morrison and S. Ross, Colloidal Dispersions-suspensions, emulsions, and foams. 2002, John Wiley and Sons, Inc., New York.

[10] M. Škarabot, U. Tkalec, and I. Muševič, *Transport and crystallization of colloidal particles in a thin nematic cell.* The European Physical Journal E, 2007, Volume 24, pp.99–107.

[11] Y. Mieda and K. Furutani, *Two-dimensional micromanipulation using liquid crystals.* Applied Physics Letters, 2005, Volume 86, Issue 10, pp.101901/1-3.

[12] O. P. Pishnyak, S. Tang, J. R. Kelly, S.V. Shiyanovskii, and O. D. Lavrentovich, *Levitation, Lift, and Bidirectional Motion of Colloidal Particles in an Electrically Driven Nematic Liquid Crystal.* PHYSICAL REVIEW LETTERS, 2007, Volume 99, pp.127802/1-4.

[13] J. L. West, K. Zhang, D. Andrienko, Yu. Reznikov, and Anatoliy Glushchenko, *Liquid crystals as a tool for forming photonic crystals.* Proceedings of SPIE, 2005, Volume 5733, pp.32-38.

[14] T. Takahashi, M. Ogawa, S. Saito, Y. Toko, K. Kobayashi, M. Kimura, and T. Akahane, *Improvement of Response Speed for Mobile Fine Particle Display Cells by Adding Charge Transfer Complex Dopant*. Molecular Crystals and Liquid Crystals, 2005, Volume 433, pp.317–328.

[15] J. Yamamoto and H. Tanaka, *Dynamic control of the photonic smectic order of membranes.* Nature Material, 2005 January, Volume 4, pp.5-80.

[16] T. Togo, K. Nakayama, M. Ozaki, and K. Yoshino, *Electric Field-induced Migration of SiO_2 Particles in Smectic Liquid Crystal.* Japanese Journal of Applied Physics, 1997, Volume 36, pp.L1520-L1522.

[17] M. Zapotocky, L. Ramos, P. Pouline, T. C. Lubensky, and D. A. Weitz, *Particle-Stabilized Defect Gel in Cholesteric Liquid Crystals*. Science, 8 January 1999, Volume 283, pp.209-212.

[18] I. Dierking, F. Giedelmann, P. Zugenmaier, W. Kuczynskit, S. T. Lagerwall and B. Stebler, *Investigations of the structure of a cholesteric phase with a temperature induced helix inversion and of the succeeding S_c* phase in thin liquid crystal cells.* Liquid Crystals, 1993, Volume 13, No.1, pp.45-55.

[19] D. M.Walba, R. T. Vohra, N. A. Clark, M. A. Handschy, J. Xue, D. S. Parmar, S. T. Lagerwall, and K. Skarp, *Design and Synthesis of New Ferroelectric Liquid Crystals. 2. Liquid Crystals Containing a Nonracemic 2,3-Epoxy Alcohol Unit*. Journal of American Chemical Society. 1986, Volume 108, pp.7424-7425.

[20] T. B. Jones, *Quincke Rotation of Spheres*. IEEE Transactions on industry application, JULY/AUGUST 1984, Volume IA-20, No. 4, pp.845-849.

[21] G. Schwarz, *A theory of the low-frequency dielectric dispersion of colloidal particles in electrolyte solution.* THE JOURNAL OF PHYSICAL CHEMISTRY, 1962, Volume 66, pp.2636-2642.A. ; Ørjan G. Martinsen, S. Grimners and H. P. Schwan, Interface phenomena and dielectric properties of biological tissue. Encyclopedia of Surface and Colloid Science, 2002, pp.2643-2652. Marcel Dekker,

Inc. ; V. Ryzhkova, F. V. Podgornov, and W. Haase, *Nonlinear electrophoretic motion of dielectric microparticles in nematic liquid crystals*. APPLIED PHYSICS LETTERS, 2010, Volume 90, pp.151901. ; Yue Hu and Michelle W. Chen, *Computer simulation of polarization of mobile charges on the surface of a dielectric sphere in transient electric fields.* Journal of ELECTROSTATICS, 1998, Volume 43, pp.19-38. ; T. Bert and H. D. Smet, *The microscopic physics of electronic paper revealed*. Displays, 2003, Volume 24, pp.103-110 (pp.223-230).

[22] J. H. Simpson and H. Y. Carr, *Diffusion and Nuclear Spin Relaxation in Water.* Physical Review, 1958, Volume 111, Number 5, pp.1201-1202.

[23] W. Helfrich, *Deformation of cholesteric liquid crystals with low threshold voltage*. Applied Physics Letters, 1970, Volume 17, pp.531-532.

[24] J. P. Hurault, *Static distortions of a cholesteric planar structure induced by magnetic or ac electric fields*. The Journal of Chemical Physics, 1973, Volume 59, pp.2068-2075.

[25] C. J. Gerritsma and P. Van Zanten, *Periodic perturbations in the cholesteric plane texture*. Physics Letters A, 1971, Volume 37, Issue 1, pp. 47-48.

[26] F. Rondelez and J.P. Hulin, *Distorsions of a planar cholesteric structure induced by a magnetic field.* Solid State Communications, 1972, Volume 10, Issue 11, pp.1009-1012.

[27] I. Dierking, G. Biddulph, and K. Matthews, *Electromigration of microspheres in nematic liquid crystals.* PHYSICAL REVIEW E, 2006, Volume 73, pp.011702.

[28] I. Dierking, P. Cass, K. Syres, R. Cresswell, and S. Morton, *Electromigration of microspheres in ferroelectric smectic liquid crystals*. PHYSICAL REVIEW E, 2007, Volume 76, pp.021707.

[29] A. V. Ryzhkova, F. V. Podgornov, and W. Haase, *Nonlinear electrophoretic motion of dielectric microparticles in nematic liquid crystals.* Applied Physics Letters, 2010, Volume 96, Issue 15, pp.151901.

Chapter 5

Motions of a Spherical Particle in the Isotropic Phase

The liquid crystal mesogens as the temperature increases on a temperature scale exhibit the following sequence; crystalline solid – liquid crystal phases – isotropic liquid. In a lower temperature range below the liquid crystalline phases, the structure of a crystalline solid exists. A crystal possesses a three-dimensional periodic lattice where the centres of the molecules are located on, over a long-range order possessed by the crystal. At the melting point of a crystal, the crystalline solid starts to melt into a liquid crystal phase. As previously mentioned, a liquid crystal phase has no positional order (or extremely reduced) and/or a long-range orientational order of the molecules (and some of liquid crystal materials have the bond orientational order in certain phases like smectic, hexatic phases). When a liquid crystal phase is heated up over the clearing point, the anisotropic nature changes into an isotropic structure. The liquid has a short-range order between the molecular centres of mass, and the structure possesses a three dimensional translational degree of freedom. Therefore, above the clearing point the director of the liquid crystal phase disappears. [1]

The previous chapter has introduced the experiments where a chiral nematic phase has been used as a dispersion medium. It also presents the electric field induced motion of a spherical particle in a chiral nematic medium. This chapter presents the

investigation of the electric field induced motion of spherical particles dispersed in the isotropic liquid.

5.1 Motivation

The electrophoretic movements in isotropic liquids are the main kinetics in traditional colloidal systems with an electric field applied. The isotropic phases formed by liquid crystal materials have no director but as temperature decreases, the isotropic phases change to more ordered phases; liquid crystal phases. In this section, a set of experiments was performed to know whether the isotropic phase of chiral nematic liquid crystals can offer any role as dispersion media to study fundamental investigations of the liquid crystals and controlled microfluidics of colloidal systems.

From the aspect of electrophoresis, spherical particles are expected to show movement along straight lines (translational motion), as the isotropic phase of liquid crystals is in the state of liquid without anisotropic properties. [1-3] On the other hand, there have been investigations about particle behaviour at the vicinity of the isotropic phase and the chiral nematic phase. Collings *et al*. investigated the optical rotatory power of chiral nematic phases and their isotropic phases, which support the fact that chirality of the liquid crystal phase may have influences on the isotropic phases. [4] Keyes *et al.* suggested that the fluctuations of the tensor order parameter modes could exist, having temperature dependence near the transition to the isotropic

phases, which are in contrast to the classical director model. [5] Experimental works in the systems of spherical particles dispersed in isotropic phases have shown several kinds of electric field induced motions of the particles. Jákli *et al*. observed random motions (chaotic flying behaviour) of glass spheres because there was considered to be no back flow effect and elastic trapping force in the isotropic phase after heating up of the smectic (layered) phase or of the nematic phase. [6] Yoshino *et al*. investigated silica spheres showing the circular pattern of motions in the isotropic phase above the clearing point of a chiral nematic phase or a smectic phase. [7-8] Haase *et al*. reported that the electrophoretic mobility of the sphere became very low compared with the motions in the isotropic phase due to the decrease of net charge in the electric double layer as the thermal motion of ions was extended. [9]

Therefore, it can be expected that the linear translation (line shape motion) along the applied electric field or perpendicular direction to the applied electric field is a general phenomenon of the traditional electrophoretic mobility. However, due to the characteristic isotropic phase affected by chirality or director field of the liquid crystal which exists just below the clearing point (temperature range under the isotropic phase), the phase can have certain kinds of the motions of particles in there for example, circle shape (circular motion)-movement or chaotic flying (random motion)-movement in the isotropic media.

This chapter will introduce the investigation of the movement of micron-sized silica particles in the isotropic phase of a liquid crystal material with the transition

temperature from chiral nematic material ((S,S)-EPHDBPE) to isotropic phase $T_{Iso\text{-}N^*}$ is 95.7 ℃.

5.2 Experimental Results

The characteristic isotropic phase appears as a dark domain just after the transition from the chiral nematic texture. The experiments in this chapter are carried out by uncrossing two polarisers (by 50º) to observe the silica sphere dispersed in the isotropic phase.

This section is the description of the results about the movements of a micron-sized spherical silica particle. The particle is dispersed in an isotropic phase, and the system is under an electric field. Too high a temperature could adversely affect the sandwiched cell, so the experiment was performed firstly in the temperature range between 96 ~ 120 ℃, then fixed to an arbitrary temperature of 110 ℃ as there was no significant temperature dependence of the particle-motion regime. Thus, this set of experiments has been done at a fixed temperature of 110. 0 ℃ (13 K above the N* to I transition temperature).

As mentioned above, various kinds of particle motions could be expected in the isotropic phase. The temperature dependence of the effect, the kinds of motion observed and the field dependence are discussed later.

5.2.1 The Stability Regime of the Silica Sphere in the Isotropic Phase

The kinds of particle motion observed in this chapter are mapped in Figure 5.1. In the low field region, below 2.2 $V\mu m^{-1}$ at 10 Hz and 4.7 $V\mu m^{-1}$ at 400 Hz, there was no motion. In the high field region, above the no-motion regime, there was a random-motion regime. Surprisingly, in the region where $E \geq 4.5$ $V\mu m^{-1}$ and $f \geq 150$ Hz, circular motion of the spherical particles has been seen.

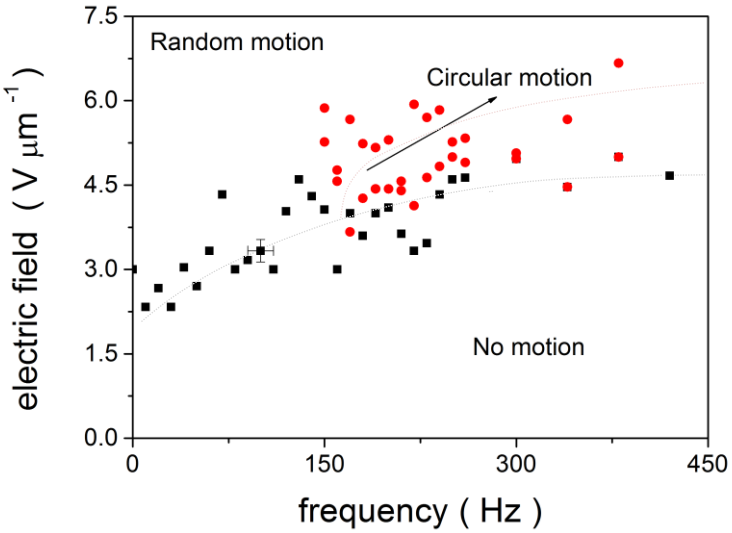

Figure 5.1 The stability regime of the motions of the silica spheres in the isotropic phase at 110℃. Three types of motions, random motion – circular motion – no motion are observed. The black squares are showing the boundary of 'Random motion' (chaotic flying) regime and 'No motion' (no movement) regime as the amplitude and frequency of the applied electric field were varied. The red circles represent the regions of electric field induced 'Circular motion' (circle shaped motions) of the particles.

5.2.2 The Circular Motion of the Silica Sphere in the Isotropic Phase

Within the circular motion regime of Figure 5.1, the track of the particle motion can be used to analyse details of the pattern of the movement. Figure 5.2 is a typical trajectory of a circular motion of the silica spheres in the isotropic phase. It can be seen that the diameter of the circular motion is ~25 μm. Using such trajectories, investigations of the electric field dependency and frequency dependency have been deduced and are presented in the following sections.

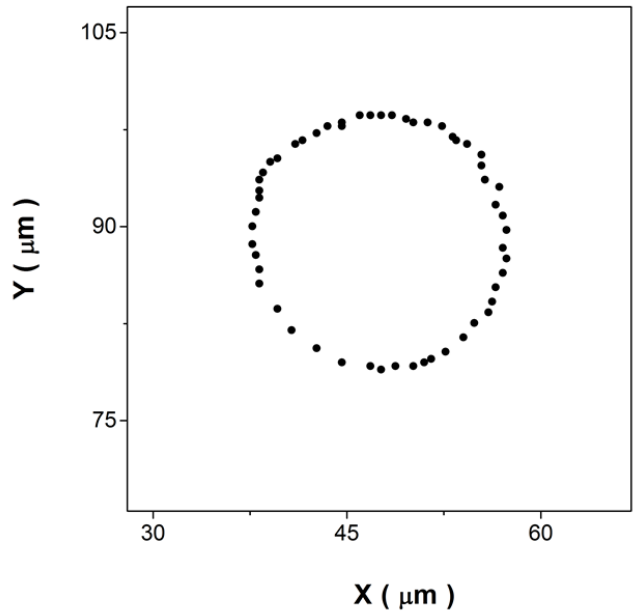

Figure 5.2 An exemplary circular trajectory of the micron-sized silica sphere at 110.0 ℃. The applied electric field has a value of E = 4.6 Vμm^{-1} and f = 160 Hz.

5.2.2.1 The Frequency Dependency of the Circular Motion of a Silica Sphere in the Isotropic Phase

Figure 5.3 is the angular velocity of the circular motion of the particle which was calculated as a function of frequency. There was no frequency dependency of the angular velocity, ω, of the particle motion, the angular velocity shows nearly constant value which was not as seen in chiral nematic phase of the material compared with Figure 4.3. The angular velocity of the particle is in the range of the value 50 ~ 60 $^{\circ}s^{-1}$ (0.87 ~ 1.05 rads s^{-1}), depending on field strength, discussed next.

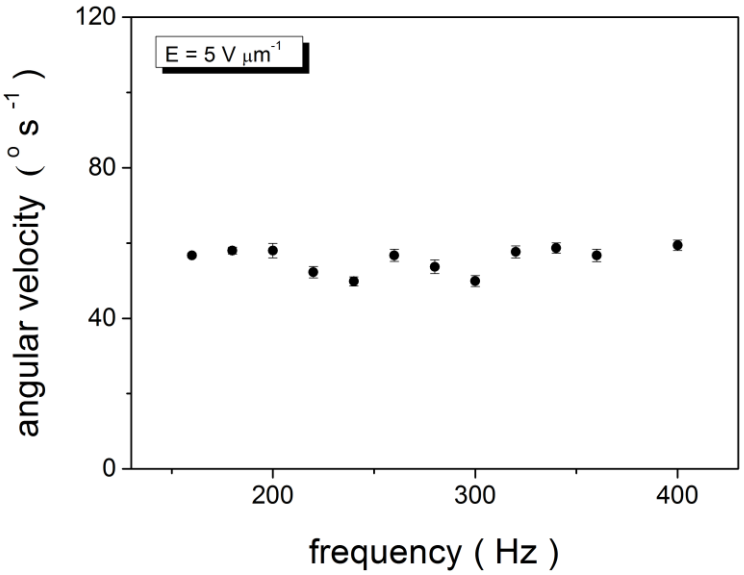

Figure 5.3 The angular velocity of the micron-sized silica sphere as a function of frequency of the applied electric field. The applied electric field is E = 5 Vμm^{-1}.

5.2.2.2 The Electric Field Dependency of the Circular Motion of a Silica Sphere

As the angular velocity of the particle has no frequency dependence, the experiment for the field dependency has been done at an arbitrary chosen frequency, 160 Hz. The dependence of the angular velocity on field is shown in Figure 5.4. A threshold field of approximately 3 $V\mu m^{-1}$ was observed, below which circular motion was not observed. However, at very low frequencies some random motion was observed below this threshold (Figure 5.1). When the amplitude of the electric field increased, the angular velocity of the silica spherical particle also increased, the as shown below.

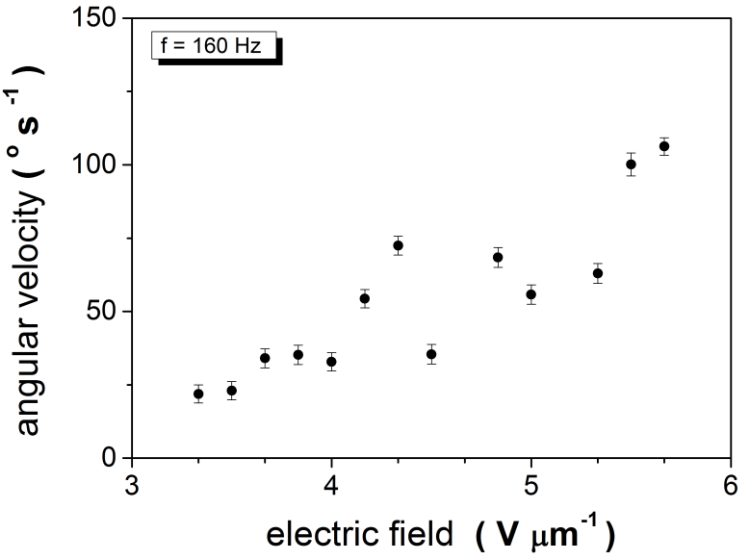

Figure 5.4 The angular velocity of the micron-sized silica sphere as a function of the applied electric field. The frequency f = 160 Hz.

5.2.3 The Diameter of the Circular Movement of the Silica Sphere in the Isotropic Phase

5.2.3.1 The Frequency Dependence of the Diameter of the Circles

At the applied electric field E = 5 Vμm^{-1}, the range of the diameter of the circular motion delivering the frequency dependency is 5 ~ 20 μm. As the frequency increased, the diameter of the circle of the silica particle's movement decreased in a non-linear way, see Figure 4.6. At the low frequency region, the diameter of the circular motion increases rapidly.

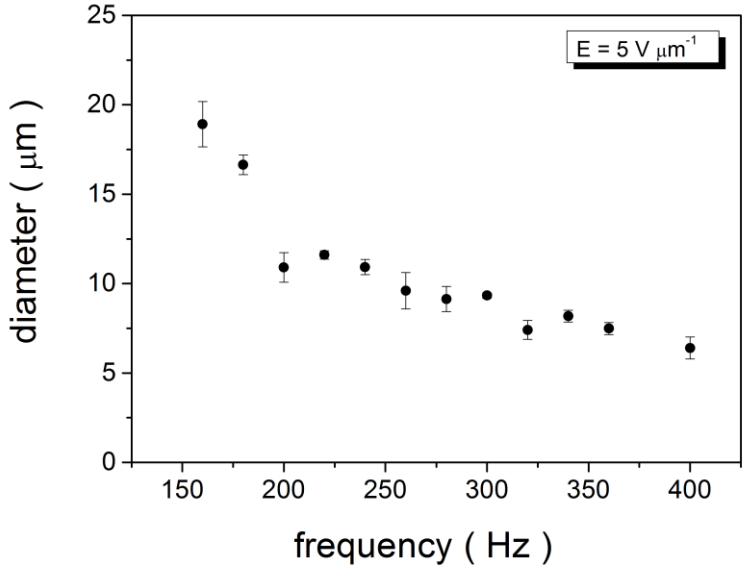

Figure 5.5 The diameter of a circular motion of the micron-sized silica sphere as a function of frequency of the electric field applied. The applied electric field is E = 5 Vμm^{-1}.

5.2.3.2 The Electric Field Dependence of the Diameter of the Circles

Figure 5.6 shows the field dependence of the diameter measurement at a fixed frequency of f = 160 Hz. The measured diameter values are 5 ~ 40 μm with the electric field dependency in the given region of the field. As the amplitude of the electric field increased, the diameter of the circular movement of the spherical particle in the isotropic phase decreased. The dependency of the diameter on the electric field is approximately linear. At fields high than 5.5 $V\mu m^{-1}$, motion is too small to measure. ($\leq$ 5 μm)

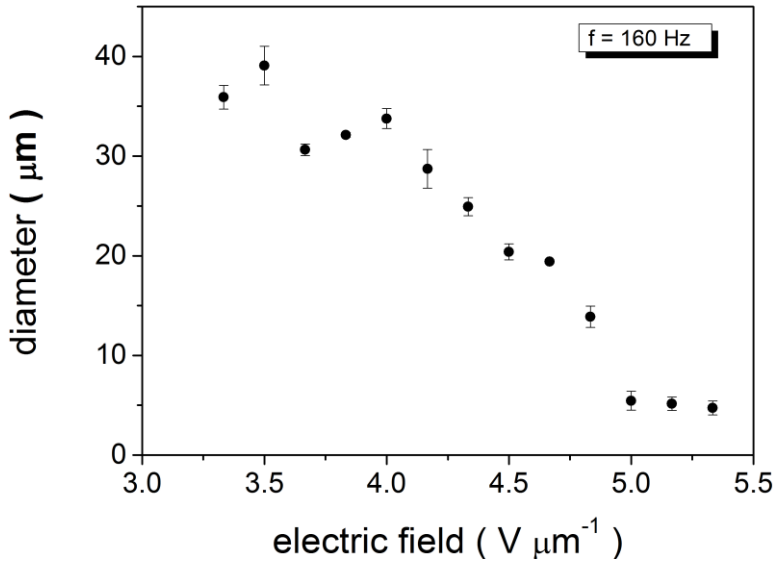

Figure 5.6 The diameter of a circular motion of the micron-sized silica sphere as a function of electric field applied to the system. The frequency f = 160 Hz.

The silica particle experienced motions of circles, therefore the size of the circle can be described by its diameter. The diameter showed specific dependency on the amplitude and frequency of the applied electric field, the diameter values are 5 ~ 40 μm with the electric field dependency in the given region of the field. The particle is particular, the diameter change is reproducible along the frequency and amplitude of the electric field applied. A further discussion of results is dealt with in the following section.

5.3 Discussion of the Results

To compare the motions of the particles in chiral nematic phase discussed in chapter 4, this section will start with pointing out the facts which can describe the difference or similarity of the motions in the two kinds of the phase. Then the motions in isotropic phase will be discussed further.

5.3.1 Comparison of the Motions of Particles in the Isotropic Phase and the Chiral Nematic Phase

In the stability regime of the motions of the particles in chiral nematic phase, there are random motion, circular motion, linear motion, and no motion regions (Figure 4.1). The stability regime of the motions of particles in the isotropic phase shows random motion, circular motion, and no motion regions (Figure 5.1). As the

amplitude and frequency of the electric field increases, the motions of particles appears similar sequence; random motion occupies the higher field region, no motion occupies the higher frequency region.

Linear motions appear in the chiral nematic phase from 15Hz and 1 $V\mu m^{-1}$, but in the isotropic phase linear motions never appear in the region studied, i.e. within f = 0 ~ 1000Hz and E = 0 ~ 10 $V\mu m^{-1}$ of the electric field.

Circular motion appears in the electric field where the region is above f = 150Hz and E = 3 $V\mu m^{-1}$ in the isotropic phase, while the circular motion appears from f = 10Hz and from E = 1 $V\mu m^{-1}$ in the chiral nematic phase. It is clear that both the field amplitude and frequency necessary to induce circular motion is higher in the isotropic phase than in the chiral nematic phase.

The velocity of the circular motion of the particle in the isotropic phase is, however, much slower than in the chiral nematic phase. As a function of frequency, the velocity in the isotropic phase (Figure 5.3) is approximately 10 times slower than in the chiral nematic phase (Figure 4.3). As a function of amplitude of the electric field, the circular motion of the particles in the isotropic phase is nearly 5 times slower than in the chiral nematic phase (Figure 4.4). This is somewhat surprising since the viscosity in the isotropic phase is considerably lower than in the chiral nematic phase, implying that different mechanisms are occurring.

The diameter of the circular motion trajectories in the isotropic phase also has a temperature dependence. Diameter of the circular motion trajectories in the isotropic phase (Figure 5.2) are approximately 4 times bigger than in the chiral nematic phase (Figure 4.2). There is a noticeable dependence on frequency, as shown in Figure 5.5,

but this dependency is not seen for the chiral nematic phase. There is also a strong dependency of the diameter on the amplitude of the electric field (Figure 5.6), which again did not appear for the chiral nematic phase.

The circular motion of particles in the chiral nematic phase result from a viscous drag force and induced charge, but the motion in the isotropic phase clearly needs to be discussed with a different theoretical background as is seen in the next section.

5.3.2 Motions of Particles in the Isotropic Phase

Figure 5.1 is a schematic diagram of the regime of motions which shows random motion and circular motion compared with the no motion regime. This section concentrates on the discussion of the circular motion, because random motion in isotropic phases have been widely observed and analysed extensively *via* measurements of the Stokes drag, Brownian motion, or stochastic behaviour. [10-19] Experiments looking at the motion of particles in this isotropic phase $T_{\text{Iso-N*}}$ (95.7 ℃) present an interesting circular motion regime which results from the electrically induced movements of the micron-sized silica particles.

The circular motion of interest in this chapter is electric field induced motion in the isotropic phase. This motion is initiated at a critical electric field, because of this the circular motion of the spherical particles in the isotropic phase has similarity with Quincke rotations. [20] This motion in the isotropic phase does not have any

symmetry-breaking processes, but there is a relaxation time difference between solids (the inclusions) and liquid media (dispersion media) observed. In this chapter, because the isotropic phase is used, the effect of the anisotropy of liquid crystals is not expected to occur, so the discussion will consider the differences between isotropic liquids and the isotropic phase of chiral nematic liquid crystals.

5.3.2.1 Dependence of Angular Velocity on Field Amplitude

The spherical particles in the isotropic phase show that their angular velocities increase as the amplitude of electric field increases (Figure 5.4), and the angular velocities are independent of the frequencies (Figure 5.3). A system of silica spheres showing Quincke rotation in liquid crystals has been studied by Liao *et al.*. In their system, the angular velocity increases as a function of electric field. [21] Their work shows that the particles (when using both spherical and cylindrical particles) have rotational motion and linear translational motion along the smectic layers under an applied electric field, and the motion is associated with a threshold voltage defined by:

$$\omega = \frac{1}{\tau_{MW}} \sqrt{\frac{E^2}{E_{cr}^2} - 1} \ , \tag{5.1}$$

where τ_{MW} is the Maxwell-Wagner interfacial polarization relaxation time, E is electric field, E_{cr} is critical voltage for moving of the particles. In this chapter, 2-Dimensional circular motion of the spherical particles occurs in the isotropic phase in a

perpendicular direction to the applied electric field. Figure 5.2 is an example of a trajectory of a circular motion of a spherical particle, which depicts an exemplary diameter of circular motion in the isotropic phase. This chapter reveals the diameter changes of the circular motion occurring in the isotropic phase with respect to modifying the amplitude of the electric field and the frequency in Figure 5.5 and Figure 5.6.

At a fixed frequency of 160 Hz, the diameter of circular motion decreases nearly to the particle's diameter as the electric field increases from 3 to 6 $V\mu m^{-1}$. (Figure 5.6) Above the 6 $V\mu m^{-1}$ at the frequency, the regimes in Figure 5.1 shows random motion region, not with stopping the motion. Therefore the diameter decrease follows a similar trend with Quincke rotation with the diameter of the circular motion becoming zero. Both cases of the decreasing diameters of the motions are close to the limit of the observation using the image analysis equipment.

Figure 5.7 shows the data of Figure 5.4 fit to Equation 5.1, rearranged so that it becomes:

$$\omega^2 = \left(\frac{1}{\tau_{MW}}\right)^2 \left(\frac{E^2}{E_{cr}^2} - 1\right). \tag{5.2}$$

The fit reveals that E_{cr} = 3.4 ± 0.3 $V\mu m^{-1}$ and τ_{MW} = 0.81 ± 0.27 s. The critical field is in excellent agreement with the observation that fields below around 3 $V\mu m^{-1}$ do not induce motion.

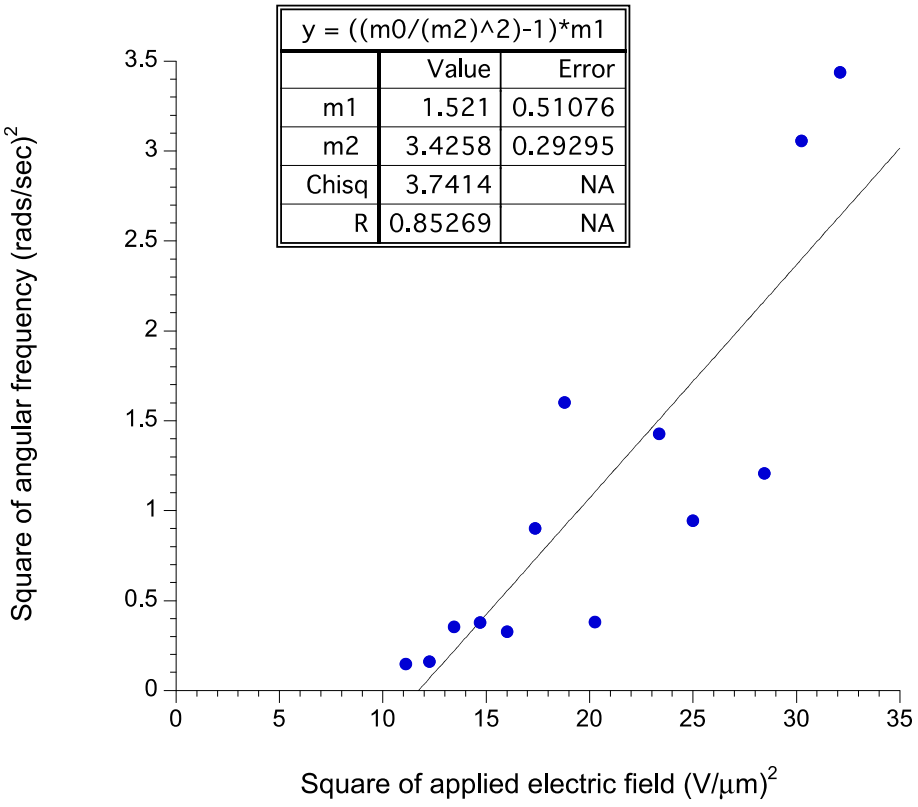

Figure 5.7 The data plot of square of critical field versus square of angular frequency. The straight line shows the fit to equation 5.2 which gives the values of E_{cr} and τ_{MW} indicated on the figure.

The Maxwell-Wagner interfacial polarization relaxation time can give a physical insight to the particle motion. During times where $t << \tau_{MW}$, no free charge has accumulated. When $t >> \tau_{MW}$, surface charge can be accumulated and the effective movement of the particle is governed by the electric field. The plot shown in Figure

5.7 gives τ_{MW} ~ 0.81 ± 0.27 s. However, it is also possible to determine τ_{MW} using equation 5.3:

$$\tau_{MW} = (\varepsilon_s+2\varepsilon_l)/(\sigma_s+2\sigma_l) , \quad (5.3)$$

Where ε_s and ε_l are permittivity of silica sphere and the isotropic liquid crystal and σ_s and σ_l are the conductivity of the material respectively. Typical values for the permittivity are ε_s ~ 3.9, ε_l ~ 5, while σ_s typically takes value $<10^{-12}$ S/m. [22-24] σ_l was measured to be ~ 1.4×10^{-7} S/m in the 110℃ in this material, but this is a rather high value and a more usual value in the isotropic phase of liquid crystals is ~ 10^{-10} S/m. Using this value we find τ_{MW} ~ 1×10^{-3} s if σ_l ~ 1.4×10^{-7} S/m, and τ_{MW} ~ 1 s if σ_l ~ 10^{-10} S/m. The figure deduced for figure 5.7 falls between these two limits (and is closer to that where a lower conductivity of the liquid crystal is answered).

5.3.2.2 Critical Field Behaviour

Another interesting value is the critical electric field, E_{cr}. In the smectic phase, the Quincke rotations of the spherical particles have critical field values 0.34 $V\mu m^{-1}$ at 59 ℃ and 2.1 $V\mu m^{-1}$ at 50 ℃ , as shown in Liao *et al.*'s work. On the other hand, in the isotropic phase of the liquid crystal used in this chapter, the critical electric field is above 3.7 $V\mu m^{-1}$ at 110 ℃ for the circular motion regime. It is a higher value than in comparable works. The critical electric field can be a tool for calculation of the viscosity of the medium:

$$E_{cr}^2 = \eta \frac{\sigma_{lc}}{\varepsilon_0^2 \varepsilon_{lc} \varepsilon_s} , \quad (5.4)$$

for colloidal suspensions of silica spheres in liquid crystals which meet the condition $\sigma_{lc} >> \sigma_s$, $\varepsilon_{lc} \sim \varepsilon_s$, where η is the viscosity, σ is conductivity, ε is dielectric constant. ε_0 is dielectric permittivity of vacuum, 8.8×10^{-12} F/m.

At higher temperatures, generally, solid particle inclusions show higher speed of movement in fluid media because of the lower viscosities, but here, the critical electric field is affected more by the conductivity of the dispersion medium than the other parameters in Equation 5.4. Whereas Togo *et al.* considered only the lower viscosity of the isotropic medium that occurs at a higher temperature. [7] In isotropic phases the anisotropy of the system is eliminated, and the critical electric field shows lower value. [9, 21] The isotropic phase used in this chapter has a higher critical electric field for the particle motion compared with the critical electric field for the onset of circular motion in the chiral nematic phase (below the transition temperature in Chapter 4). Using equation 5.4 to calculate a viscosity, note that the parameters that change most from the liquid crystal to the isotropic phase are viscosity (η) and conductivity (σ_{lc}). Using the value for E_{cr} and typical value for the other parameters,

$$E_{cr}^2 = \eta \frac{\sigma_{lc}}{\varepsilon_0^2 \varepsilon_{lc} \varepsilon_s} \rightarrow \eta = \frac{E_{cr}^2 \varepsilon_0^2 \varepsilon_{lc} \varepsilon_s}{\sigma_{lc}} = \frac{(3.7 \times 10^6)^2 \times (8.8 \times 10^{-12})^2 \times 5 \times 4}{\sigma_{lc}} , \quad (5.5)$$

here, the calculated value becomes 0.2 Pa s when $\sigma_{lc} \rightarrow 10^{-10}$ S/m, and 212 Pa s when $\sigma_{lc} \rightarrow 10^{-7}$ S/m. These appear to be rather high, when compared with the

viscosity of a typical liquid crystal; 5CB has η ~ 0.01 Pa s close to the nematic isotropic transition. The higher value for viscosity obtained could be interpreted as either because the uncertainty in conductivity dominates the calculation, or, perhaps more likely, the similarity of the motion to Quincke rotation cannot realistically be extended to viscosity calculations. Indeed, in this experiment, the particle is severely constrained by the device substrates and this could lead to the high effective viscosity calculated.

5.3.2.3 Frequency Dependence of Circular Motion

Within the circular regime shown in Figure 5.1, at a fixed electric field of E = 5 Vμm^{-1}, the circular motion of a particle in the isotropic phase shows a diameter-decrease upon an increase of frequency. (Figure 5.5.) Above 400 Hz, the diameter of circular motion tends towards zero. Figure 5.1 shows the 'No motion' area is predominant when the frequency becomes higher, so there may be an associated delay time in this system related to the frequency of electric field. This kind of frequency effect which is stopping the colloidal particle motion has been observed in various other systems of liquid crystals. [25-27] When the electric field frequency time period is faster than a delay time, the motions tend to be seized. Equation 5.6 describes the maximal frequency given by:

$$f_{max} = \frac{1}{\tau_{\mathrm{DEL}}} \quad . \tag{5.6}$$

The circular motion's f_{max} is ~ 400 Hz, thus the delay time is 2.5 × 10^{-3} s. Due to the observation of zero motion upon the high frequency electric field application, the ion diffusion coefficient also important when explaining the electric field effect on the colloidal system. Schwarz's formula is used to calculate the delay time by considering the ion diffusion coefficient (*D*) and the radius of the particle (*r*):

$$\tau_{\mathrm{DEL}} = \frac{r^2}{2D} \ . \tag{5.7}$$

Using τ_{DEL} = 2. 5× 10^{-3} s and *r* = 1.25 μm, the ion diffusion coefficient is found to be *D* ~ 3.1 × 10^{-10} m^2 s^{-1}. The delay time for a system of dielectrophoretic motions can only occur in a system when the dielectrophoretic force is zero. [9] The ion diffusion coefficient in the isotropic phase is typically 4 times larger when compared with *D* in the chiral nematic phase (~ 7.8 × 10^{-11} m^2 s^{-1}), calculated from Figure 4.1 (f_{max} ~ 100 Hz) and Figure 5.1 (f_{max} ~ 400 Hz). While *D* in the isotropic phase is ~ 3.1 × 10^{-10} m^2 s^{-1} which is a comparable a value to Na^+ ion's in sea water. *D* = 8 × 10^{-10} m^2 s^{-1} at 5℃. [28]

5.3.2.4 Diameter Variation with Electric Field

The diameter of the circular motion is introduced by the spin-induced propulsion force under the applied electric field. Spinning of the axis can occur at higher electric fields in a fixed frequency regime, but the onset of circular motion requires further understanding of the exact initiating force. Representative observations

by Togo *et al*. and Nakayama *et al*. show that the circular motion in liquid crystals and their isotropic phases have most similarity with the work presented in this chapter, with the literature qualitatively describing the spherical particle's movement in chiral nematic liquid crystals and isotropic phases of the chiral nematic liquid crystal. In both cases the observations could not be fully explained by the background theory, and hence requires further investigation. [7-8]

5.4 Conclusions

The form of the movement of the micron-sized particles in the isotropic phase is not linear, but moves either randomly or circularly upon 2-dimensional observation (using 2.5 μm diameter spherical silica particle, 6 μm thickness cell). These two kinds of motion are symmetry-breaking behaviours, and are different from the traditional electrophoresis in isotropic fluids which follow symmetric translations along the applied electric fields. General random motion of the particles throughout the isotropic phases was observed in this experiment as has been reported in previous work as mentioned. However, not only random motion occurs, but also systematic circular motion appears above a critical electric field. In this chapter, the experimental measurements suggest that the behaviour is similar to the field induced Quincke rotation of micron-sized spherical particles in the isotropic phase.

The similarity to Quincke rotation has been considered in detail and analysis of the dependence of the angular velocity on field amplitude gives a reasonable value

for τ_{MW} but one which is strongly dependent on the value of conductivity used. However, using the Quincke analysis to deduce a viscosity for the isotropic liquid gives a much higher value than expected. It is suggested that this high value could be related to the confinement of the particle in the device in this experimental geometry.

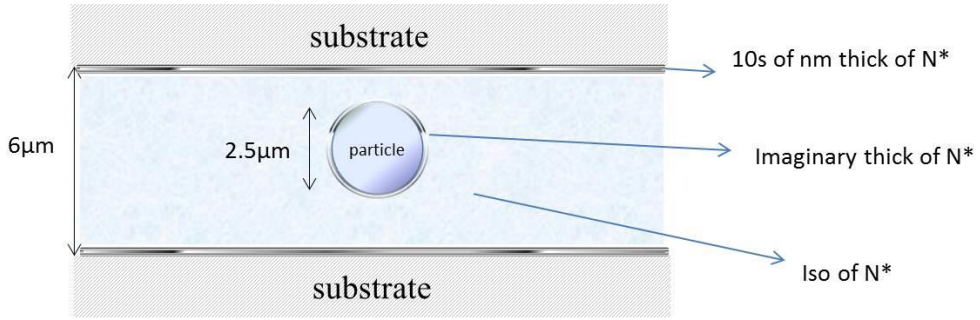

Figure 5.8 Schematic diagram of the confinement of a spherical particle in an isotropic liquid crystal phase. When electric field applied across the cell depth, a stable Quincke rotation is available as the condition $\varepsilon_s/\sigma_s > \varepsilon_l/\sigma_l$ is given by this system.

It is noted that the motion stops when the delay time is longer than frequency of the electric field, so the ion diffusion of the system affects the motion regime.

We should finally consider the fact that circular motion occurs at all in the isotropic phase. In other isotropic systems with applications of electric fields, either linear motion or Quincke rotation (on an axis) has been observed. In this case, we cannot rule out 'traditional' Quincke rotation; the experiment cannot easily observe it. It is possible that the circular motion is caused by a combination of 'traditional' Quincke rotation, coupled with a tendency for linear motion. However, it isn't clear why simple linear motion is not seen, as it is observed in the chiral nematic phase

(chapter 4). It is clear that the isotropic liquid crystal system is different from other isotropic liquid: it is possible that even 10K above the $T_{N^*\text{-Iso}}$, the surface of the device and the silica sphere induce liquid crystalline strongly influences the dynamics of the system, including the effective viscosity.

5.5 References

[1] G. Vertogen and W. H. de Jeu, Thermotropic liquid crystal fundamentals. 1988, Springer-Verlag Berlin Heidelberg.

[2] I. D. Morrison and S. Ross, Colloidal dispersions. 2002, WILEY-INTERSCIENCE.

[3] A. T. Andrews, Elecrtophoresis. 1986, Oxford University Press.

[4] M. B. Atkinson and P. J. Collings, *Optical Rotatory Power in the Isotropic Phase of Four Cholesteric Esters*. 1986, Molecular Crystals and Liquid crystals.

[5] M. A. Pantea and P. H. Keyes, *Fluctuations of the tensor order-parameter modes in a cholesteric liquid crystal*. 2005, PHYSICAL REVIEW E, Volume 71, pp.031707.

[6] A. Jákli, B. Senyuk, G. Liao, and O. D. Lavrentovich, *Colloidal micromotor in smectic A liquid crystal driven by DC electric field*. Soft Matter, 2008, Volume 4, pp.2471-2474.

[7] T. Togo, K. Nakayama, M. Ozaki, and K. Yoshino, *Electric Field-Induced Migration of SiO_2 Particles in Smectic Liquid Crystal*. Japanese Journal of Applied Physics. 1997, Volume 36, pp.L1520-L1522.

[8] K. Nakayama, M. Ozaki, and K. Yoshino, *Influence of Smectic Layer Structure on Electric Field-Induced Migration of SiO_2 Particles.* Molecular Crystals and Liquid crystals, 1999, Volume 329, pp.129-135.

[9] A. V. Ryzhkova, F. V. Podgornov, and W. Haase, *Nonlinear electrophoretic motion of dielectric micoparticles in nematic liquid crystals.* APPLIED PHYSICS LETTERS, 2010, Volume 90, pp.151901.

[10] M. Pumpa and F. Cichos, *Slow Single-Molecule Diffusion in Liquid Crystals.* The Journal of Physical Chemistry B, 2012, Volume 116, Issue 49, pp.14487-14493.

[11] Y. Y. Hidaka, *A nonequilibrium temperature and fluctuation theorem for soft-mode turbulence.* Physica D: Nonlinear Phenomena, 2010, Vol. 239, Issue 11, pp.735-738.

[12] M. P. Lettinga, E. Barry, and Z. Dogic, *Self-diffusion of rod-like viruses in the nematic phase.* 2005, Europhysics Letters, Volume 71, Issue 4, pp.692-698.

[13] G. Eric, L. M. Paul, B. Markus, van R. Rene, and van der S. Paul, *Dynamical and structural insights into the smectic phase of rod-like particles.* Journal of Physics: Condensed Matter, 2008, Volume 20, Issue 49, pp.494213.

[14] A. A. Verhoeff, J. van Rijssel, V. W. A. de Villeneuvea, and H. N. W. Lekkerkerkera, *Orientation dependent Stokes drag in a colloidal liquid crystal. Soft matter,* 2008 Volume 4, Issue 8, pp.1602-

[15] J. C. Loudet, P. Hanusse, P. Poulin, *Stokes drag on a sphere in a nematic liquid crystal.* Science, 2004 November, 26th, Volume 306, Issue 5701, pp.1525.

[16] M. Vergeles, P. Keblinski, J. Koplik, and J. R. Banavar, *Stokes Drag at the Molecular Level.* Physical Review Letter, 1995, Volume 75, pp.232-235.

[17] D. M. Heyes, M. J. Nuevo and J. J. Morales, *Translational and rotational diffusion of dilute solid amorphous spherical nanocolloids by molecular dynamics simulation.* MOLECULAR PHYSICS, 1998, Volume 93, No. 6, pp.985- 994.

[18] K. S. Chu and D. S. Moroi, *Self-diffusion in nematic liquid crystals*. Journal de Physique Colloques, 1975, Volume 36, Number C1, pp.99-101.

[19] M. P. B. van Bruggen, H. N. W. Lekkerkerker, G. Maret, and J. K. G. Dhont , *Long-time translational self-diffusion in isotropic and nematic dispersions of colloidal rods.* Physical review E, 1998 Volume 58, Issue 6, pp.7668 -7677.

[20] T. B. Jones, *Quincke Rotation of Spheres*. IEEE Transactions on industry application, JULY/AUGUST 1984, Voulme IA-20, No. 4, pp.845-849.

[21] G. Liao, I. I. Smalyukh, J. R. Kelly, O. D. Lavrentovich, and A. Jákli, *Electrorotation of colloidal particles in liquid crystals.* Physical Review E, 2005, Volume 72, pp.031704/1-5.

[22] P. R. Gray, P. J. Hurst, S. H. Lewis, and R. G. Meyer, Analysis and Design of Analog Integrated Circuits (Fifth ed.). 2009, Wiley New York, p.40.

[23] R. Nozaki, T. K. Bose, and J. Thoen, *Broadband dielectric relaxation study in a ferroelectric liquid crystal by time domain reflectometry*. Ferroelectrics, 1991, Volume 121, pp.1-11.

[24] J. A. Voorthuyzen, K. Keskin, and P. Bergveld, *Investigations of the surface conductivity of silicon dioxide and methods to reduce it*. Surface Science, 1987, Volume 187, pp.201-211.

[25] A. K. Srivastava, M. Kim, S. M. Kim, M. Kim, K. Lee, Y.H. Lee, M. Lee, and S. H. Lee, *Dielectrophoretic and electrophoretic force analysis of colloidal fullerenes in a nematic liquid-crystal medium*. Physical Review E, 2009, Volume 80, pp.031704/1-5.

[26] S. Hernàndez-Navarro, P. Tierno, J. Ignés-Mullola, and Francesc Saguésa, *AC electrophoresis of microdroplets in anisotropic liquids: transport, assembling and reaction*. Soft Matter, 2013, Volume 9, Issue 33, pp.7999

[27] O. D. Lavrentovich, I. Lazo, and O. P. Pishnyak, *Nonlinear electrophoresis of dielectric and metal spheres in a nematic liquid crystal*. Nature, 2010. Volume 467, pp.947-950.

[28] Y. Li and S. Gregory, *Diffusion of ions in sea water and in deep-sea sediments*. Geochimica et Cosmochimica Acta, 1974, Volume 38, pp.703-714.

Chapter 6
Motions of an Elongated Particle in the Nematic Liquid Crystal Phase

The nematic liquid crystal phase is the simplest liquid crystal phase and is widely used for electronic displays, microfluidics, and bioengineering. [1] A nematic liquid crystal material in a sample cell can have its physical properties controlled by temperature, electric field, and cell geometry (thickness, alignment) etc. [2] As a colloidal system, nematic liquid crystals can be used to disperse various particles in the system, allowing an investigation of fundamental science. [3-7] This chapter describes the observation of particle motions in several geometries of the nematic phase. An explanation of the geometries employed will be introduced in the next section.

6.1 Motivation

Previous chapters dealt with spherical particles in both the chiral nematic phase and its isotropic phase. That work was of interest because there are few investigations that deal with chiral nematic phases for electrophoretic mobility observations. Though our experiment does not observe 3-dimensions in the sample cells (the cell gap is such that the system is 2-dimensional), there are several interesting motions that appear. In particular, motion with similarities to Quincke rotational motions and electrophoretic movement were described in chapters 4 and 5.

This chapter concerns the nematic phase, which has been relatively widely studied, and different shapes of particle are included. In particular, the experiments use several kinds of geometries with a nematic liquid crystal dispersion medium and elongated spheroid inclusions, and the aim is to investigate specifically whether the particles show mobility which are similar to those reported in chapter 4 and 5. There are many experiments that have used spherical particles in nematic liquid crystals, which report electrophoretic mobility along the electric field. [3-5] Also, there are investigations using nanowires or carbon nanotubes that switch with the liquid crystal director when the electric field is applied to the particle liquid crystal composite. [6-8]

The experiments in this chapter used elongated particles dispersed in nematic liquid crystals. Such experiment can be considered as 'model' experiments for systems that include nanotubes or nanowires in nematic liquid crystals, and offer an insight into the contribution of electrophoresis to the interesting phenomena. The 4 types of geometries which are considered are summarised in table 6.1.

<table>
<tr><th></th><th>Elongated particle size</th><th>Cell gap</th><th>Boundary conditions</th><th>Dielectric anisotropy</th></tr>
<tr><td rowspan="4">information</td><td rowspan="4">$l = 5.4 \pm 1.3$ μm
$d = 1.4 \pm 0.1$ μm</td><td rowspan="2">L = 9.9 μm</td><td rowspan="2">Homogeneous</td><td>$\Delta\varepsilon > 0$</td></tr>
<tr><td>$\Delta\varepsilon < 0$</td></tr>
<tr><td rowspan="2">L = 9.1μm</td><td rowspan="2">Homeotropic</td><td>$\Delta\varepsilon > 0$</td></tr>
<tr><td>$\Delta\varepsilon < 0$</td></tr>
</table>

Table 6.1 A summary of the elongated particle (silica) included in different nematic liquid crystal geometries.

The thin cell geometries are of 4 types with two boundary conditions. The nematic liquid crystal host is chosen to have either positive or negative dielectric anisotropy, thus the sample cells have different kinds of dispersion media for the elongated particles. The movement of the elongated particles will show unusual new phenomena related to the length scale, and cell geometry.

6.2 Experimental Results

The object of the experiment is the observation of the novel movement of particles. There have been reports that spheres, nanowires and nanotubes move in nematic liquid crystals by Stokes drag or under the influence of an electric field, but there are very few theoretical approaches that describe the phenomena. Therefore, these experiments are focused on describing and where possible explaining the unusual motion of elongated particle in the simplest liquid crystal phase, using 4 types of geometry. The following section will analyse the displacement of the elongated particles in nematic materials observed when electric fields were applied to the devices.

6.2.1 Homogeneous Boundary Condition

A homogeneous (HG) boundary condition is formed when the alignment of the calamitic nematic liquid crystal is constrained to be parallel to the two glass substrates

(The cell gap is 9.9 μm.). The schematic diagram in Figure 6.1 depicts the geometry with an arbitrary cell gap.

Figure 6.1 A schematic diagram of homogeneous (**HG**) boundary conditions in a calamitic liquid crystal material in an arbitrary cell gap (a side view). The elongated particle's geometry can be observed as lying particles (**LP**) or standing particles (**SP**), each with positional distributions between the two substrates (it is not possible to detect the angles of 3 dimensional positions).

The following sections will describe the experimental results of the elongated particle motions in the HG boundary conditions with two types of nematic liquid crystals.

6.2.1.1 Motions of an Elongated Particle in a Nematic Material with a Negative Dielectric Anisotropy: Homogeneous Alignment

Negative dielectric anisotropy nematic liquid crystals in homogeneous boundary conditions stay in the parallel alignment with respect to the glass substrates during the application of the electric field to the sample cell, i.e. no Freedericksz transition will occur for this geometry, though under some circumstances electroconvection could occur. Any particle motion is observed using a polarizing microscope, with the polarizers at 30º and individual frames are recorded by a video camera.

The first result of the observations is that the motion regimes are located over a narrow electric field region, shown in Figure 6.2. The motions are either linear or random displacement (chaotic flying motion). Lying particles are the major inclusions which move. Only the linear motion that is observed is available for analysis using our system which calculates the displacement in particular time intervals. The critical field for the linear motion is 7 $V\mu m^{-1}$ and frequency region is below 70 Hz. In the frequency region above 70 Hz, the linear motion disappears and random motion occurs, but above 200 Hz all motions stop.

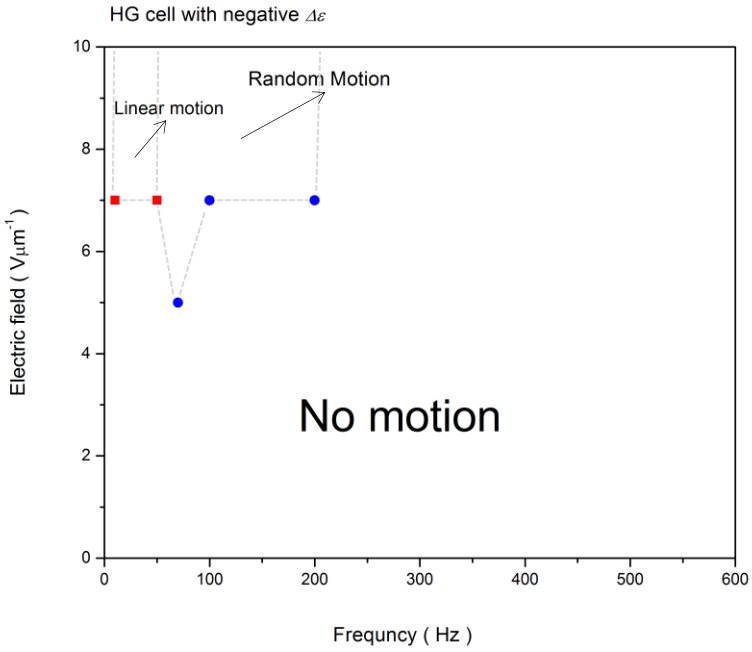

Figure 6.2 The stability regime of the motions of the elongated particles in a nematic phase with homogeneous boundary conditions, and a negative dielectric anisotropy liquid crystal material.

The observation is also focused on understanding whether the direction of the movement influences the speed, i.e. is motion faster or slower along the director? Analysis reveals that the linear motion of the elongated particle in the sample cell can be in any arbitrary direction; there is no preference parallel or perpendicular to the director. In the linear motion regime, the velocity of the linear motion as a function of angle with respect to the director can be calculated and this is shown in Figure 6.3. The angle is the difference in value between the rubbing direction and the long axis of the particle, with observed-clockwise as positive and observed-counter clockwise as

negative the values in radians. The velocity is measured for fixed electric field conditions. The linear velocity is found to be between 50 ~ 260 μms^{-1} and is independent of the angle.

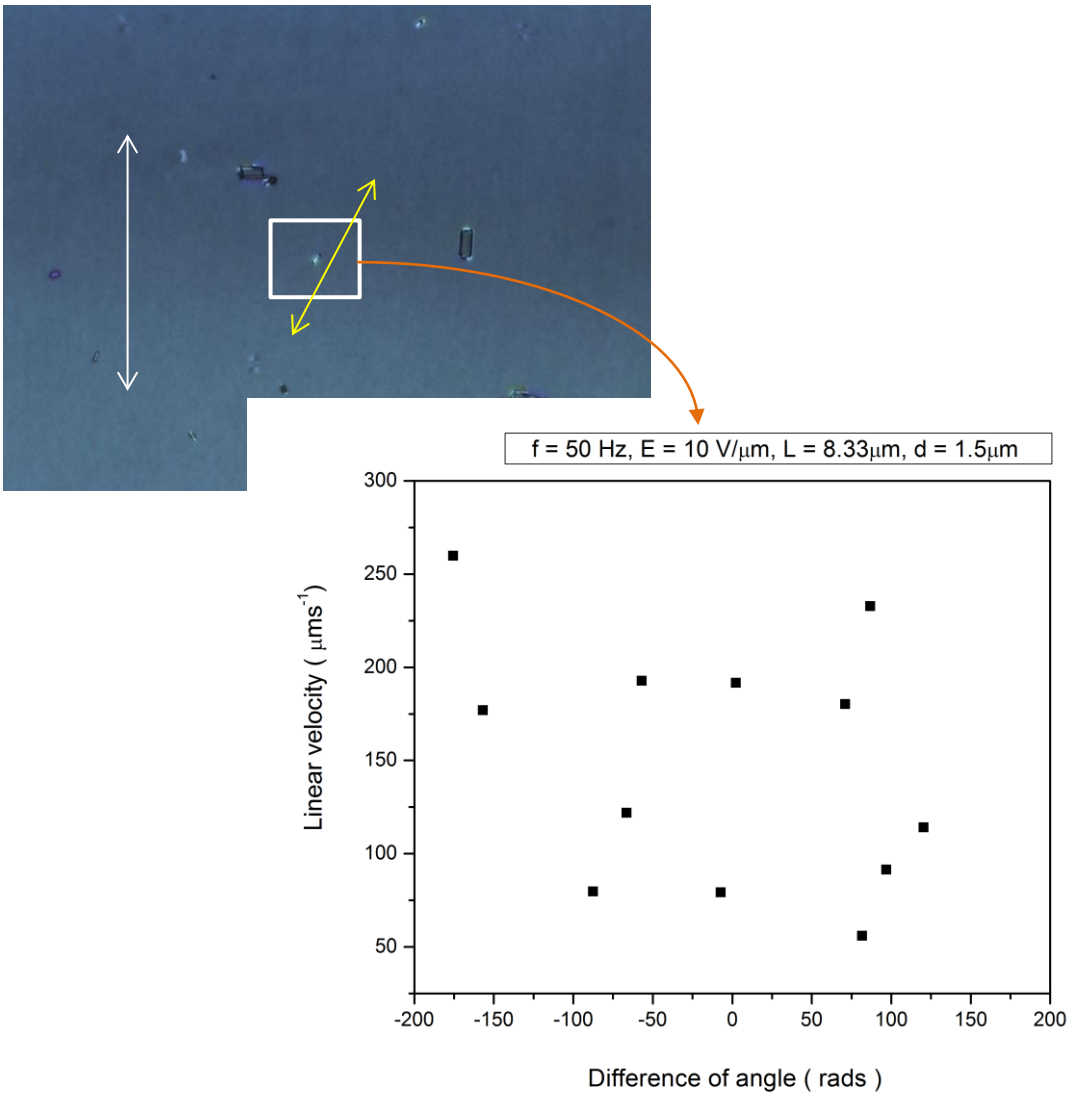

Figure 6.3 (a) A lying particle in the liquid crystal material in the cell showing a difference of angle between the director and the particle's long axis; the white double arrow line is the director and the yellow line is the particle's long axis. (b) The linear velocity of the elongated silica particle as a function of angular difference between the

long axis of the particle and director alignment along the rubbing direction of the cell. The observation is at f = 50 Hz and E = 10 Vμm^{-1}. The diameter of the particle is 1.5 μm and length is 8.33 μm.

The elongated particles in this cell geometry prefer to move remaining in their lying positions (LP) in the cell once subjected to the applied electric field. The velocities of linear motions of the lying particles measured as a function of the distribution of their length scale are shown in Figure 6.4. The percent weight (%wt) of particles in the sample is very low, the observed elongated particles are not many, and the linear velocity has the lowest value when the length is ~ 9 μm. Interestingly, 9 μm is also the cell gap in this experiment.

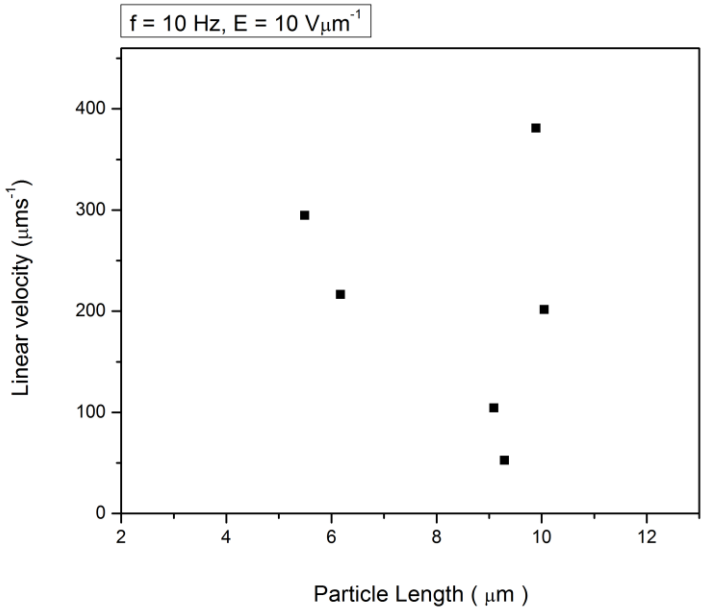

Figure 6.4 The linear velocity of the elongated silica particle as a function of

particle's length scale. The applied electric field is f = 10 Hz and E = 10 Vμm^{-1}. The length is 5 μm ~ 10 μm.

6.2.1.2 Motions of the Elongated Particle in a Positive Dielectric Anisotropy Nematic Material: Homogeneous Alignment

In section 6.2.1.1, the liquid crystal director did not change on application of the field as the system has negative dielectric anisotropy. In this section, the experiment has been done using the positive dielectric anisotropy nematic material. The stability regime for different kinds of particle motion is shown in Figure 6.5.

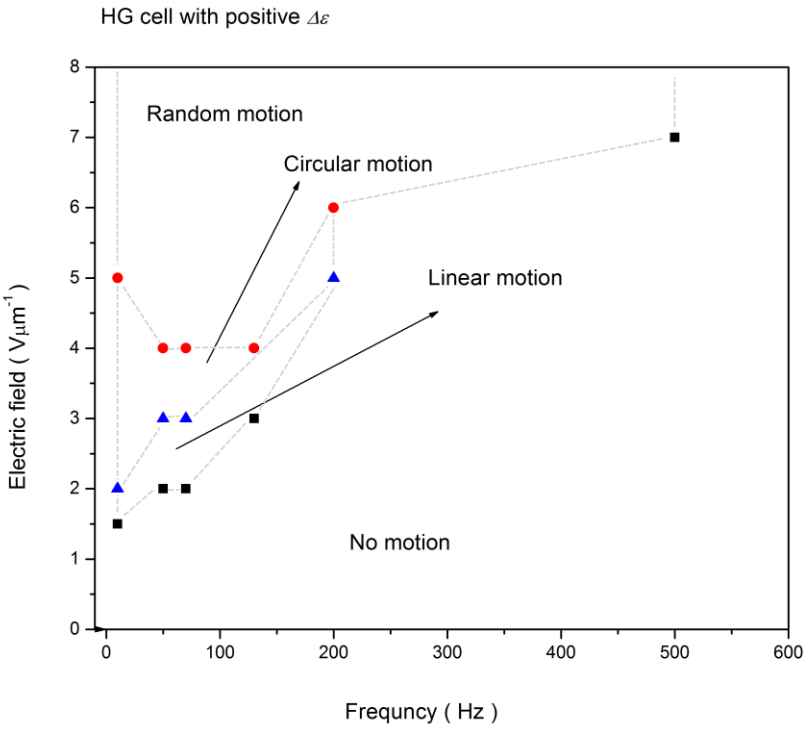

Figure 6.5 A stability regime of the motions of the elongated particles in a nematic

phase. With homogeneous boundary conditions and a positive dielectric anisotropy liquid crystal material. The Fréedericksz threshold is at 2.6 $V\mu m^{-1}$.

In contrast to the negative dielectric system, the field-frequency regime for motion is larger and several kinds of motion are observed. In the region of circular motion, the particles are seen to move in a somewhat random way show spinning or randomly circulating motion. Consequently, the motion cannot be analysed as it was in chapter 4. In the linear motion regime, an electric field dependency of the velocity could be measured, but the linear velocity did vary as a function of the length of the elongated particle. The observation in this system shows that the possible particles' length scales are 3 ~ 12 μm.

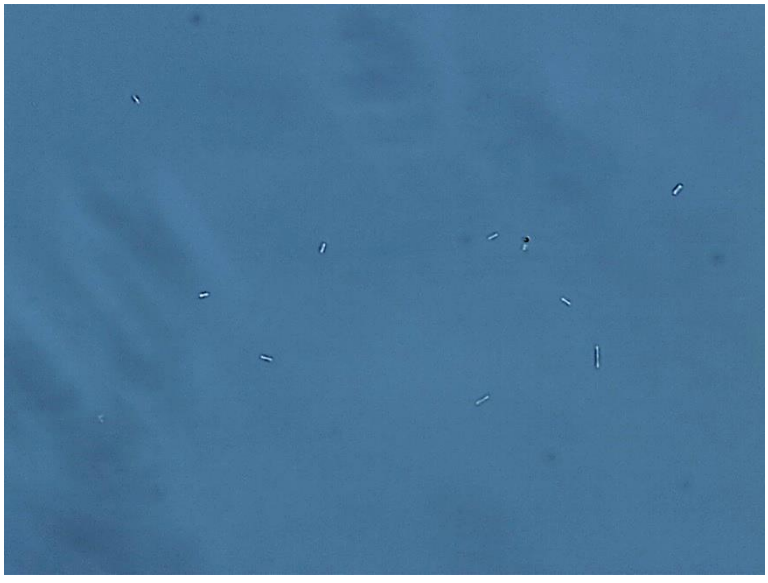

Figure 6.6 An exemplary photograph showing the length distribution of the moving

particles (in a state of LP) in the sample cell. The linear velocity of the elongated silica particle as a function of particle's length scale could be measured in this texture with the motion of different particles. The moving directions have no dependency with respect to the director.

There is a difficulty to find the proper particles with specific length scales for the measurement and analysis was only possible for a few particles in the most well optimized conditions for the observation and measurement. The elongated particles' length distribution which is available in the experiment in this section is 3 ~ 12 μm. Figure 6.7 shows that the linear velocity decreased up to a length of ~ 9 μm, then shows a large increase above the length scale within our measurement.

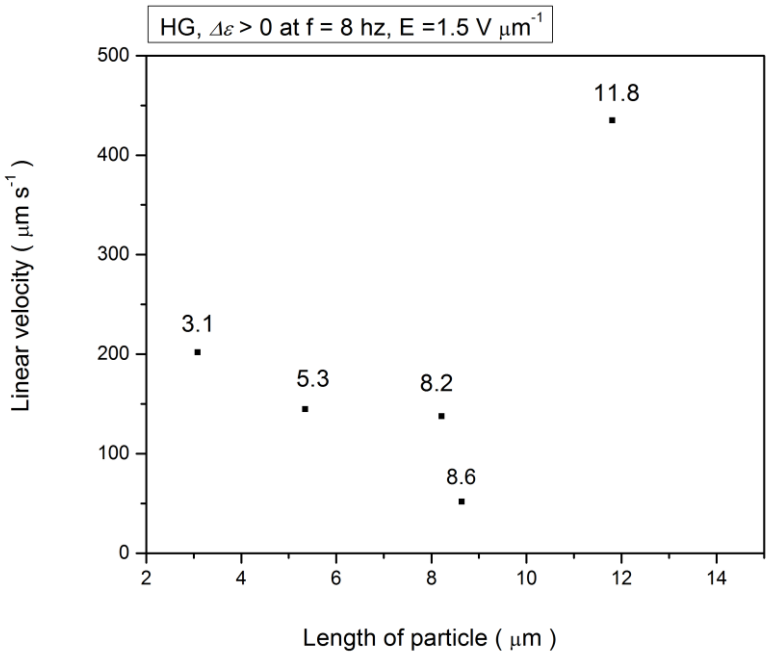

Figure 6.7 The linear velocity of the elongated silica particle as a function of particle's

length scale 3 µm ~ 12 µm at f = 8 Hz and E = 1.5 Vµm^{-1} in homogeneous boundary condition with positive dielectric anisotropic nematic liquid crystal.

6.2.2 Homeotropic Boundary Conditions

In homeotropic (HT) boundary conditions, the alignment of the calamitic nematic liquid crystal is perpendicular to the two glass substrates (The cell gap for the experiments is 9 µm.). The schematic diagram depicts the geometry with an arbitrary cell gap.

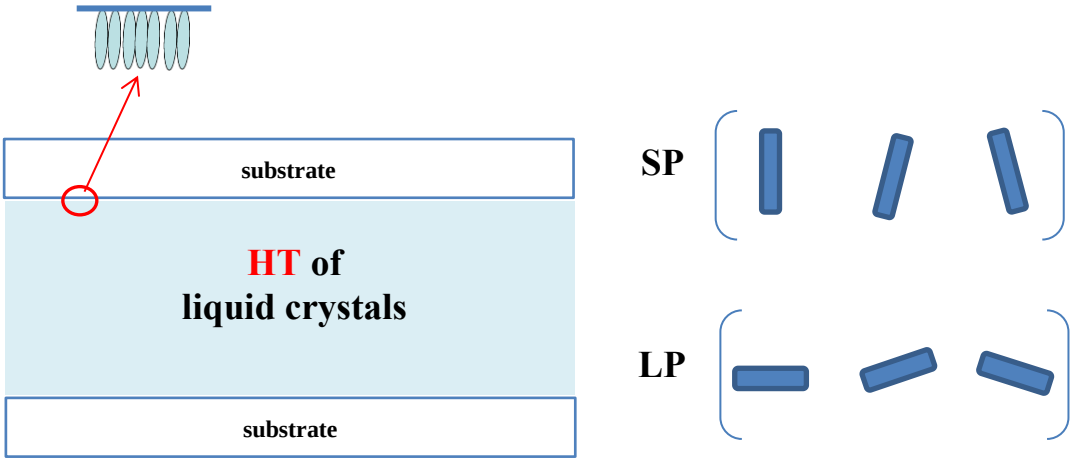

Figure 6.8 The schematic diagram of homeotropic (**HT**) boundary condition of calamitic liquid crystal material in an arbitrary cell gap (a side view). Elongated particle's geometry is observed lying particles (**LP**) and standing particles (**SP**) with

the position distributions (not possible to detect the angles of 3-dimensional positions) between the two substrates.

6.2.2.1 Motions of the Elongated Particle in a Negative Dielectric Anisotropy Nematic Material: Homeotropic Alignment

In homeotropic boundary conditions with a negative dielectric anisotropy nematic liquid crystal, the application of a field to the cell induces topological defects which have a dramatic influence on the motion of the dispersed particles. Indeed, if the particles interact with a defect, it tends to move in a complicated way with the defect. The different regimes are shown in Figure 6.9.

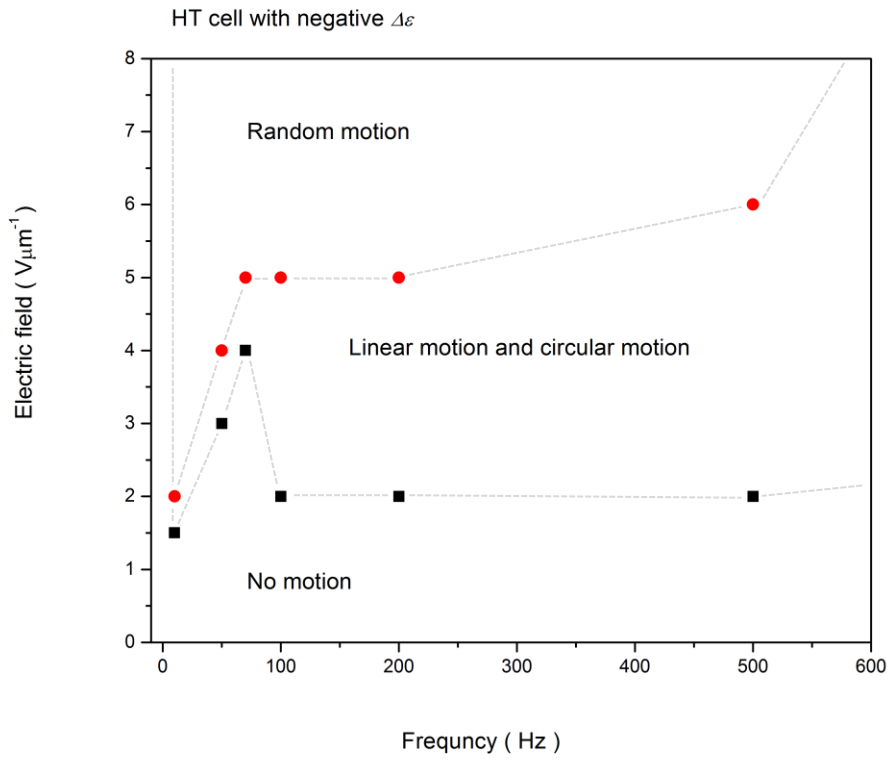

Figure 6.9 A stability regime of the motions of the elongated particles in a negative

dielectric anisotropy nematic phase with homeotropic boundary conditions. The threshold for defect formation in this geometry is 0.6 $V\mu m^{-1}$.

As shown in figure 6.9, there is no motion regime under the threshold field related to a wide range of frequency, and random motion regime with higher electric field. While circular motion occurs either with the defects or around a point defect, also there is linear motion area along with the complicated circular motions of the particles. In the circular motion regime, the appearance is as interesting moving textures.

In this geometry, the circular motion of the elongated particle is related to the defects in the nematic phase, but the particles can also experience random directional linear motion. In this section, observations of the unusual motion will be focused on, and it should be noted that details of the defect and particle composite motions are not always clearly captured by our experimental system. Above the threshold field (0.6 $V\mu m^{-1}$), the liquid crystal medium dynamically changes as the defect structure is induced and both the linear motion and the circular motion of the elongated particles are consequently much more complicated than in any other geometry described. The linear motions and the circular motions start to appear above a threshold of ~ 1.5 $V\mu m^{-1}$ (a higher field than the threshold field for inducing defects). Both of the motions simultaneously exhibit the dramatic displacements caused by the attraction to the defects, and particles can move in a manner that is effectively a combination movement caused by the particle-defect interaction, together with the unidirectional linear motions which occur without the interaction with (dragging by)

the defects. The linear motions occur over a much broader regime than in other geometry including a higher frequency region of the applied electric field, but the directions of the movements and the displacements at specific time intervals are not as regular. Therefore, in this section the extraordinary features are observed as a function of time to try to understand the novel phenomena that occur in this sample geometry of and two kinds of qualitative analysis have been considered, detailed in the next section.

An unusual feature of the circular motion in this geometry is the relationship with the defects. Two kinds of motions are observed. The first one is the motion of the elongated particles which move with the defects and therefore occurs when the defects appear above the threshold field. The motion picture is saved as the frames with the unit frame rate, t (t = 0.0175s in the following figures). Figure 6.10 is a set of the frames of such motions which show the moving defects and a particle which exhibit a combined motion under the application of the electric field. The applied electric field is f = 800 Hz, and E = 5.5 Vμm^{-1} (the polarizer at 30º). Each photo shows a same area at a different time as indicated.

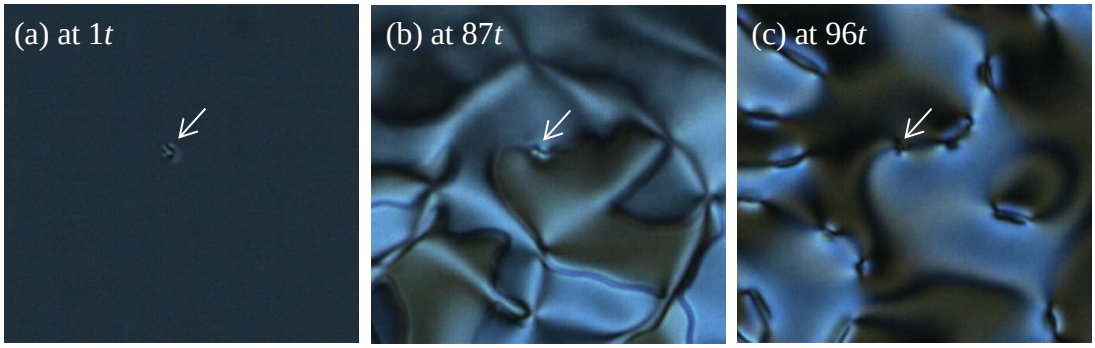

Figure 6.10-1 A negative dielectric liquid crystal phase with homeotropic boundary conditions including an elongated particle. (a) initial state (HT) at 1t. The liquid crystal director and the particle are all perpendicular to the substrates. (b) after applying an

electric field, (the threshold field for defect is 0.6 V μm^{-1}) the texture changes and topological defects appears. At 87*t*, the particle is at the interface between the defect domains. (c) Just before the transition to the point defects in the texture at 96*t*.

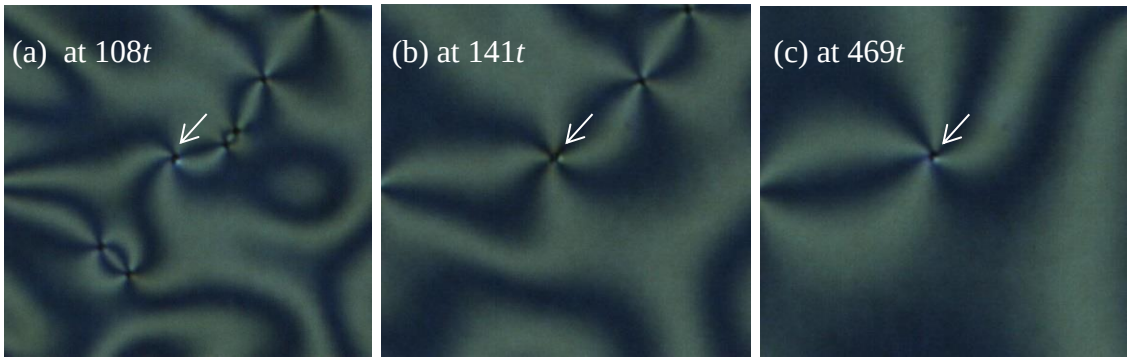

Figure 6.10-2 A negative dielectric liquid crystal phase with homeotropic boundary conditions including an elongated particle. (a) the particle is kept in the interface during stabilizing the topological defect at 108*t*. (b) around the particle, there are still a fluctuations of the defects exists at 141*t*. (c) the particle is standing in the middle of the point defect and starts to exhibit circular motion holding the centre of the defect at 469*t*.

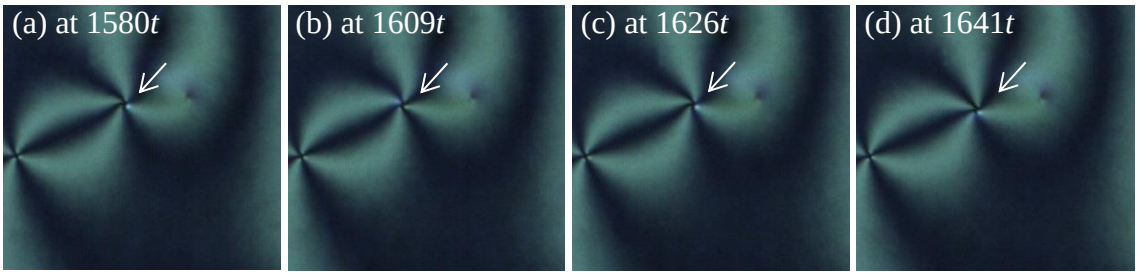

Figure 6.10-3 A negative dielectric liquid crystal phase with homeotropic boundary conditions including an elongated particle. The particle combined with a defect and shows a 360º circular motion with the clockwise movement from the view. The pictures from (a) at 1580*t* to (d) at 1641*t*.

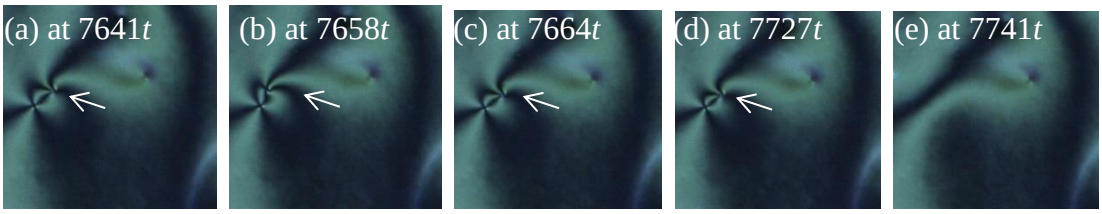

Figure 6.10-4 A negative dielectric liquid crystal phase with homeotropic boundary conditions including an elongated particle. From (a) at 7641*t* ~ (e) at 7741*t*, the defects become smaller and disappear, the particle shows a displacement along the edge of the defect and is propelled away when the defects disappear by annihilation.

The circular motions of the standing elongated particles occur across the widest range observed for any geometry, including in the higher frequency range over 500 Hz. In this section, the circular motions of the standing particles were measured within the field amplitude range E = 7 ~ 10 Vμm^{-1} and the diameter of the motion was also determined. In Figure 6.11-1, the particles' circular motions show the angular velocity between 16 ~ 22 rads s^{-1} (much faster than the angular velocities in our chiral nematic system or our isotropic system). The angular velocities do not show a dependency on the amplitude of the field increases. The diameter takes values between 4 ~ 8 μm in the electric field region as shown in Figure 6.11-2. (These values can be compared with ~ 5 μm in the chiral nematic phase and 5~20 μm in the isotropic phase as described in chapters 4 and 5.)

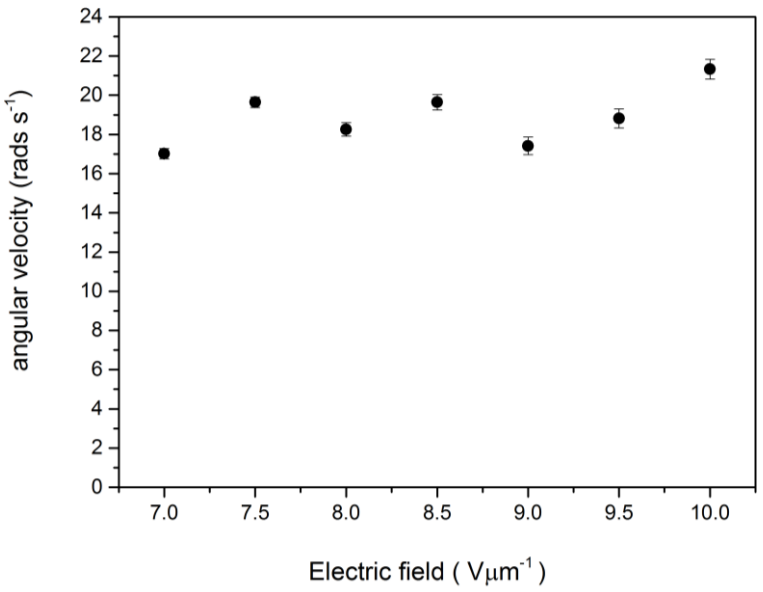

Figure 6.11-1 The angular velocity of the elongated silica particle as a function of the applied electric field. The frequency f = 800 Hz. (HT, $\Delta\varepsilon < 0$, Standing particles).

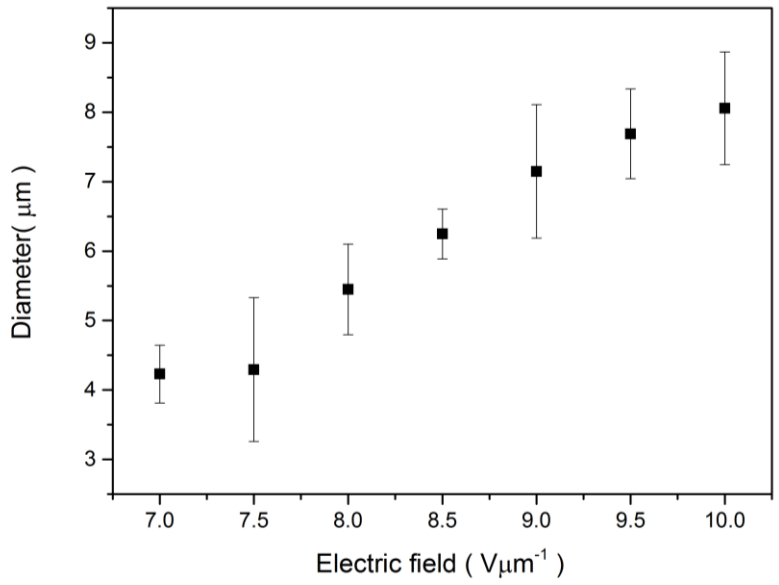

Figure 6.11-2 The diameter of a circular motion of the elongated particle as a function of amplitude of the applied electric field. The frequency of the field is f = 800 Hz. (HT,

$\Delta\varepsilon < 0$, Standing particles).

6.2.2.2 Motions of the Elongated Particle in a Positive Dielectric Anisotropy Nematic Material: Homeotropic Alignment

The particles exhibit only circular motion in a positive dielectric nematic phase with homeotropic boundary conditions. The regime that shows the widest region of stability in this case is that of the circular motion (Figure 6.12). The critical field of the circular motion is 1 $V\mu m^{-1}$ and the dependence of the amplitude is measured (Figure 6.13).

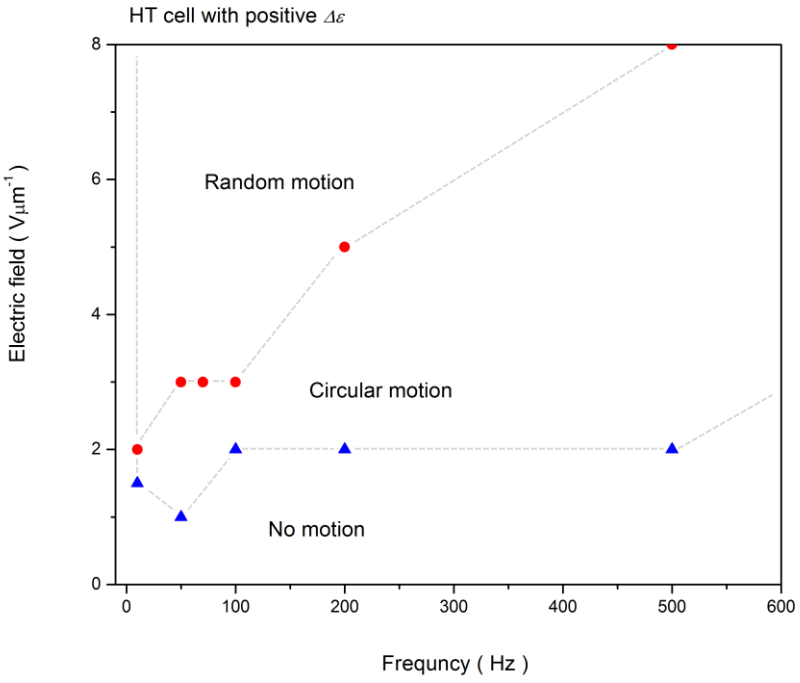

Figure 6.12 A stability regime of the motions of the elongated particles in a positive dielectric anisotropy nematic phase with homeotropic boundary conditions.

In this geometry, the circular motions with perpendicular to the substrates are preferred in high frequency fields (around 400 Hz) and the angular velocity increases from 2 to 12 rads s^{-1} as the amplitude of the field increases from 2.5 to 5.5 $V\mu m^{-1}$. The figure 6.13 shows the results.

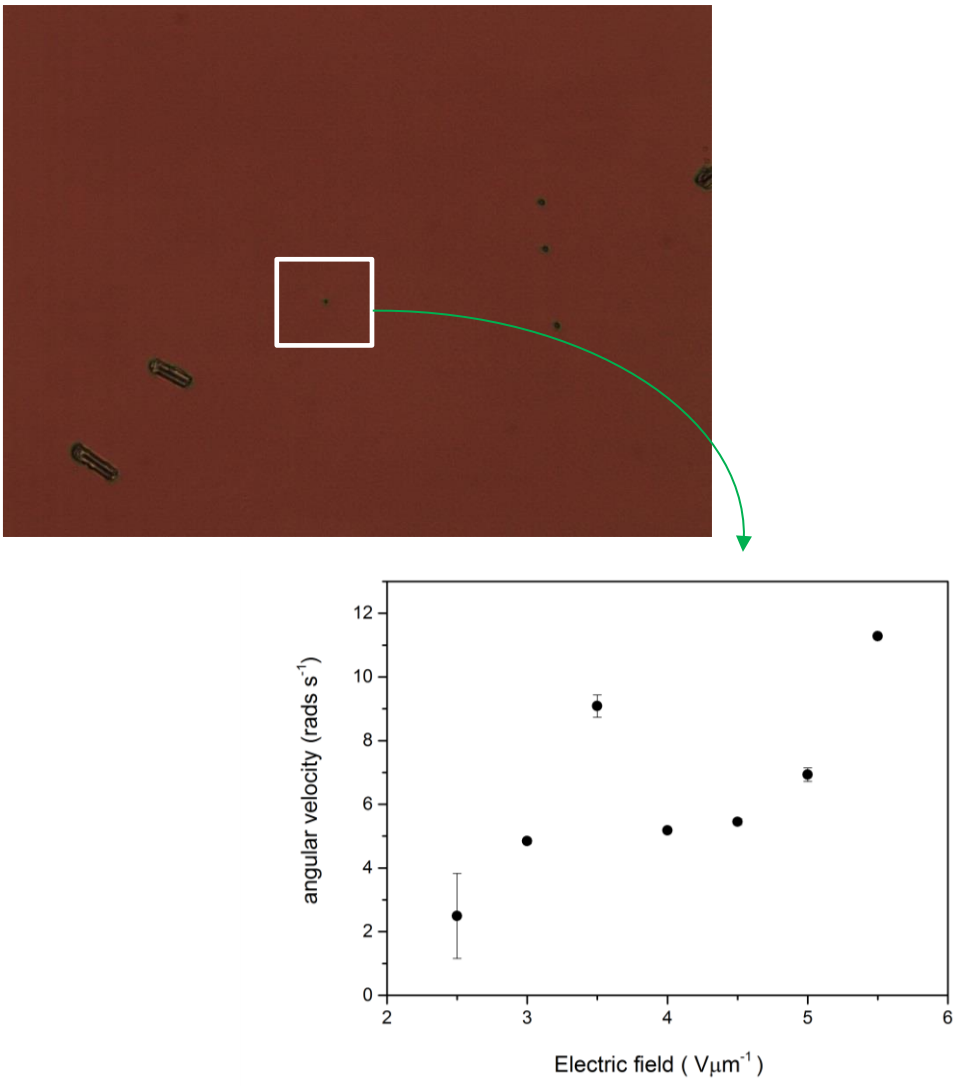

Figure 6.13 The angular velocity of the elongated particles in the nematic liquid

crystal phase, the velocity is shown as a function of amplitude of the electric field. The standing particle's circular motion becomes faster as the amplitude of the field is higher. (HT, $\Delta\varepsilon > 0$, f = 400Hz).

6.3 Discussion of the Results

6.3.1 Homogeneous Boundary Condition with $\Delta\varepsilon_{lc} < 0$ and $\Delta\varepsilon_{lc} > 0$

In a homogenous cell geometry, the particles tend to preferentially be normally lying between the substrates, which means that the elongated particles are parallel to the two glass substrates. This is true irrespective of whether the liquid crystal is of positive or negative dielectric anisotropy. The major difference between the two types of system with homogeneous boundary conditions is that in the case of $\Delta\varepsilon_{lc} < 0$ there is no response of the liquid crystal to the field (no Freedericksz transition), whereas for $\Delta\varepsilon_{lc} > 0$, a Freedericksz transition is observed. The major difference between the field-induced particle motion in the positive and negative dielectric anisotropy devices with homogeneous boundary conditions is that more kinds of motion were observed for particles in the positive dielectric material. Unfortunately, only the linear motion was sufficiently regular that a detailed analysis could be carried out.

The critical field for particle motion for the case of $\Delta\varepsilon_{lc} < 0$ shows the highest value for any of the 4 types of cell geometries considered in this chapter. For the random motion, the E_{cr} is 5 $V\mu m^{-1}$, while the linear motion needs E_{cr} = 7 $V\mu m^{-1}$.

The frequency above which no motion is observed is 200 Hz and this is similar irrespective of the sign of the dielectric anisotropy of the liquid crystal. Also, in both cases experiments show that the directions of the particles' displacements are not related to the director of the liquid crystal in the cell (see, for example the measured motions of the particles for $\Delta\varepsilon_{lc} < 0$ with L = 8.33 μm, electric field of $E = 10$ Vμm^{-1}, f = 50 Hz.) We can conclude, therefore, that the particle motions are not strongly affected by the liquid crystal's alignment on the substrates in homogeneous geometries.

The experiments considered a distribution of the length scale of the particles, and investigated the relation between the length and the linear velocity for motions. Again, both geometries show similar behaviour; the linear velocity decreases significantly as the particle length decreases, reaching a minimum when the particle length is approximately the same size as the cell gap. For the $\Delta\varepsilon_{lc} < 0$ nematic material, observed in a field of $E = 10$ Vμm^{-1}, f = 10 Hz the linear velocity reduced from around 400 μms^{-1} for particles of length ~ 4 μm and reached a minimum of 50 μms^{-1} at a particle length of ~ 9.2 μm; the velocity then significantly increases again above this particle length. The interesting fact is that in both cases, the critical length (9 μm) is nearly same as the cell gap, i.e. 9 μm.

The results from this cell geometry with the homogeneous boundary conditions exhibit unusual characters of the motion. The observations of spherical or elongated particles' linear motion by electric field [3] or by Brownian motion [9] in nematic liquid crystal phases reveal that the direction of the motion is similar direction with the nematic directors. Also, nanowires move along their long axes in nematic liquid

crystals related to the directors [6], but in this system, the elongated micron sized particles move with random direction which is not related to the directors of nematic liquid crystal phase They are hardly reported that the relationship of the length scales of the particles and the velocity, but here, the particle's length similar with the cell gap shows a lowest velocity of the linear motion in the cell geometry.

6.3.2 Homeotropic Boundary Conditions with $\Delta\varepsilon_{lc} < 0$

The remarkable observations of particle motion in this combination of geometries are due to the fact that the application of an electric field can induce topological defects in the nematic film. The motion of the particles is strongly coupled to the defects, which means that the analysis that was carried out for particle motion in chapters 4 and 5 is likely not to be valid here. Nonetheless, it is interesting to consider the behaviour of the particle motion to see whether some insight can be obtained into the mechanisms that are responsible for the particle motion. It was not possible to analyse the linear motion as the direction was not sufficiently uniform. However, a detailed analysis of the circular motion revealed that the angular velocity was much faster in this system than in the chiral nematic or isotropic phases, and that it was independent of the amplitude of the applied field (Figure 6.11-1). The diameter of the circular motion exhibits a strong dependence on the applied field (Figure 6.11-2) which appears approximately linear. This can be analysed in more detail as follows. First consider an equation of the form:

$$D = D_0 + C(E - E_{th}),$$

which is the fit applied in Figure 6.14. This assumes that the diameter of circular motion has a minimum possible value it can take, given by $D_0 = 3.8 \pm 0.4\ \mu m$ and that there is a threshold field, $E_{th} = 6.7 \pm 0.3\ V/\mu m$. The constant of proportionality, C is $C = 1.4 \pm 0.2\ \mu m^2/V$.

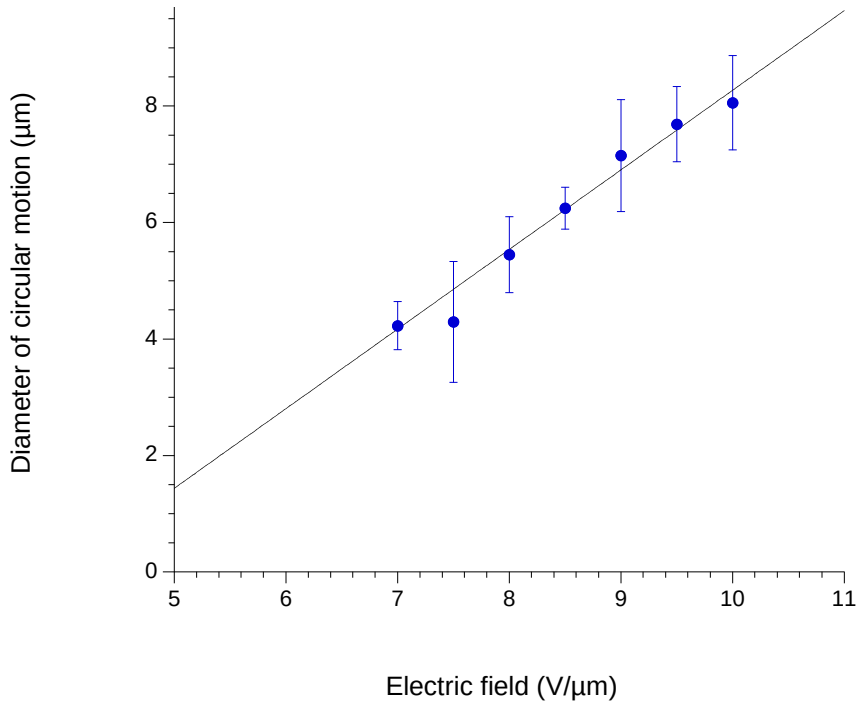

Figure 6.14 A linear fit to the graph that describes the diameter of the circular motion with respect to the applied electric field (from Figure 6.11-2).

An alternative behaviour that reflects that many of the field dependencies observed in liquid crystal systems (square-law dependences) fits of the data to the equation

$$D = D_0 + \chi(E^2 - E_{th}^2)$$

as shown in Figure 6.15. Then the values of the parameters are: $D_0 = 3.6 \pm 0.4\ \mu m$, $E_{th} = 6.4 \pm 0.4\ V/\mu m$ and the constant of proportionality is $\chi = 0.8 \pm 0.01\ \mu m^3/V^2$. In fact there is nothing to distinguish between these two analyses of the data.

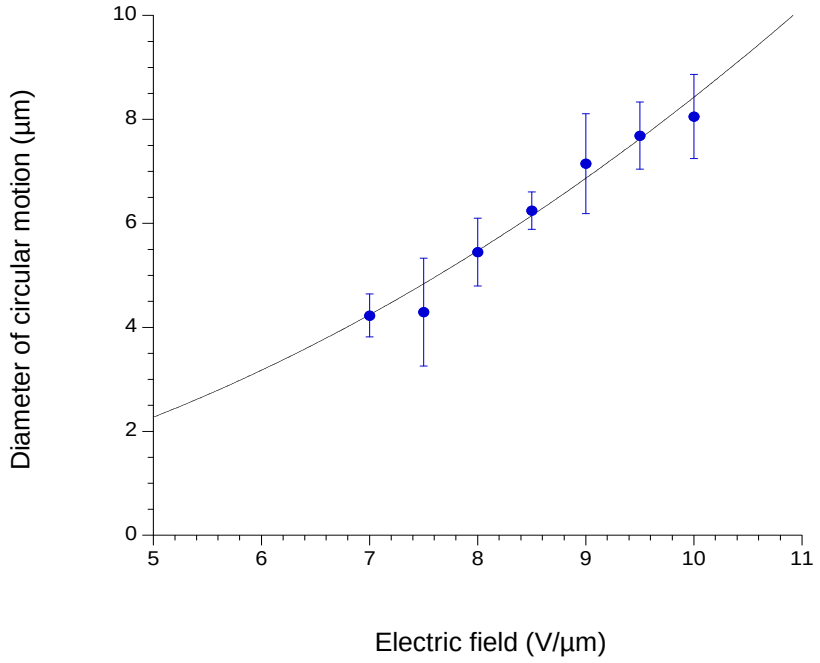

Figure 6.15 A square law dependence fitted to the data of figure 6.11-2.

6.3.3 Homeotropic Boundary Conditions with $\Delta\varepsilon_{lc} > 0$

This case gave perhaps the most similar situation to those considered in Chapters 4 and 5, and it is appropriate to therefore consider similar analyses to those applied to spherical particles in defect-free systems. Figure 6.16 considers whether the

data of Figure 6.13 can be described by a Quincke-type rotation, where the square of the angular velocity is related to the square of the field. This doesn't seem to give a good fit, indeed the fit implies that there is no threshold to the circular motion, which is not consistent with the observations. It can be concluded that in this case, the circular motion is not related to a Quincke-type rotation, unlike in the other cases where spherical particles moved in a defect-free sample.

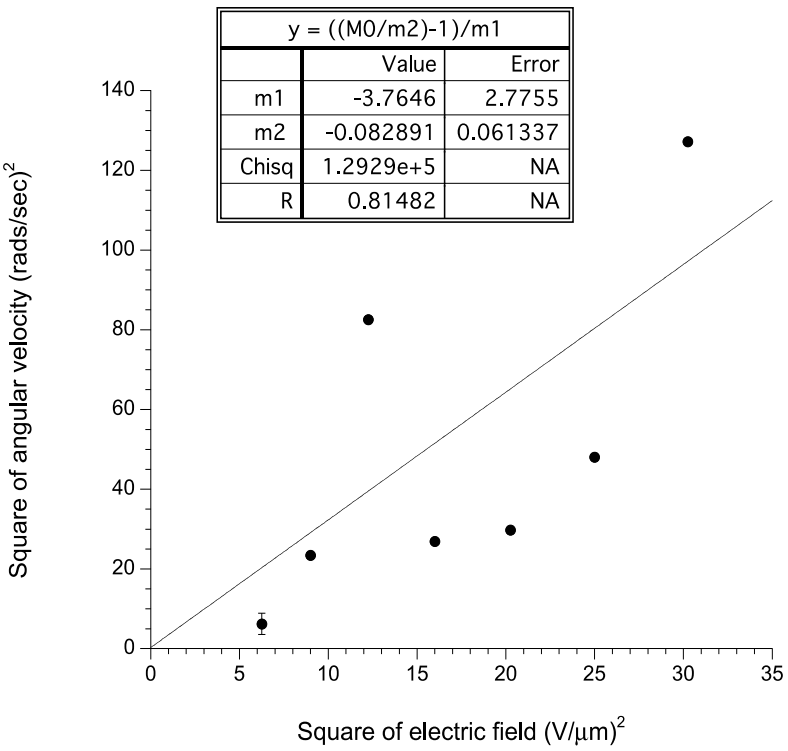

Figure 6.16 The relationship between the square of the angular velocity and the square of the applied electric field for the circular motion of elongated particles coupled with defects. The fit describes a Quincke-type rotation.

Figures 6.17 (a) and (b) consider linear and cubic fits to the data of Figure 6.13. Again, such fits were used to gain an insight into earlier types of particle motion, but it must be remembered that in those cases the particle velocity being analysed was linear, while here it is an angular velocity. Nonetheless, the linear dependency gives a good fit, with a threshold of 1.7 $V\mu m^{-1}$. Including the cubic term seems to give a better fit, but as before when a cubic fit was considered, the coefficients are unphysical. m2, which describes the threshold field, is negative (which cannot be the case), and the additional cubic factor (defined by the coefficient m3), is too small to justify. Overall, it is reasonable to say that including the cubic term in the fit is not appropriate and that the data can be described best by a linear fit with respect to the field.

(a)

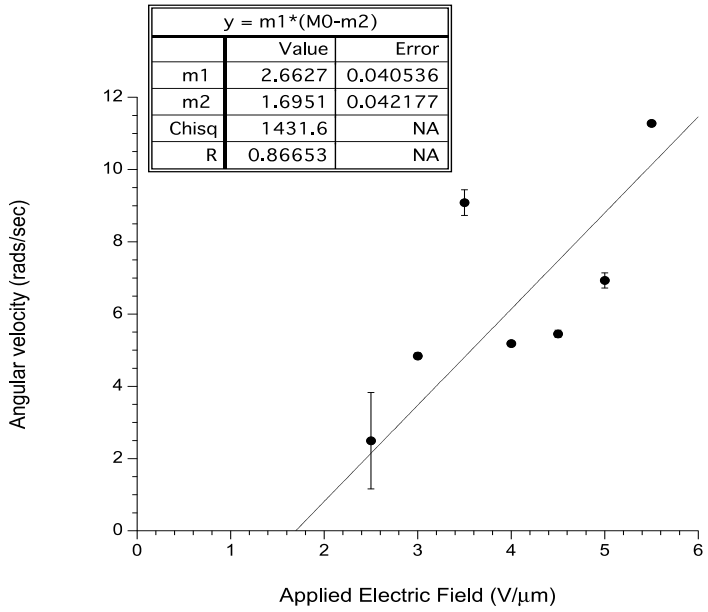

(b)

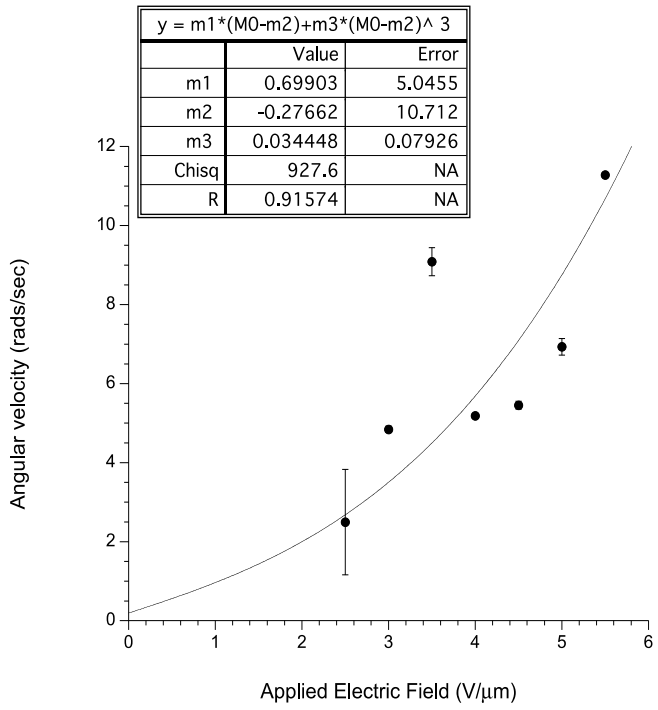

Figure 6.17-(a) and (b) Linear and cubic fits applied to the dependence of the angular velocity to the applied electric field for the circular motion of the elongated particles coupled with defect motion.

There are differences between the results of the experiments described in Sections 6.3.2 and 6.3.3, which show that the circular motion combined with the defects in the nematic phase of negative dielectric material, and without the defects in the positive dielectric nematic material. The moving particle's velocity is not related to the difference of the field amplitude in the negative dielectric material, but shows the diameter of the circular motion combined by the defect increases as the field increases. This measurement is an interesting result possessing a big potential for the future work.

In the positive dielectric nematic liquid crystal, the motion of the circle of the particle increase its velocity with higher field, the linear fit shows the best analysis, therefore the elongated particle in this nematic liquid crystal with the homeotropic boundary conditions exhibits the linear electrophoretic movement in this system. The classic linear electrophoretic mobility of colloidal particles in isotropic liquid is described in the traditional text books [10], and there are previous works using liquid crystals to show the linear electrophoretic mobility. [11]

The difference of the elongated particle's motion regime between homogeneous (higher threshold field of the particle motion in the cell) and homeotropic aligned samples (lower threshold field) could be compared with the nanotubes in homogeneous aligned sample and in homeotropic aligned sample in Lee's work. [7] Lee *et al* reported that the higher electric field was required to translate the elongated particle (CNT) in homogeneous aligned cell rather than homeotropic aligned cell.

6.4 Conclusions

This chapter has examined the behaviour of electric-field induced motion of elongated particles in four different nematic liquid crystal geometries. The area is a rich one to study and clearly this work is only a starting point to the study of these interesting systems. Nonetheless, some clear conclusions can be drawn, summarised below.

1. In both positive and negative dielectric anisotropy systems where linear motion of the lying particle is induced, there is no obvious influence of the liquid crystal director on the particle motion. However, in both cases, the linear velocity of the particle is lowest where the particle length is approximately the same as the cell gap. The dependence of linear velocity on particle size is extremely strong and the deep minimum associated with the cell gap suggests that the mechanism inducing the motion must be such that there is a cross-over between the particle length and width at this point. It will be interesting to explore this further in future work as understanding the relationship between particle velocity and the geometry of it and the cell offers an approach to controlling the particle velocity.
2. In the case of a negative dielectric anisotropy system with homoetropic boundary conditions, the topological defects that are induced by the field have a significant influence on the particle motion. Indeed the particle and defect motion is strongly coupled. Both linear and circular motion occur in this system, though the former could not be fully analysed. In the case of the circular motion:
    a. The angular velocity is much faster than observed for spherical particles in the isotropic or chiral nematic phase;
    b. The angular velocity is independent of field strength;
    c. The diameter of the circle of motion depends approximately linearly on the applied field and a detailed analysis shows that there is a good fit if the dependence is considered to be proportional to $E^2 - E_{th}^2$.

3. Unlike previous observations of circular motion in defect-free samples, there is no similarity between the features of the circular motion of the elongated particle in a homeotropic nematic sample with positive dielectric anisotropy with Quincke-rotation.

Finally, we can say that our system is the first report about the motions of the elongated micron sized silica particles in nematic liquid crystals with 4 types of geometries. The most fascinating result is the particle's circular motions with defect movement in the high velocities. Galerne *et al* investigated drag force and elastic force on the colloidal particles in the interaction field of a disclination lines in a nematic phase using optical tweezing. [12] Muševic et al manipulated micro rod in nematic phase to determine the symmetry around the particles. [9] Both of the self-assembled colloidal particles have a driving mechanism due to the elastic distortions around the particles causing the disturbance of the order of the nematic liquid crystal phase, then long-range forces between particles as a consequence of the coupling between liquid crystal molecules and the surface of the particles. Yeomans *et al* investigated the defect pairs and annihilations only under the electric field in nematic liquid crystals. [13]

As seen from previous works, the measuring velocity of the elongated micron sized silica particles moving with the nematic defects related to electric field is an extraordinary phenomenon, and quite delicate to find and measure. Therefore these observations are the first report presented in this experimental chapter and related theory is hardly figured.

6.5 References

[1] B. Bahadur, Liquid crystals applications and uses. Volume l, 1990, World Scientific Publishing Co.Ptd.Ltd.

[2] P. J. Collings, M. Hird, Introduction to liquid crystals. 1997, Taylor & Francis Ltd.

[3] I. Dierking, G. Biddulph, and K. Matthews, *Electromigration of microspheres in nematic liquid crystals*, PHYSICAL REVIEW E, Volume 73, pp.011702.1-6.

[4] Israel Lazo and Oleg D. Lavrentovich, *Liquid-crystal-enabled electrophoresis of spheres in a nematic medium with negative dielectric anisotropy*, 2013, Philosophical Transactions of the Royal Society A, 2013, Volume 371, p.20120255.

[5] Clayton P. Lapointe, Thomas G. Mason, and Ivan I. Smalyukh, *Shape-Controlled Colloidal Interactions in Nematic Liquid Crystals*, SCIENCE, Volume 326, 20 NOVEMBER 2009. pp.1083-1086.

[6] Giusy Scalia, Jan P. F. Lagerwall, S. Schymura, M. Haluska, F. Giesselmann, and Siegmar Roth, *Carbon Nanoparticles in Nematic Liquid Crystals*, CHINESE PHYSICS LETTER, 2008, Volume 25, No.1, pp. 212-215.

[7] Anoop Kumar Srivastava, Seok Jin Jeong, Myong-Hoon Lee, and Seung Hee Lee, *Dielectrophoresis force driven dynamics of carbon nanotubes in liquid crystal medium*, JOURNAL OF APPLIED PHYSICS, 2007, Volume102, pp.043503.1-5.

[8] Cécile Zakri and Philippe Poulin, Phase behavior of nanotube suspensions: from attraction induced percolation to liquid crystalline phases, Journal of Materials Chemistry, 2006, Volume16, pp.4095–4098.

[9] Uroš Tkalec,a Miha Škarabot and Igor Muševic, *Interactions of micro-rods in a thin layer of a nematic liquid crystal*, Soft Matter, 2008, Volume 4, pp.2402–2409.

[10] W.B.Russel, D.A.Saville, and W.R.Schowalter, Colloidal dispersions. 1989, Cambridge University Press.

[11] S.A.Tatarkova, D.R.Burnham, A.K.Kirby, G.D.Love and E.M.Terentjev, *Colloidal interactions and transport in nematic liquid crystals*, Physics Review Letter, 2010, Volume 98, p157801.

[12] D.Pires, J. Fleury, and Y.Galerne, *Colloid Particles in the Interaction Field of a Disclination Line in a Nematic Phase*, Physical Review Letters, 2007, Volume 98. pp.247801.1-3.

[13] I. Dierking, M. Ravnik, E. Lark, J. Healey, G. P. Alexander, and J. M. Yeomans, *Anisotropy in the annihilation dynamics of umbilic defects in nematic liquid crystals*, PHYSICAL REVIEW E, 2012, Volume 85, pp.021703.1-11.

Chapter 7
Conclusions and Future Work

7.1 Conclusions

The motivation of the experiments in this thesis is the finding any novel movement of micron sized particles in liquid crystal materials. In this work, the experiments focus on new types of geometry (silica sphere without surface treatment in chiral nematic phase and its isotropic liquid, elongated silica particle in nematic phase in 4 types of geometry) compared with previous works introduced in chapter 1 and 2. The experimental results are discussed in each chapter. The main conclusions of the experiments are summarized below.

In chapter 4, an investigation of spherical silica particles in a chiral nematic phase was made. The results showed both circular and linear motions of the micron-sized particles in the chiral nematic liquid crystal phase. The main findings are:

- The direction of the circular motion has no dependence on the handedness of the chiral nematic phase;
- The field dependence of the angular velocity can be analysed by Quincke rotation and the critical frequency allows an estimated of the ion diffusion coefficient which is physically reasonable.
- The unusual temperature dependence of the circular motion cannot be

explained with the relation to viscosity, but could depend on undulation in the sample texture.

- The linear motion of the particle starts above a critical field. Where linear motion occurs, it has similar features to nematic and other electrophoretic systems, but the constrained geometry of the thin cell gap results in electrophoretic mobility without cubic term.
- The motions become faster with amplitude of electric field. Frequency did not have such a strong effect on the motion but a maximum frequency occurs as ion diffusion may have an effect on the liquid crystal-particle composite system.

Chapter 5 examined a surprising form of motion of particles in the isotropic phase of a chiral nematic liquid crystal that was either random or circular. In other isotropic systems with applications of electric fields, either linear motion or Quincke rotation (on an axis) has been observed. The circular motion observed in the isotropic phase appeared above a critical electric field, suggesting that the behaviour is similar to the field induced Quincke rotation of micron-sized spherical particles in the isotropic phase. It is possible that the circular motion observed here is caused by a combination of 'traditional' Quincke rotation, coupled with a tendency for linear motion. However, it isn't clear why simple linear motion is not seen, as it is observed in the chiral nematic phase (chapter 4). We suggested that the isotropic liquid crystal system is different from other isotropic liquid and that even 10K above the $T_{N^*\text{-Iso}}$, the surface of the device and the silica sphere induce liquid crystalline order that influences the dynamics of the system, including the effective viscosity.

The similarity to Quincke rotation led to an analysis of the dependence of the angular velocity on field amplitude that gives a reasonable value for the Maxwell relaxation time, but one which is strongly dependent on the value of conductivity used. It is noted that the motion stops when the delay time is longer than frequency of the electric field, suggesting that the ion diffusion of the system affects the motion regime. However, using the Quincke analysis to deduce a viscosity for the isotropic liquid gives a much higher value than expected and we suggested that this high value could be related to the confinement of the particle in the device in this experimental geometry as mentioned above.

Chapter 6 examined the behaviour of electric-field induced motion of elongated particles in four different nematic liquid crystal geometries. The area is a new one and the work led to some interesting conclusions. For planar samples, the following conclusions were made:

- In both positive and negative dielectric anisotropy systems where linear motion of the lying particle is induced, there is no obvious influence of the liquid crystal director on the particle motion.
- The linear velocity of the particle is always lowest where the particle length is approximately the same as the cell gap. The dependence of linear velocity on particle size is extremely strong and the deep minimum associated with the cell gap suggests that the mechanism inducing the motion must be such that there is a cross-over between the particle length and width at this point.

In the case of the negative dielectric anisotropy system with the homeotropic boundary conditions, the topological defects that are induced by the field had a significant influence on the particle motion.

- The particle and defect motion are strongly coupled.
- Both linear and circular motions occur in this system, though the former could not be fully analysed. In the case of the circular motion, the angular velocity is much faster than observed for spherical particles in the isotropic or chiral nematic phase, the angular velocity is independent of field strength.
- The diameter of the circle of motion in the case where field-induced defects couple with the motion depends approximately linearly on the applied field. A detailed analysis shows that there is a good fit if the dependence is considered to be proportional to $E^2 - E^2_{th}$.

Finally, unlike all of the previous observations of circular motion in defect-free samples, there is no similarity between the features of the circular motion of the elongated particle in a homeotropic nematic sample with positive dielectric anisotropy with Quincke-rotation.

7.2 Future Work

The behaviour of the spherical particles in the chiral nematic phase appears to depend strongly on the balance of different length scale, i.e. pitch length, particle

diameter and cell thickness as the experimental result. Therefore, it would be interesting to know how the dependency changes with the variation of the ratios between the pitch length, particle's diameter, and the cell gap by the measuring the motions of the particles in the different atmosphere of the modified ratios. The linear velocity can be investigated as the electrophoretic mobility and the angular velocity can be analysed by using the Quincke rotation.

Another interesting suggestion of the future work is the measuring the elongated particle's linear velocity with the modification of the its length and cell gap, because the minimum velocity was observed where the particle length was nearly same as the cell gap. The understanding of the relation between cell gap and the length of the particle as with the ratio of diameter/the length of the particle can offer a methodology to control the motions of the particles.

In addition, the defect movement with the elongated particle shows the fascinating moving texture. The observation is a novel texture (the simultaneous movements of a particle and the defects in the quick manner), therefore the measurement which focuses on the defect's type and the motion's regime is the next step of this experimental work. [1]

The motions of the micron sized particles can be affected by the electric atmosphere around the particles in the dispersion system. This influence of the electric properties of the liquid crystal media can be investigated for the Quincke rotation when the conductivity of the liquid crystal medium can be varied.

Finally, combining the measurement technique can give much more details about the motions of the micron-sized silica particles in liquid crystals. The technology

of laser tweezing would be a nice combination because the measurement of the forces in the colloidal system could be a precise approach to the fundamental research of the system. [2] The Confocal Fluorescence Microscopy application can be a combination for the 3-D measurement of the system. [3]

The motion regime could be an indication for the controlled mechanics of the micron sized unit motor when the relation of the variations can be measured throughout the experimental investigations

7.3 References

[1] T. C. Lubensky, David Pettey, and Nathan Currier, *Topological defects and interactions in nematic emulsions*. PHYSICAL REVIEW E, 1998, Vol. 57, No. 1, pp.610-625.

[2] Jennifer L. Sanders, Yiming Yang, Mark R. Dickinson and Helen F. Gleeson, *Pushing, pulling and twisting liquid crystal systems: exploring new directions with laser manipulation*. PHILOSOPHICAL TRANSACTIONS of THE ROYAL SOCIETY A, 2013, Vol. 371, 20120265.

[3] Shuming Nie, Daniel T. Chiu, and Richard N. Zaret, *Probing Individual Molecules with Confocal Fluorescence Microscopy*. SCIENCE, 11 November, 1994, Vol.266, pp.1018-1021.

Appendix

This thesis is an investigation of unusual field induced particle motions in chiral nematic phase and isotropic phase and nematic phase. The attachment contains motion pictures of the particles for showing the characteristic behaviour of them. The list in the table describes the geometry of sample cells and the exemplary motions of the movie attached.

1. List of Motion Pictures

(1) File Name

1. L7 in Chiral nematic phase
2. C1 in Chiral nematic phase
3. Isotropic phase (CDV)
4. 2(Important 4min26sec to 4min 50sec BRUSHES and ORBITING particle)
5. HT positive 3-1(CDV)
6. HG negative (CDV)2
7. HG positive (CDV)2

(2) Summary of the Sample Cell

No.	LC phase	Motion regime	Temperature & field			Cell gap (μm)	Boundary condition	Particle shape/size(μm)
			T(ºC)	E(V/μm)	f(Hz)			
1	N*	linear	90.3	~ 3	~ 60	6	homogeneous	sphere/ 2.5 diameter
2		circular		0 ~ 3	~ 25			
3	Iso	circular	110.0	~5	~ 160	6		
4	N (Δε<0)	various	23.0	0 ~ 6	~ 800	9.1	homeotropic	elongated/ 1.5 diameter & ~ 5.4 length
5	N (Δε>0)			0 ~ 6	~ 300			
6	N (Δε<0)			~ 10	~ 50	9.9	homogeneous	
7	N (Δε>0)			0 ~ 5	~ 100			